

LITHOFACIES AND DEPOSITIONAL ENVIRONMENT SPANNING
THE CRETACEOUS-PALEOGENE BOUNDARY
ON THE NEW JERSEY COASTAL PLAIN

By

HENDRA WAHYUDI

A thesis submitted to the

Graduate School-New Brunswick

Rutgers, The State University of New Jersey

in partial fulfillment of the requirements

for the degree of

Master of Science

Graduate Program in Geological Sciences

written under the direction of

Professor Gail M. Ashley

and approved by

New Brunswick, New Jersey

October, 2010

LITHOFACIES AND DEPOSITIONAL ENVIRONMENTS SPANNING
THE CRETACEOUS-PALEOGENE BOUNDARY
ON THE NEW JERSEY COASTAL PLAIN

By HENDRA WAHYUDI

Thesis Director:
Professor Gail M. Ashley

ABSTRACT OF THESIS

The sedimentary record spanning the Cretaceous-Paleogene (K/Pg) boundary was examined in outcrop and in seven cores recovered from a 50 km long transect along the outcrop belt on the New Jersey coastal plain. The objectives were to: (1) conduct a high-resolution study of the K/Pg lithofacies, (2) document spatial and temporal changes in composition and texture of the sediments, and (3) interpret any changes in the depositional environment across this important geological boundary when a mass extinctions occurred. Analyses include core description, textural, petrographic, microprobe, and XRD analyses. Five lithofacies were interpreted in the Upper Cretaceous sediments and three lithofacies were recognized from the lowermost Paleogene deposits.

Microprobe studies show the chemistry of Upper Cretaceous and lowermost Paleogene glauconite are identical (~7-8% K₂O), but their color difference may suggest

different redox condition. XRD analyses show the Upper Cretaceous clay contains more land-derived detritus than the lowermost Paleogene clay.

The following sequence of events is interpreted from the sediment record spanning the K/Pg boundary: (1) deposition in near-shore setting and slow sedimentation in middle shelf when sea level was falling, albeit still shelfal depth; (2) deposition of K/Pg lithofacies when sea level was falling possibly creating a diastem but not a sequence boundary, *per se*; (3) a transgression above the K/Pg boundary; and (4) deposition in middle shelf possibly with decreased ocean productivity and a more reducing environment.

There is no sedimentological evidence above the K/Pg boundary, suggesting tsunami-related deposition associated with a bolide impact. Either a tsunamite was eliminated by bioturbation, or NJCP was too far from the impact site to be affected. A transgressive lag, instead, was formed by normal sedimentation during the subsequent transgression in the early Paleocene.

Acknowledgements

I would like to express my deepest gratitude to Dr. Gail M. Ashley for her suggestions and comments throughout the course of this research, and her critical review and evaluation of the various forms of this manuscript.

I would like to thank Dr. Kenneth G. Miller who gave me the opportunity to study the K-Pg cores as well as invaluable advice, funding, and critical feedback.

I am indebted to Dr. James V. Browning for providing excellent support during my research. He has made available his support in a number of ways.

I would like to thank Dr. Richard K. Olsson and Dr. Peter J. Sugarman for great discussions on K-Pg stratigraphy.

I would also like to thank Dr. Victoria C. Hover from University of Louisiana, Lafayette, for her critical comment and suggestions on XRD analysis. My appreciation is equally extended to Dr. Jeremy S. Delaney for assisting me on the microprobe analysis.

I thank Linda Godfrey and Alex Cotet for helping me on X-ray diffraction slide preparation, Dr. Paul Falkowski for generously providing me centrifuge facilities, Dr. Thomas J. Emge for his assistance on the X-ray diffraction machine, and Bang Taufan Ladjantja for giving me a ride during field trips.

Nicole A. Abdul is gratefully acknowledged for assistance of my English writing, constructive and encouraging support.

The former and current graduate students in the Rutgers Geological Sciences Department are deserving of thanks as well: Zulfitriadi, Ika Sulistyaningrum, Triyani Nur Hidayah, Ethika, Dennis M. Sanchez, Selen Esmeray, Madhavi V. Parikh, Zuhal Seker, Kelsey Bitting, David M. Bord, Ashley Harris, Livia Montone, Morgan Schaller, Tali

Babila, Christopher A. Vidito, Sara Mana, Paulo A. Ruiz, Deniz Kustu, Huapei Wang, Jonathon LaCarruba, Jesse Thornburg, Catherine Beck, Emily Beverly, Beatriz E. Serrano, Aurora Elmore, Svetlana Mizintseva, Alex Nikulin, Emily Poorvin, and Ayda R. Schookohi. They all helped make this educational journey enjoyable.

Special thanks to ExxonMobil Oil Indonesia and the government of Indonesia for granting me the scholarship and giving me an opportunity to grasp an education journey in United States.

Finally, I would like to thank my family in Indonesia for their prayers and support. Alhamdulillah!

Table of Contents

	Page
Title Page	i
Abstract	ii
Acknowledgment	iv
Table of Contents	vi
List of Tables	ix
List of Figures	x
List of Appendices	xiii
I. Introduction	1
I.1. Background	1
I.2. Geologic setting	4
I.2.1. General stratigraphy	6
II. Research approach	10
II.1. Sites considered	10
II.2. Laboratory studies	10
II.2.1. Textural and binocular microscopic examinations	10
II.2.2. Petrographic analyses	11
II.2.3. Microprobe analyses	12
II.2.4. X-Ray diffraction (XRD) analyses	13
III. Results	15
III.1. Lithofacies	15
III.1.1. Upper Cretaceous sand-rich lithofacies	15

Brown, muddy glauconite sand facies (mgs-1)	15
Brown, bioturbated, muddy glauconite sand facies (mgs-b1)	15
Indurated, muddy glauconite-quartz sand facies (mgs-2)	16
Muddy quartz sand facies (mqs)	17
III.1.2. Upper Cretaceous mud-rich lithofacies	18
Quartzose sandy mud facies (qsm)	18
III.1.3. Lowermost Paleogene sand-rich lithofacies	19
Green, muddy glauconite sand facies (mgs-3)	19
Green, bioturbated, muddy glauconite sand facies (mgs-b3)	19
III.1.4. Lowermost Paleogene mud-rich lithofacies	20
Glauconitic mud facies (gm)	20
III.2. Stratigraphy	21
III.3. Glauconite chemistry	23
III.3.1. Black glauconite	24
III.3.2. Dark green glauconite	25
III.4. Clay mineralogy	26
III.4.1. Upper Cretaceous clay	26
III.4.2. Lowermost Paleogene clay	27
IV. Discussion	29
IV.1. Paleoenvironmental implications	29
IV.1.1. Upper Cretaceous	29
Brown, muddy glauconite sand (mgs-1)	29
Brown, bioturbated, muddy glauconite sand (mgs-b1)	30

Indurated, muddy glauconite-quartz sand (mgs-2)	31
<i>Pinna</i> layer	32
Muddy quartz sand (mqs)	33
Quartzose sandy mud (qsm)	34
IV.1.2. Lowermost Paleogene	34
Green, muddy glauconite sand (mgs-3)	34
Green, bioturbated, muddy glauconite sand (mgs-b3)	35
Glauconitic mud (gm)	38
IV.2. K/Pg boundary placement	38
IV.3. Dynamics of sedimentation	40
V. Conclusions	44
References	46

List of Tables

		Page
Table 1	Diffraction data for common clay minerals and their association	56
Table 2	Authigenic glauconite and its environment of deposition	57
Table 3	Clay minerals and their interpretation of origin.	58
Table 4	Sedimentological criteria of offshore tsunamite, tempestite, and transgressive fill deposits	59

List of Figures

		Page
Figure 1	<i>Pinna</i> layer, Main Fossiliferous Layer, and Krakatau Event Layer	60
Figure 2	Stratigraphy of on the NJ coastal plain spanning the K/Pg boundary	62
Figure 3	Study location	63
Figure 4	Sediment classification based on percentage of grain sizes	64
Figure 5	The Upper Cretaceous sand-rich lithofacies	65
Figure 6	Microphotograph of brown, bioturbated, muddy glauconite sand from Meirs Farm 1 core	67
Figure 7	Bioturbated clay on granulariferous, indurated, muddy glauconite- quartz sand from USGS-NJGS Freehold core	68
Figure 8	Microphotograph of indurated muddy glauconite sand from Tighe Park 1 core	69
Figure 9	Microphotograph of indurated muddy glauconite sand from Agony Creek outcrop	70
Figure 10	The Upper Cretaceous mud-rich lithofacies	71
Figure 11	The lowermost Paleogene sand-rich lithofacies	72
Figure 12	Microphotograph of green, muddy glauconite sand from Meirs Farm 1 core.	73
Figure 13	Microphotograph of green, bioturbated, muddy glauconite sand from Agony Creek outcrop	74
Figure 14	The lowermost Paleogene mud-rich lithofacies	75
Figure 15	Microphotograph glauconitic mud facies from Buck Pit 1 core	76

Figure 16	Stratigraphic column of Buck Pit 1 core	77
Figure 17	Stratigraphic column of USGS-NJGS Freehold core	80
Figure 18	Stratigraphic column of Tinton Falls outcrop	82
Figure 19	Stratigraphic column of Tighe Park 1 core	83
Figure 20	Stratigraphic column of Agony Creek outcrop	85
Figure 21	Stratigraphic column of Meirs Farm 1 core	86
Figure 22	Stratigraphic column of Fort Monmouth 3 core	88
Figure 23	Stratigraphic column of Search Farm 1 core	90
Figure 24	Stratigraphic column of Low Meadow 1 core	92
Figure 25	Fence diagram of K/Pg deposits	94
Figure 26	Sediment characteristics and lithofacies boundary of K/Pg deposits	95
Figure 27	Glaucinite morphotypes	97
Figure 28	Backscattered electron images of glauconite morphotypes	98
Figure 29	Stages of development of glauconitization in granular substrate	99
Figure 30	Relationship of K ₂ O with SiO ₂ as determined by microprobe analysis	100
Figure 31	Relationship of K ₂ O with FeO as determined by microprobe analysis	102
Figure 32	Relationship of K ₂ O with Al ₂ O ₃ as determined by microprobe analysis	104
Figure 33	Relationship of FeO with Al ₂ O ₃ as determined by microprobe analysis	106
Figure 34	X-ray diffractograms of the Upper Cretaceous samples	108

Figure 35	X-ray diffractograms of the lowermost Paleogene samples (1)	109
Figure 36	X-ray diffractograms of the lowermost Paleogene samples (2)	110
Figure 37	K/Pg deposits from Bass River, New Jersey	111
Figure 38	Sea level curve across the K/Pg boundary	112
Figure 39	A depositional model of sedimentation across the K/Pg boundary, NJ	113

List of Appendices

	Page
Appendix 1 Detailed locations of K/Pg bore-holes and outcrops at NJCP	114
Appendix 2 Location and depth of petrographic, microprobe, and XRD samples	115
Appendix 3 List of XRD peaks	116

I. Introduction

I.1. Background

The Cretaceous/Paleogene (K/Pg) boundary has been the focus of numerous studies because it records of mass extinction and sea level change (*e.g.*, MacLeod and Keller, 1991; Olsson *et al.*, 1997; Olsson *et al.*, 2002; Keller, 2008; Schulte *et al.*, 2010). It ranks third in magnitude among the major mass-extinction events, with a 40% loss of genera including planktonic foraminifera, calcareous nannoplankton, brachiopods, mollusks, ammonites, land and marine reptiles (Bambach, 2004). Currently, extraterrestrial impact (Alvarez *et al.*, 1980) is the favored hypothesis by many scientists, supported by the detection of a global Iridium (Ir) anomaly at the level of mass extinction in planktonic foraminifera and calcareous nannoplankton (*e.g.*, Alvarez *et al.*, 1980; Smit, 1999). In addition, the identification of a ~180 km diameter crater near Chicxulub, Mexico on the Yucatan Peninsula (Hildebrand *et al.*, 1991), associated with ejecta-rich deposits, including altered impact glass, shocked minerals, and carbonate accretionary lapilli (Bohor, 1987; Smit, 1999; Yancey and Guillemette, 2008) support the correlation of an impact event with the K/Pg boundary.

However, the emplacement of hot spot volcanism of the Deccan Traps (a Large Igneous Province that consists of more than $3 \times 10^6 \text{ km}^3$ of flood basalt) is another possible explanation for the extinction event (*e.g.*, Officer and Drake, 1985; Officer *et al.*, 1987; Duncan and Pyle, 1988; Courtillot *et al.*, 1988; Keller *et al.*, 2008). The Deccan Traps could have caused the extinctions through several mechanisms, including the release of dust and sulphuric aerosols into the air which might have blocked sunlight and thereby reducing plant photosynthesis (*e.g.*, Courtillot *et al.*, 1988; Keller *et al.*, 2008).

This scenario proposes a period of intense volcanic activity associated with volatile emissions leading to acid rain and global cooling (Officer *et al.*, 1987). Acid rain may have caused a reduction in the alkalinity and pH of the surface oceans that could explain the observed decrease in surface-water productivity and carbonate dissolution at depth (Officer *et al.*, 1987). These combined effects could explain the mass extinction at the K/Pg boundary (Officer *et al.*, 1987; Keller, 1989). However, the Deccan Traps volcanism likely began by ~0.5 Myr before the extinction (Vonhof and Smit, 1997), although Keller *et al.* (2008) proposed that the main volcanism phase occurred at the K/Pg boundary.

The position of sea level at the K/Pg boundary is also controversial (MacLeod and Keller, 1991; Pospichal, 1994). Donovan *et al.* (1988) concluded that global sea level fell in the latest Maastrichtian based on the identification of lowstand deposits in central Alabama. This hypothesis is supported by the finding of coarse-grained clastic and limestone breccia deposits in Northern Mexico (Stinnesbeck and Keller, 1996). However, the magnitude of sea level fall and the subsurface distribution of the lowstand deposits are not precisely known (Olsson and Liu, 1993). In addition, sea level had already started to fall during the late Maastrichtian and was relatively low both before and after the K/Pg boundary (Olsson and Liu, 1993).

The New Jersey coastal plain is an excellent location for studying the K/Pg boundary because it is located ~2,500 km from the Chicxulub crater and strata there consist of a relatively undisturbed succession, unlike the localities near the crater on the Gulf coastal plain (Olsson *et al.*, 1997; Olsson *et al.*, 2002). Olsson *et al.* (1997) described K/Pg boundary sediments in cores drilled at Bass River, New Jersey (Ocean

Drilling Program Leg 174AX). They are comprised primarily of glauconitic clay that contains the planktonic foraminiferal Zones P0 and P α . These beds abruptly overlie a spherule bed that contains shocked quartz. Thus, Olsson *et al.* (1997) hypothesized that this sediment deposition was connected to the Chicxulub impact. The impact hypothesis is supported by both the presence of carbonate accretionary particles originated from carbonate crystals generated within the vapor plume of the impact at K/Pg sediment in Bass River borehole, New Jersey (Yancey and Guillemette, 2008) and an elevated concentration of Ir (~2 ppb) in the Bass River corehole (Olsson *et al.*, 2002). However, detection of another, more modest Ir anomaly in New Jersey in a lower stratigraphic position, posed an enigma. Landman *et al.* (2007) reported a ~0.5 ppb Ir anomaly at the base of a very fossiliferous *Pinna* layer containing Cretaceous fossils found in the Manasquan River Basin, south of Freehold, Monmouth County, New Jersey. This inconsistency could result either by the extinctions post dating the impact or from a downward displacement of Ir due to bioturbation, chemical diffusion, and/or groundwater leaching (Landman *et al.*, 2007). But, on the other hand, the poorly sorted fossiliferous sediment of the *Pinna* layer in the New Jersey coastal plain as described by Landman *et al.* (2007) and the Main Fossiliferous Layer (MFL) (Gallagher, 2002) near the K/Pg boundary share similar characteristics to the poorly sorted fossiliferous sediment of Krakatau Event Layer in Teluk Banten which have been interpreted as a tsunami deposit triggered by the devastating Krakatau eruption in 1883 (Figure 1) (Van den Bergh *et al.*, 2003).

Bourgeois *et al.* (1988) described an Ir anomaly and paleontologic K/Pg boundary, which directly overlies a sandstone bed at sites near the Brazos River, Texas.

Interestingly, they proposed that the sandstone bed was deposited from a tsunami that was generated by the impact. The finding of mass-flow deposits containing K/Pg boundary impact ejecta in cores at Bermuda Rise, which is located more than 700 km from the continental margin, also supported the tsunami hypothesis (Norris *et al.*, 2000). Olsson *et al.* (1997) indicated that calcareous clay clasts in the basal 6 cm of the Paleocene from the Bass River core might also have originated from the erosive action due to an earthquake triggered by the impact on the Cretaceous seabed. It is thus possible that the *Pinna* layer represents a tsunamite deposited immediately after the impact. In addition, Gallagher (2002) found complete and partial skeletons of vertebrates in the MFL and supported the tsunami hypothesis. However, other possible scenarios such as a major storm or a normal marine transgressive deposition could also result in the same unusual coarse deposits (*e.g.*, Bourgeois, 1990; Landman *et al.*, 2007; Morton *et al.*, 2007).

Despite the many studies of K/Pg boundary deposits, few have focused on the details of the sediments (Bourgeois, 1990). This study presents the results of detailed sedimentological and mineralogical analyses of deposits below and above the K/Pg boundary along a 50 km transect of the New Jersey coastal plain. The objectives were to: (1) conduct a high-resolution study of the lithofacies present in cores and outcrop, (2) document spatial and temporal changes in composition and texture of the sediments and (3) interpret any changes in the environment of deposition across this important geological boundary.

1.2. Geologic setting

The New Jersey coastal plain is located at the northern part of the mid-Atlantic coast of North America, a well known passive-thermoflexural continental margin, that formed subsequent to Late Triassic to Early Jurassic rifting and volcanism (Watts and Thorne, 1984; Steckler *et al.*, 1999; Benson, 2003; Kominz *et al.*, 2008). The coastal-plain sediments were deposited atop of basement: the northern Raritan Embayment, located at the present junction of the Raritan and Hudson Rivers in Raritan Bay and a minor arch which known as the South Jersey High (Owens and Gohn, 1985). The coastal plain was exposed and eroded during the global sea-level lowstands of the Plio-Pleistocene (Stanford *et al.*, 2001), resulting in the exposure of Upper Cretaceous and Cenozoic strata (Kulpecz *et al.*, 2008).

The New Jersey coastal plain was tectonically stable during the K/Pg boundary (Kominz *et al.*, 1998; Kominz *et al.*, 2008) and was mainly influenced by minimal siliclastic input and glauconite deposition (Olsson, 1963; 1975; 1987; Sugarman *et al.*, 1995; Olsson *et al.*, 1997; Olsson *et al.*, 2002; Landman *et al.*, 2004; Landman *et al.*, 2007; Miller *et al.*, 2004; Browning *et al.*, 2008), which was deposited on a gentle-ramp (gradient $\sim 1:1000$) physiography (Steckler *et al.*, 1999).

The K/Pg boundary occurs in a highstand systems tract (HST) within the Navesink sequence (Olsson *et al.*, 2002; Miller *et al.*, 2004). Global sea level fell to ~ 70 m prior to the K/Pg boundary and slightly rose to ~ 75 m at the boundary and then fell again during Paleocene (Kominz *et al.*, 2008). Browning *et al.* (2008) interpreted that the K/Pg deposits were deposited in middle (30-100 m) to outer neritic (>100 m) shelf environments. Olsson *et al.* (2002) suggested that paleowater depth gradually shallowed from about 90 m to 50 m during this period based on analysis of foraminifera from

borehole record from Bass River.

I.2.1. General stratigraphy

The K/Pg coastal plain section of New Jersey contains one unconformity-bounded unit that is called the Navesink II sequence (Sugarman *et al.*, 1995; Olsson *et al.*, 2002; Miller *et al.*, 2003; Kulpecz, 2008). This sequence is interpreted as a shelf deposit (Kulpecz, 2008). It consists of the Upper Cretaceous Navesink Formation which grades to Upper Cretaceous Red Bank, Tinton, and New Egypt Formations (Figure 2). Landman *et al.* (2007) assigned the very fossiliferous *Pinna* layer, located on the upper part of the Tinton Formation to the Danian. Below is a detailed description of the individual formations:

- Navesink Formation

The Upper Cretaceous Navesink Formation is a transgressive glauconite-rich deposit that accumulated on the middle shelf (Olsson, 1987; Olsson *et al.*, 2002). It is light gray to gray and burrowed (Olsson, 1963; Owens *et al.*, 1998; Landman *et al.*, 2004; Landman *et al.*, 2007). It grades upward into the Red Bank Formation in northeastern Monmouth County and into the New Egypt Formation on the southwestern part of this county (Olsson, 1963; Landman *et al.*, 2004; Landman *et al.*, 2007).

- Red Bank Formation

The Red Bank Formation consists of two members: the lower Sandy Hook Member and the upper Shrewsbury Member (Olsson, 1963). The Sandy Hook Member is dark gray feldspathic silty quartz sand to silt which grades upward into the fine- to coarse-grained, micaceous sand of the Shrewsbury Member (Olsson, 1963). The

Shrewsbury Member is interpreted as a regressive unit that was deposited on the inner to middle shelf (Olsson, 1975; 1987).

- Tinton Formation

The Tinton Formation is a glauconitic quartz sand (Olsson, 1963; Landman *et al.*, 2004; Landman *et al.*, 2007). It is the only indurated unit in the Upper Cretaceous section of New Jersey (Olsson *et al.*, 1975). It is dark gray to dark yellow where unweathered; where weathered, siderite changes color of unit to orange brown because of iron oxides, and the formation is stained or cemented in exotic patterns (Owens *et al.*, 1998). Olsson (1975) estimated the thickness of the Tinton Formation as approximately 6.7 m, and that it is very limited in its geographic extent. Olsson (1987) interpreted the Tinton Formation as being deposited in an inner shelf environment and is related to the Red Bank regressive facies. Its upper contact is unconformable with the Hornerstown Formation (Olsson, 1987; Sugarman *et al.*, 1995; Owens *et al.*, 1998; Landman *et al.*, 2004; Landman *et al.*, 2007).

Based on exposures in the Manasquan River, Landman *et al.* (2007) described a very fossiliferous layer, called the *Pinna* layer, at the top of the Tinton Formation. This abundantly fossiliferous 20 cm thick unit contains internal and external molds without any calcareous shell material. They found two notable bivalve fossils: *Cucullaea vulgaris* and *Pinna laqueata*, the latter only appears in this layer and is often found in living position suggesting an autochthonous accumulation with little or no postmortem transport. The color of this unit is “gray-green on fresh exposures, but is orange-brown when weathered”. It is less lithified than the underlying part of the Tinton Formation and contains small siderite nodules (1-5 cm in diameter), which are sometimes fossiliferous,

scattered throughout the unit. Landman *et al.* (2007) also observed that the *Pinna* layer is thoroughly bioturbated without any evidence of bedding. The *Pinna* layer conformably overlies Tinton Formation.

- New Egypt Formation

The New Egypt Formation is “dark gray, glauconitic, clayey sand to sandy clay with some siderite nodules, minor mica and lignite” (Landman *et al.*, 2004; Landman *et al.*, 2007). It is approximately 10–10.5 m thick and thins to the south (Olsson, 1963). Olsson (1975; 1987) interpreted it as the downdip, shelf facies equivalent with the Tinton and Red Bank Formations. The New Egypt Formation conformably overlies the Navesink Formation (Olsson, 1987; Landman *et al.*, 2004). Olsson *et al.* (1997; 2002) interpreted that the Hornerstown Formation conformably overlies the New Egypt Formation. In contrast, Landman *et al.* (2004) interpreted that the Hornerstown Formation unconformably overlies the New Egypt Formation (Figure 2).

- Hornerstown Formation

The Hornerstown Formation is a dark gray to gray-green, burrow mottled, glauconitic clayey sand to glauconite sand (Owens *et al.*, 1998; Landman *et al.*, 2004; Landman *et al.*, 2007). Locally, it has small amounts of quartz at its base (Owens *et al.*, 1998). Olsson *et al.* (1997) described a spherule layer at the base of the Hornerstown Formation in the Bass River corehole. Below the spherule layer is the uppermost Maastrichtian calcareous nannofossil *Micula prinsii* Zone and above the spherule layer is the basal Danian planktonic foraminiferal *Guembelitra cretacea* P0 Zone. The Hornerstown Formation is deposited in mid-neritic depths (Olsson 1963; Olsson *et al.*, 2002).

Landman *et al.* (2007) found a thin and discontinuous layer that was extensively bioturbated, sandwiched between the *Pinna* layer and the concentrated bed of siderite nodules of the Hornerstown Formation. They referred to this layer as the Burrowed Unit (Figure 2) and assigned it tentatively to the Hornerstown Formation. The burrows in this zone are very large, *e.g.* 10 cm long by 2.5 cm wide. It contains numerous siderite nodules, which are similar to those that occur sporadically throughout the *Pinna* layer. In the northeastern and southeastern part of coastal plain the Burrowed Unit is equivalent with the Main Fossiliferous Layer (MFL), a concentrated layer of *Cucullaea vulgaris*, gastropods, baculites, and vertebrate remains (Gallagher, 1993; Landman *et al.*, 2004; Landman *et al.*, 2007) (Figure 2).

The interpretation of the unconformable basal contact of the Hornerstown with the underlying formations has been controversial (Olsson, 1963; Gallagher, 1993; 2004; Olsson *et al.*, 1997; Olsson *et al.*, 2002; Owens *et al.*, 1998; Landman *et al.*, 2004; Landman *et al.*, 2007). Olsson (1963) also found in many areas that the basal contact is characterized by an intensely bioturbated zone in which many burrows filled with bright green glauconite sand from the Hornerstown Formation project down into the dark gray matrix of the underlying New Egypt Formation.

II. Research approach

II.1. Sites considered

K/Pg boundary coreholes located at Buck Pit 1, Fort Monmouth 3, Low Meadow 1, Meirs Farm 1, Search Farm 1, Tighe Park 1, and Freehold were examined (Figure 3; Appendix 1). These seven coreholes have relatively complete K/Pg sections. Percent recovery of sediment was high for each corehole with an average recovery of 90%. The thickness of those cores range from 5.3-22.5 m (17.5-73.8 ft).

Supporting fieldwork was conducted on September 20, 2009, October 11, 2009, and April 30, 2010 at an outcrop in “Agony Creek” tributary to river, about 200 m from the Tighe Park core hole and to Campo Pit, about 100 m from Buck Pit core. Additional K/Pg samples from Tinton Falls and Hockhocks Brook were also studied. The purpose was to compare the K/Pg deposits on the outcrops with the cores. The field study involved description and collection of samples for laboratory analyses.

II.2. Laboratory studies

The seven cores were logged and described. Physical characteristics of sediments, bedding, sedimentary structures and color were made. Both sediments from cores and outcrops were sampled to perform textural, petrography, microprobe and X-ray diffractometry (XRD) analyses.

II.2.1. Textural and binocular microscopic examinations

Sediment textures for all samples were determined using a combination of wet and dry-sieve techniques. A small sample of each sediment (minimum 30 gm) was dried,

weighed and disaggregated. Samples were then wet-sieved through a 63 μm screen to separate the silt and clay fractions from sand. Clay and silt were qualitatively distinguished by the level of plasticity of the sediment. Clayey sediments feel sticky and form ribbons when moist. Silty sediments have a slick feel and form no ribbon when moist. Some clay was retained to perform XRD analysis. The sand-sized fraction was removed from the screen, dried, weighed, and then dry-sieved manually for 5 to 10 minutes using a 250 μm screen to separate the fine-very fine sand from the coarser grain (medium-very coarse sand). Sand content (% sand) was determined by dividing the weight of sand fraction by total starting weight of sample.

The sand fraction was examined under a binocular microscope to determine the mineralogic composition. The mineralogic composition of these sands was grouped into glauconite, very fine-fine quartz, medium-very coarse quartz, mica, and other (*e.g.*, skeletal fragment, siderite) and estimated semi-quantitatively. Their percentage was plotted to observe their distribution at various depths. The glauconite color variation was also qualitatively observed at K/Pg coreholes and was the subject of microprobe analysis to examine their chemistry.

Color (based on Munsell soil color chart), grain size (sand vs. mud; adapted from Folk, 1954 in North American Geologic-Map Data Model Science Language Technical Team, 2004) (Figure 4), dominant mineral, and induration of sediment are basis of the lithofacies name.

II.2.2. Petrographic analyses

A total of 9 thin sections (3 samples collected in the field, 6 samples from coreholes; Appendix 2) were commercially prepared for petrographic analyses by Spectrum Petrographics Inc. Thin sections were examined under a petrographic microscope to describe sediment textures and various components, including glauconite (color and morphotypes), clastic or detrital grains (*e.g.*, quartz), skeletal fragments, and matrix and cements. Representative fabrics, textures, and grain types were documented via digital photography.

II.2.3. Microprobe analyses

A total of 26 grains of glauconite (17 grains of dark green and 9 grains of black glauconite; Appendix 2) from representative Upper Cretaceous and lowermost Paleogene sediments were selected for the microprobe analyses. Selected samples were manually picked, mixed with an embedding medium (epoxy resin), and set in a 1-inch diameter clear lucite disk. After the epoxy set, lower portions of the disk were polished with the SiC and a series of diamond laps (a 6 μ m lap followed by a 1 μ m lap) to expose grains for microprobe analysis. Then, samples were coated with carbon using the evaporated carbon-coating method to make the samples conductive. The carbon-coated polished samples were studied using the microprobe facility in the Department of Earth and Planetary Sciences at Rutgers University. Analyses were performed using a JEOL JXA-8200 Scanning Electron Microprobe equipped with 5 WDS detectors.

Quantitative (WDS) microprobe analyses were carried out using the crystals TAP (Al, Si) at spectrometer 1, TAP (Na, Mg) at spectrometer 2, PETH (Ti) at spectrometer 3, PET (K, Ca) at spectrometer 4, and LIF (Mn, Fe) at spectrometer 5. All quantitative

major element analyses were calibrated with the following standards: 127 Plagioclase Lake County for Silicon (Si), 120 Hornblende Kakanui for Titanium (Ti), 103 Anorthite Great Sitkin for Aluminum (Al) and Calcium (Ca), 101 Fe₂SiO₄ for Iron (Fe), 102 Mn₂SiO₄ for Manganese (Mn), 134 Enstatite Norton County for Magnesium (Mg), 139 Albite Tiburon for Sodium (Na), and 123 Microcline NMNH for Potassium (K). The analysis were run at an accelerating voltage of 20 KeV with a primary beam of 20 nA and counting times of 5-20 second per element. Results of analyses are displayed as oxides and calculated with stoichiometric Oxygen method.

II.2.4. X-Ray diffraction (XRD) analyses

Mud (silt and clay) from eight samples were collected to perform XRD analyses (Appendices 2 and 3). Separation of clay-sized fractions (<2 µm) from silt was obtained through centrifuging (3500 revolutions per minute [rpm] for 10 minutes). After each centrifugation, the supernatant (clay and water) was separated from the precipitated fraction (silt). Distilled water was added to each supernatant until they reached the same weight (90 grams) before conducting faster centrifugation on Thermos Scientific Sorvall RC 6+ centrifuge (max. speed 14000 rpm) at 12000 rpm for 20 minutes at 4°C (acceleration 8, deceleration 8). The centrifugation processes are conducted in the Institute of Marine and Coastal Sciences at Rutgers University.

The extracted clay was dried using an oven at ~40°C for 24 hours and then were ground in an agate mortar separately to make a homogenous powdered-clay. XRD slides were prepared using the technique of Chiu *et al.* (2005). The slides were made by

mounting ~8 mg clay powder on microscope glass covers (1-in diameter) using a mixture of one part of DucoCement diluted with 10 parts acetone.

X-ray diffraction was conducted on the air-dried condition in a Philips XPert powder diffractometer with sample changer at the Department of Chemistry, Rutgers University. Samples were run using a Cu K α radiation source at a speed of 0.01°/s. through the range of 4 to 34° 2 θ . X-ray diffractograms were used to qualitatively evaluate the clay mineralogy and their mineral associations (Appendix 3).

III. Results

III.1. Lithofacies

III.1.1. Upper Cretaceous sand-rich lithofacies

Brown, muddy glauconite sand facies (mgs-1)

Mgs-1 dominantly consists of sand-size sediment (Figure 5). Its color varies from very dark grayish brown (2.5Y 3/2) to black (5YR 2.5/1). It is loose, massive, and contains abundant clay. The composition is mostly black glauconite (54-86%) with 11-43% mud. Mgs-1 has 1-4% mica and 1-3% fine to coarse quartz. It has clay clasts that are composed of diagenetic siderite in Meirs Farm 1 core. Scattered diagenetic gypsum appeared when this sediment was dry. It also has a sulfur smell.

Mgs-1 appears in every K/Pg core, except Buck Pit, Tighe Park, and Freehold. Its thickness ranges from 0.4-9.2 m (1.3-30.3 ft). It is commonly found alternating with- and grading upward into brown, bioturbated, muddy glauconite sand (mgs-b1). Based on its lithologic character and position, it is assigned to the Upper Cretaceous New Egypt/Navesink Formations.

Brown, bioturbated, muddy glauconite sand facies (mgs-b1)

Brown, bioturbated, muddy glauconite sand (mgs-b1) is the same as facies mgs-1, but with very intense bioturbation (Figure 5). Mineralogically, mgs-b1 is similar to the mgs-1 but has slightly higher fine quartz content and clay (judging by the ribbon texture). In Meirs Farm it contains more diagenetic siderite (10-30%).

Mgs-b1 is distinguished by its extensive bioturbation. Near the formation contact, *i.e.* the lowermost Paleogene Hornerstown and the Upper Cretaceous New

Egypt/Navesink Formations, the sediment in the bioturbation is similar to the overlying green, muddy glauconite sand (mgs-3) from the lowermost Paleogene Hornerstown sediment. Burrows are generally circular (~3 to 5 cm) and elongate (up to ~10 cm long and ~2.5 cm in diameter). The thickness of this unit ranges from ~20-60 cm. Lower in the section, the sediment in the bioturbation unit consists of brown clay. The burrows are lens-shaped. The total thickness of this facies is 1.0-1.6 m (3.3-5.1 ft).

In thin section, the matrix of mgs-b1 is mainly composed of very fine-grained, randomly oriented black clay (Figure 6). Glauconite grains dominantly show mammilated-lobate and ovoidal-spheroidal morphology. Capsule shaped and vermicular grains are minor. Curvy sutures are common in mammilated-lobate grains. They commonly exhibit two-color variation. The core of the grains are dark green or cloudy brownish green and lighter green or yellowish green on their edge. Quartz grains are monocrystalline and angular to subangular. Fecal pellets are rare and are sometimes replaced by glauconite (Figure 6).

Mgs-b1 appears in the Meirs Farm, Search Farm, and Fort Monmouth cores. It usually alternates with the brown, muddy glauconite sand (mgs-1). This facies belongs to Upper Cretaceous New Egypt /Navesink Formation.

Indurated, muddy glauconite-quartz sand facies (mgs-2)

The indurated, muddy glauconite-quartz sand (mgs-2) is granulariferous and iron-cemented (Figure 5). Mud comprises up to 45% of this deposit. Mgs-2 is mainly composed of detrital glauconite and quartz; however the percentages of the minerals vary. Glauconite is more abundant at Tighe Park/Agony Creek (up to 85%) and less

abundant at Hockhocks Brook outcrop (~50%) and Freehold core (~10%). On the other hand, quartz grains are coarser and more abundant at Freehold (~75%) and Hockhocks Brook (~25%) compared to quartz at Tighe Park/Agony Creek (<5%). This facies is more indurated at Freehold and Hockhocks Brook than at Tighe Park/Agony Creek. Mica appears as an accessory minerals. It contains *Cucullaea vulgaris* and *Pecten* molds without any calcareous shells. Those molds are partially and completely sideritized and occur as nodules. Bioturbated clay is common in this facies (Figure 7).

In thin section, facies mgs-2 is reddish brown due to diagenetic siderite cement (Figure 8). The matrix fraction is characterized by very fine-grained, randomly oriented clays, and very fine mica. The original shapes of glauconite grains are difficult to assess due to weathering. Most glauconite grains are covered by siderite. Some relict glauconite grains still show two-color variation, but they exhibit a worm-like texture instead of a distinct curvy fracture. Quartz grains are monocrystalline and angular to subangular. Phosphate grains are rare. Skeletal fragments recognized include fecal pellets, bivalves, and planktonic foraminifera (Figures 8 and 9).

The thickness of this facies varies from 1.0-2.7 m (~3.0-8.75 ft). Based on its degree of induration, glauconite and quartz content, mgs-2 is assigned to the Upper Cretaceous Tinton Formation. The upper part of this facies near the contact with the overlying Hornerstown Formation sediment is equivalent to the *Pinna* layer of Landman *et al.* (2007) (Figures 1 and 2).

Muddy quartz sand facies (mqs)

The muddy quartz sand facies (mqs) is dark yellowish brown (10YR 4/4)-grayish brown (10YR 5/2), poorly sorted, angular-subrounded sand (Figure 5). Mqs is dominantly composed of quartz. Medium-coarse quartz is up to 90% at Tinton Falls and about 70% at Buck Pit and Freehold. Fine quartz is ~10% in average. The rest of mqs is mud (~25%); detrital glauconite is less than 6% and mica ~1%. This lithofacies is indurated at Tinton Falls and friable at Buck Pit and Freehold.

This facies is only found at the Tinton Falls, Buck Pit and Freehold. The thickness is ~0.6-3.7 m (2.0-12 ft). Mqs belongs to the Upper Cretaceous Tinton Formation at Tinton Falls and Buck Pit, but most likely belongs to the Upper Cretaceous Red Bank Formation at Freehold.

III.1.2. Upper Cretaceous mud-rich lithofacies

Quartzose sandy mud facies (qsm)

The quartzose sandy mud-rich facies (qsm) is dark gray (5Y 4/1) to dark yellowish brown (10 YR 4/4) (Figure 10). It is dominantly granulariferous mud and has ~30% medium-coarse quartz and <3% fine quartz. Quartz grains are angular to subrounded; some grains are iron stained. It also composed of less than 1% mica and glauconite.

This facies is thin (15 cm) and is only found in the Buck Pit 1 core and Campo Pit outcrop. Qsm has an abrupt contact with the overlying lowermost Paleogene glauconitic mud (gm) facies. It grades downward to the muddy quartz sand (mqs) facies. It likely belongs to the Upper Cretaceous Tinton Formation.

III.1.3. Lowermost Paleogene sand-rich lithofacies

Green, muddy glauconite sand facies (mgs-3)

Green, muddy glauconite sand (mgs-3) is widely found in every K/Pg core (Figure 11). It is very dark grayish green (GLEY 1 3/5G) and dominantly sand. The composition is dominantly dark green glauconite (up to 90%). It has 15% mud on average. Mgs-3 contains <1-12% fine quartz. Medium to coarse quartz and mica are accessory (less than 3%). Fecal pellets and fish teeth are present. A colorless mineral, likely a phosphatic vivianite (Sugarman, *pers. comm.*), is occasionally present.

In thin section, the matrix is mainly composed of very fine grained, randomly oriented black clay. Mammilated-lobate and ovoidal-spheroidal shapes showing curvy sutures are the dominant morphology of glauconite grains. Two-color variation of the grains also appears. Quartz is monocrystalline, angular to subrounded. Skeletal fragments including fecal pellets and benthic foraminifera are present (Figure 12).

Mgs-3 is typical of the lowermost Paleogene Hornerstown Formation. It often overlies the Upper Cretaceous brown, bioturbated, muddy glauconite sand (mgs-b1). However, in the Tighe Park and Agony Creek sites it grades to the lowermost Paleogene green, bioturbated, muddy glauconite sand (mgs-b3). Its thickness is 1.0-10.6 m (3.3-35.0 ft).

Green, bioturbated, muddy glauconite sand facies (mgs-b3)

The green, bioturbated, muddy glauconite sand (mgs-b3) is very dark grayish green (GLEY 1 3/5G) - very dark grayish olive (10Y-5GY 5GY/4) (Figure 11).

Mineralogically, it resembles the lowermost Paleogene green, muddy glauconite sand

(mgs-3). In the Tighe Park core it is characterized by circular (~5 mm) to elongate burrows, *e.g.* cm long by ~10 mm and wide by ~2.5 mm. In outcrop the burrows are more complex. They are composite-lenses filled by brown, glauconite sand. The burrows are often sideritized. Molds of *Cucullaea vulgaris* are found in the outcrop. In general, the fossils are sideritized forming small nodules. The thickness is up to 0.7 m (2.3 ft).

Thin section shows similar features as shown in mgs-3 facies (Figure 13). Mgs-b3 is only found in the Tighe Park core and Agony Creek outcrop. It belongs to the lowermost Paleogene Hornerstown Formation. It is equivalent to the Burrowed Unit of Landman *et al.* (2007) and the Main Fossiliferous Layer (Gallagher, 2002)(Figures 1 and 2).

III.1.4. Lowermost Paleogene mud-rich lithofacies

Glauconitic mud facies (gm)

The glauconitic mud facies (gm) is thin (~30 cm) and is only found in the Buck Pit and Campo Pit (Figure 14). It is olive (5Y 4/3) to dark gray (5Y 4/1). Mud dominates (93-97%) and it contains more clay than silt based on its plasticity. This facies has a small amount of glauconite (up to 4%), little quartz (<2% medium-coarse quartz and <0.5% fine quartz), and a trace of mica. Scattered light brown clay clasts appear in this facies.

Thin section shows the matrix is composed of very fine-grained, randomly oriented brown clay/mica (Figure 15). It has some glauconite and quartz grains. Glauconite is mottled and shows worm-like features.

This facies characteristic has not been recognized previously in Cretaceous-Paleogene formations in New Jersey. It might be a facies in the New Egypt Formation.

III.2. Stratigraphy

The K/Pg deposits of the New Jersey coastal plain are composed of a complex lithostratigraphic package of sediments. There is significant variation of lithofacies in a relatively close distance (*e.g.*, distance of Buck Pit to Tighe Park is ~ 11 km) (Figure 3). The age control of the deposit is based on limited of dinocyst, pollen and macrofossil data (Landman *et al.*, 2007; Miller *et al.*, 2010). The correlations of the K/Pg deposit are also made using pattern changes of echinoid fecal pellets and Ir data near the boundary (Miller *et al.*, 2010).

The Uppermost Cretaceous sediments are heterogeneous. In the most updip section they are represented by Buck/Campo Pit locality, where they consist of a few meters thick poorly sorted muddy quartz sand (mqs) and an overlying ~15 cm thick granular, quartzose sandy mud (qsm) (Figure 16). There is a ~10 cm highly iron cemented layer between these two facies. The contact of these facies appears gradational. These facies belong to the Tinton Formation. They pinch out to the southeastern part of coastal plain (Figure 25).

About 10 meters thick mqs of the Red Bank Formation grades to more than 10 meters thick of qsm sand of Tinton Formation in the Freehold core (Figure 17). The same lithostratigraphic succession appears at Tinton Falls locality (Figure 18). The contact between these facies is not present at either the Freehold core or Tinton Falls outcrop. The indurated, muddy glauconite-quartz sand (mgs-2) of the Tinton Formation is the only

Upper Cretaceous lithofacies at Tighe Park (Figure 19) and Agony Creek (Figure 20).

The age of the Tinton Formation, including the overlying *Pinna* layer is based on the appearance of indicative uppermost Maastrichtian species of ammonite *Discoscaphites iris* and the dinoflagellate *Palynodinium grallator* (Landman *et al.*, 2007). Scattered white clay clasts appear on the Upper Cretaceous and lowermost Paleogene facies at Agony Creek site (Figure 20).

The Uppermost Cretaceous sediments at Meirs Farm, Fort Monmouth, Search Farm, and Low Meadow are intercalated with brown, muddy glauconite sand (mgs-1) and brown, bioturbated, muddy glauconite sand (mgs-b1) from the New Egypt/Navesink Formations (Figures 21-24). These facies are more widespread throughout New Jersey coastal plain. A white clay clast appears at Meirs Farm corehole, which corresponds with an Ir peak and an increase upsection of echinoid epifaunal fecal pellets occurs within the mgs-b1 facies (Figure 21). Assuming the Ir anomaly at this site is *in situ*, it is a possibility that this facies is diachronous.

The lowermost Paleogene sediments at New Jersey coastal plain are more homogenous. They predominantly consist of green, muddy glauconite sand (mgs-3), which is up to 10 meters thick. This lithofacies belongs to the Hornerstown Formation. About 60 cm thick of green, bioturbated, muddy glauconite sand (mgs-b3) (Burrowed Unit) at Tighe Park/Agony Creek and a 30 cm thick green glauconitic mud (gm) at Buck Pit underlie this deposit. The presence of *Senoniasphaera inornata* in glauconitic mud indicates Danian age (Miller *et al.*, 2010). The stratigraphic correlation of deposits bracketing the K/Pg boundary are shown in a fence diagram (Figure 25).

The contact between the Upper Cretaceous and the lowermost Paleogene lithology (Figure 26) is mostly abrupt suggesting a significant change either of paleoenvironmental settings or diagenetic history during the K/Pg transition. At the most updip section, *e.g.*, Buck Pit, this sharp contact is between a quartzose sandy mud (qsm) which is overlain by glauconitic mud (gm) facies. In the more downdip section, *e.g.*, at Tighe Park, green, bioturbated, muddy glauconite sand (mgs-b3) abruptly overlies the indurated, muddy glauconite-quartz sand (mgs-2). A siderite nodule appears near the contact. Mgs-b2 is abruptly overlain by mgs-1 and a *Cucullaea vulgaris* mold appears at the contact at Search Farm which corresponds with the Ir peak. The same lithofacies succession is present in the Meirs Farm core although the contact here appears more gradational. At the Low Meadow site, brown, muddy glauconite sand (mgs-1) grades upward to green, muddy glauconite sand (mgs-3) (Figure 24).

III.3. Glauconite chemistry

K/Pg sediments on the New Jersey coastal plain are dominated by glauconite. There are two types of glauconite: allochthonous/detrital and autochthonous/authigenic glauconite (Amorosi, 1997). Allochthonous glauconite is found in muddy quartz sand (mqs) and the indurated, muddy glauconite-quartz sand (mgs-2) of the Upper Cretaceous Tinton Formation. Allochthonous glauconite can be distinguished because it covaries with quartz, lacks sutures, and is generally not associated with marine biological remains such as fish teeth, fecal pellets, and phosphate grains. Autochthonous glauconite is observed in sediments from the Upper Cretaceous New Egypt (brown, muddy glauconite sand; brown, bioturbated, muddy glauconite sand) and lowermost Paleogene

Hornerstown Formations (green, muddy glauconite sand; green, bioturbated, muddy glauconite sand). Authigenic glauconite abundance does not covary with quartz. It has distinctive curvy sutures and is associated with fecal pellets, fish teeth, and phosphate grains.

The autochthonous glauconite from K/Pg sediments show various morphologies. Based on Triplehorn (1966) glauconite morphology, the K/Pg authigenic glauconite is categorized into spheroidal-ovoidal, mammilated-lobate, capsule-shaped, and vermicular forms (Figures 27 and 28). These glauconite types exhibit two different colors under the reflected microscope, black and dark green (Figure 27). Upper Cretaceous glauconite from the New Egypt/Navesink Formation is black, while the lowermost Paleogene glauconite from the Hornerstown Formation has dark green glauconite. This difference may reflect different chemical compositions that in turn may relate to different environments of deposition. A total of 26 grains of black (9) and dark green glauconite (17) from various morphologies were analyzed by microprobe to look for compositional variations.

III.3.1. Black glauconite

Black glauconite from the Upper Cretaceous New Egypt/Navesink Formation has an average composed of SiO_2 (51.82-55.30%), K_2O (6.84-8.13%), FeO (21.44-25.64%), and Al_2O_3 (4.86-10.28%). Occasionally, it has some brighter spots representing higher atomic number and Fe content (Figure 28). There are no significant oxide composition among the different morphological types. Based on the classification of glauconite at

different stages of maturity (Odin and Fullagar, 1988; Figure 29) this glauconite on average is evolved to highly evolved (6.84-8.13%K₂O).

Weight percent K₂O is plotted versus weight percent of SiO₂, FeO, Al₂O₃ to observe their relationships as shown in Figures 30-32. They show that K₂O has a linear relationship with FeO and inverse relationship with Al₂O₃, but does not have a distinctive correlation with the SiO₂ content. The weight percent FeO is also plotted versus weight percent of Al₂O₃, which shows an inverse relationship (Figure 33).

III.3.2. Dark green glauconite

The composition of dark green glauconite from the lowermost Paleogene Hornerstown Formation is almost identical with the black glauconite from the Upper Cretaceous New Egypt/Navesink. It consists of SiO₂ (51.36-55.06%), K₂O (7.10-8.30%), FeO (21.04-26.20%), and Al₂O₃ (3.68-10.81%). It does not show oxide variation among different types of morphologies. It also falls into evolved to highly evolved glauconite stages of maturity (Odin and Fullagar, 1988). Plots of K₂O versus FeO, Al₂O₃, and SiO₂ and FeO versus Al₂O₃ demonstrate similar relationships as black glauconite (Figures 30-33). Therefore, it is likely that major element chemistry of glauconite cannot be used to differentiate between black and dark green glauconite, as well as among any glauconite grain morphology.

Supply of iron is important to form glauconite (Burst, 1958a; 1958b). The high abundance of glauconite in the K/Pg deposit may imply the high amount of iron released from continental waters, which is possibly controlled by the hinterland geology during the K/Pg period. The chemical weathering of glauconite-rich deposits from the older

strata in the coastal region, *e.g.* Bass River, Merchantville, and Marshalltown Formations, may have contributed abundant iron which in turn was utilized for the formation of glauconite. The color difference of the two kinds of glauconite may be due to the valence state of the iron in these minerals, *i.e.* Fe^{+2} and Fe^{+3} , related to the redox states under which they exist (Fanning *et al.*, 1989). Using Mössbauer spectroscopy, Fanning *et al.* (1989) examined glauconite from the oxidized and reduced zones of soil in the Maryland and New Jersey coastal plains. They concluded that in the oxidized zones the glauconite was more yellow under plane-polarized light, as opposed to more green for the glauconite in the reduced zones. Thus, the dark green glauconite in the lowermost Paleogene deposit may possibly have been generated in more reduced environment than the black glauconite from the Upper Cretaceous strata.

III.4. Clay mineralogy

X-ray diffraction analyses were conducted on eight samples of selected clay-mineral separates from the Upper Cretaceous and the lowermost Paleogene formations to qualitatively observe variations of clay mineralogy within the strata (Figures 17, 20-22; Appendix 2). Table 1 is used to interpret the diffractogram pattern.

III.4.1. Upper Cretaceous clay

The Upper Cretaceous clays are derived from two lithofacies: quartzose sandy mud facies (qsm) from the Buck Pit 1 core (Figure 17) and brown, bioturbated, muddy glauconite facies (mgs-b1) from the Fort Monmouth 3 core (Figure 22). These two facies show the same diffraction peaks corresponding to interplanar spacings of $\sim 10.1 \text{ \AA}$, ~ 7.11

Å, ~ 5.00 Å ~ 4.53 Å, 3.53 Å, and ~ 3.33 Å but different relative intensities (Figure 34; Appendix 3). In general, the qsm has more prominent peaks on ~ 10.1 Å, ~ 5.00 Å ~ 4.53 Å, and ~ 3.33 Å but less intense on ~ 7.11 Å and ~ 3.53 Å compared to the mgs-b1. In addition, the mgs-b1 have other peaks at interplanar spacings of ~ 4.26 Å, ~ 3.21 Å, ~ 3.13 Å, ~ 2.82 Å, and ~ 2.71 Å.

Diffraction peaks at ~ 10.1 Å, ~ 5.00 Å ~ 4.53 Å, and ~ 3.33 Å suggest the presence of glauconite or illite. The two peaks at ~ 7.11 Å and ~ 3.53 Å indicate the presence of chlorite, kaolinite, or vermiculite. Additional X-ray diffraction analyses of ethylene-glycol solvated samples and/or of samples heated to 400° and 550° C, are required to have a more definite answer. A possible trace chlorite/vermiculitic peak is suggested also by the presence of weak hump at 14.4 Å.

Additional peaks on mgs-b1 diffractrogram are considered as non-clay mineral peaks, *e.g.* ~ 4.26 Å is a quartz peak, ~ 3.21 and ~ 2.82 Å are halite peaks (likely appear due to imperfect sample preparation), ~ 3.13 Å and ~ 2.71 Å are a pyrite peaks, and ~ 3.0 Å may be a calcite peak. Also sharp portion of peak at 3.34 Å is both quartz and glauconite/illite.

III.4.2. Lowermost Paleogene clay

Eight samples from the lowermost Paleogene clays were derived from three lithofacies in different cores. They are from a green, muddy glauconite sand (mgs-3) (Fort Monmouth 3, Meirs Farm 1, and Tighe Park 1 bore-holes; Figures 20-22); a green, bioturbated, muddy glauconite sand (mgs-b3) (Tighe Park 1; Figure 20); and glauconitic mud (gm) (Buck Pit 1; Figure 16). These three facies show the same diffraction peaks

corresponding to interplanar spacings of $\sim 10.1 \text{ \AA}$, $\sim 5.00 \text{ \AA} \sim 4.53 \text{ \AA}$, and $\sim 3.33 \text{ \AA}$ with but with different intensities among the XRD patterns (Figures 35 and 36; Appendix 3). The glauconitic mud (gm) has two more additional peaks at $\sim 7.18 \text{ \AA}$ and $\sim 3.58 \text{ \AA}$ which also appear in the underlying Upper Cretaceous sediment at the same borehole (quartzose sandy mud). All lithofacies show a $\sim 4.17 \text{ \AA}$ peak and weak peak at $\sim 2.70 \text{ \AA}$, except the gm and mgs-3 facies from Fort Monmouth borehole. There are also small peaks at $\sim 3.66 \text{ \AA}$, $\sim 3.07 \text{ \AA}$, and $\sim 2.79 \text{ \AA}$.

The diffraction peaks corresponding to interplanar spacings of $\sim 10.1 \text{ \AA}$, $\sim 5.00 \text{ \AA} \sim 4.53 \text{ \AA}$, and $\sim 3.33 \text{ \AA}$ indicate the presence of glauconite or illite which appear in all lowermost Paleogene facies. An additional peak at $\sim 3.66 \text{ \AA}$ also indicates the presence of illite. The peaks corresponding to 7.18 \AA and $\sim 3.58 \text{ \AA}$ in the glauconitic mud suggests the presence of chlorite, kaolinite or vermiculite. The peak on $\sim 4.17 \text{ \AA}$ and weak peak at $\sim 2.70 \text{ \AA}$ indicate the presence of goethite. Siderite may occur, indicated by the $\sim 2.79 \text{ \AA}$ peak. A minor peak at $\sim 3.07 \text{ \AA}$ suggests the presence of gypsum.

In general, Upper Cretaceous clay is more heterogeneous than the lowermost Paleogene clay. The Upper Cretaceous clay is composed of glauconite or illite and chlorite, kaolinite, or vermiculite. The lowermost Paleogene clay is dominantly composed of glauconite or illite. Only in glauconitic mud at Buck Pit core, chlorite, kaolinite, or vermiculite are present. The variation of the type of clay in the Upper Cretaceous sediments probably indicates various sources during the Late Cretaceous period as opposed to more homogenous sources in the Paleocene.

IV. Discussion

IV.1. Paleoenvironmental implications

Paleoenvironmental information is deduced mainly from (1) the micro- and macroscopic analyses performed on the named lithofacies, (2) the characteristics of glauconite, *i.e.* authigenic versus detrital, and (3) the lateral and vertical facies changes.

IV.1.1. Upper Cretaceous

Brown, muddy glauconite sand (mgs-1) (New Egypt/Navesink Fm.)

This facies is found at Fort Monmouth, Low Meadow, Meirs Farm and Search Farm (Figure 3). It is mainly composed of highly evolved authigenic glauconite. Authigenic glauconite typically forms in open marine environments, far away from zones of active sedimentation (*i.e.* near river mouths), at relatively low temperatures, and under most climate conditions (Odin and Letolle, 1980). However, in unusual cases authigenic glauconite can also be generated in shallow lagoons (Albani *et al.*, 2005) and tidal flats (Chafetz and Reid, 2000) (Table 2). Chafetz and Reid (2000) argued that it is unwise to use glauconite solely as an environmental indicator of either mid-shelf and deeper water. Sedimentary structures, benthic foraminifera assemblages, and trace fossil criteria should be used to have a more confident interpretation of environments of deposition.

Mgs-1 is found at Low Meadow (Figures 3 and 26). This sand is dominantly massive without significant sedimentary structures, occurs in association with fish teeth and echinoid fecal pellets and lacks quartz. It shows faint lamination in a few cores. These characteristics suggest this facies was likely deposited where there was limited sediment supply, such as in the middle shelf. Paleobathymetry data from one of the complete K/Pg sections from Bass River borehole indicated the glauconitic silty clay,

which is equivalent with this facies, was deposited in mid-shelf environment, approximately 100 m deep (Olsson *et al.*, 2002). The location of the sandy glauconite mud is up dip of Bass River. If we assume the ramp gradient is 1:1000, the environment of deposition of this facies would be ~50 m shallower than the silty clay at Bass River.

The occurrence of kaolinite, vermiculite, and chlorite in the clay fraction of this facies suggests that clays produced by bedrock weathering (Table 3) contributed to the sediment on the mid-shelf. The occurrence of pyrite in this glauconite-rich deposit likely indicates diagenesis following burial.

This facies is distributed in a K/Pg belt running in a northeast-southwest direction and pinches out to quartz-rich facies to the northwest along the dip direction which suggests that the basin likely was deeper towards to the southeast (Figure 25).

Brown, bioturbated, muddy glauconite sand (mgs-b1) (New Egypt/Navesink Fm.)

This facies occurs at Fort Monmouth, Low Meadow, Meirs Farm and Search Farm (Figure 3). It is basically the brown, muddy glauconite sand (mgs-1), but with extensive bioturbation. Thus, it is interpreted to have been deposited in the same environment as mgs-1, *i.e.*, mid-shelf. This lithofacies is often found overlain by the lowermost Paleogene green, muddy glauconite sand (mgs-3). The bioturbation on this lithofacies composed of green sand (mgs-3) may reflect the intensified activity of Paleocene fauna into the relatively nutrient-rich Upper Cretaceous sediment (Landman *et al.*, 2007). The intense bioturbation has been attributed to the dramatic decrease in export of organic material following the K/Pg extinction event (Ortega-Huertas *et al.*, 2002; D'Hondt, 2005).

Indurated, muddy glauconite-quartz sand (mgs-2) (Tinton Fm.)

The type section for the Tinton Formation that comprises this unique lithofacies is Tinton Falls (Figures 18). It is poorly sorted, *i.e.*, muddy yet granuliferous, and consists of an unusual quartz and glauconite association. Those characteristics suggest that this facies is the result of mixing sediment from different sources. The analysis of glauconite and quartz grain orientation in this facies also indicates that this deposit contains reworked sediment (Robertson, 1972). Thus, it is likely the glauconite in this facies is detrital. However, the glauconite at Tighe Park and Agony Creek sites possibly is authigenic since the quartz content is not abundant (Figures 19 and 20). The induration is due to siderite cement possibly originating from the combination of iron from the weathering of glauconite and carbonate from the leaching of the fossil shell material (Robertson, 1972).

The mud and granule content of mgs-2 indicates this lithofacies was deposited in a nearshore setting where mixed energy (waves and tides) affect deposition. The high abundance of mud suggests this deposit was generated in the lower energy zone of the lower shoreface setting (Siringan and Anderson, 1994). The occurrence of *in situ* *Protocallianassa* (ghost shrimp) claws and burrows implies deposition in very shallow water possibly, such as intertidal to shallow subtidal settings (Robertson, 1972). Landman *et al.* (2007) extensively studied macrofossils in this facies and also suggests that it likely was deposited in the nearshore, subtidal environment.

Mgs-2 is restricted to the northeast and the central parts of study area (Figure 25). The quartz is more abundant and coarser in the northeast section suggesting that the sediment source provenance was to the northeast, possibly ancient Hudson River. This is

consistent with the mapping of the paleo-Hudson river by Kulpecz *et al.* (2008). Mgs-2 does not occur in the most southwest sections of the coastal plain. It is also absent at Fort Monmouth which lies approximately 5 km to the northeast from the type of locality of this facies. Thus, Fort Monmouth was likely located between the lower shoreface where quartz is more abundant and off shore with minimum siliciclastic sedimentation and thus a favorable place for glauconite generation.

- *Pinna* layer

The upper part of the indurated, muddy glauconite-quartz sand (mgs-2), in the central part of the K/Pg outcrops including Tighe Park and Agony Creek, contains of abundant bivalve molds without any calcareous shells is referred to as the *Pinna* layer (Landman *et al.*, 2007). A modest Ir anomaly is found at the basal of this layer, which had been interpreted marking the K/Pg boundary (Landman *et al.*, 2007). *Pinna* layer is under- and overlain by a bioturbated unit which apparently shares similar characteristics to the poorly sorted fossiliferous sediment of the Krakatau Event Layer (KEL) in Teluk Banten. The KEL has been interpreted as a tsunami deposit triggered by the devastating Krakatau eruption (Figure 1) (Van den Bergh *et al.* (2003). Thus, the *Pinna* layer may be result of tsunami-related impact. However, although the elevated Ir value is present at the base of the *Pinna* layer, the biostratigraphic age of this layer is late Maastrichtian (Landman *et al.*, 2007), and thus predates the impact and makes the tsunami origin interpretation implausible. Miller *et al.* (2010) recently studied the *Pinna* layer and other K/Pg deposits at New Jersey coastal plain and suggested that the concentrated Ir at *Pinna* layer is due to downward mobilization. They theorized that the Ir was originally deposited at the top of the layer and then displaced down section due to differences in

redox potential. Even if the Ir is in place, the tsunami origin of *Pinna* layer is still unlikely because the occurrence of *Pinna laqueata* are in life position (Landman *et al.*, 2007) and *in situ Protocallianassa* (Robertson, 1972). In addition, my study shows that the *Pinna* layer does not show grain size sorting and is laterally limited which are both characteristic of tsunamites (Table 4). The sediment analysis results on the *Pinna* layer at the Manasquan River Basin support this non-tsunami origin hypothesis (Bennington *et al.*, 2010).

A more reasonable explanation of the origin of the *Pinna* layer is it is the result of river influx of sea level fall (Landman *et al.*, 2007). This layer was likely deposited in a nutrient-rich, nearshore setting. However, this environment was probably subject of occasional rapid sedimentation, possibly from riverine influx when sea level relatively fall during the K/Pg period, which buried the animals.

Muddy quartz sand (mqs) (?Tinton/Red Bank Fm.)

Muddy quartz sand (mqs) contains poorly sorted sediment. It is characterized by the abundance of mud (up to 36%) and medium-coarse quartz grains (more than 50%) indicating that the sediment was deposited in a mixed high and low energy environment (*e.g.*, Siringan and Anderson, 1994), possibly on an upper to lower shoreface environment. In Campo Pit, this facies overlies quartz-rich sediment of the Red Bank Formation whose hummocky cross stratification could have been generated in the upper to lower shoreface setting (*e.g.*, Dashtgard *et al.*, 2009; Hill *et al.*, 2003; Saito, 1989). Mqs facies has a limited distribution which may represent isolated shallow marine sand bodies (Snedden and Bergman, 1999; Tillman, 1999). It is the up dip equivalent of the

glaucinite-rich (mgs-1 and mgs-b1) sediment which were likely deposited further offshore.

Quartzose sandy mud (qsm) (Tinton Fm.)

Quartzose sandy mud (qsm) is similar to with the muddy quartz sand (mqs), but it has more mud (~66%). These characteristics suggest that they formed in a similar environment, but qsm was likely deposited in a quieter setting because it contains more mud. The presence of detrital chlorite, kaolinite, or vermiculite indicates contribution of sediment from land. This facies is interpreted as an isolated shallow marine sand body, the up dip equivalent of glauconite-rich sediment (mgs-1 and mgs-b1) accumulating offshore in deeper water.

IV.1.2. Lowermost Paleogene

Green, muddy glauconite sand (mgs-3) (Hornerstown Fm.)

This facies has similar composition as the Upper Cretaceous brown, muddy glauconite sand (mgs-1). They are both composed of dominantly evolved to highly evolved, authigenic glauconite and minimum amount of quartz. However, mgs-3 sediment is siltier, has dark green glauconite, more homogenous clay (glauconite or illite) and more abundant echinoid epifaunal fecal pellets than mgs-1 (Olsson, *pers. comm.*).

Mgs-3 was likely deposited in the similar setting as the brown, muddy glauconite sand facies (mgs-1), but probably under slightly higher energy because mgs-1 has more silt. The color difference might be related to the relative amount of Fe^{2+} and Fe^{3+} in the glauconite (Fanning *et al.*, 1989). Ferrous (Fe^{2+}) represents a more reduced

environment, whereas Ferric Fe^{3+} a more oxidized environment (Fanning *et al.*, 1989).

Based on study of glauconite from the oxidized and reduced zones of soil in the Maryland and New Jersey coastal plains the green color indicates reduced environment. The homogenous clay (*i.e.*, glauconite) within the mgs-3 indicates that deposition was very slow and there was little or no sediment from the land. The more abundant echinoid epifaunal fecal pellets may indicate that the nutrient availability was likely enough to support epifaunal organisms.

As previously stated mgs-3 is a homogenous, glauconite-rich deposit and is common throughout the K/Pg section of the New Jersey coastal plain. This deposit is underlain by sedimentologically diverse Upper Cretaceous deposits which suggests the presence of a marine transgression. Cretaceous shorelines NW of the NJ coastal plain's updip section were submerged by rising sea-level and this glauconite-rich offshore sediments deposited.

Green, bioturbated, muddy glauconite sand (mgs-b3) (lowermost Hornerstown Fm.)

Mgs-b1 occurs only at Tighe Park and Agony Creek (Figures 19, 20, and 25). This facies is similar to the green, muddy glauconite sand (mgs-3), but with extensive bioturbation. Landman *et al.* (2007) referred to this facies as the Burrowed Unit (Figure 2). Based on its similar characteristics with mgs-3, it is interpreted to have been deposited in the same middle shelf environment. The dense bioturbation in mgs-b3 indicates that the sea floor experienced bioturbation after it was deposited. The bioturbation was terminated near the contact of underlying indurated muddy glauconite-quartz sand (mgs-2) suggesting the induration occurred before the deposition of mgs-b3. The distribution of

this facies is restricted, likely related to the patchy source of nutrients during the sediment deposition.

Gallagher (2002) studied southeastern part of New Jersey coastal plain and found very high abundance of fossils, including complete and partial skeletons of vertebrates in the same stratigraphic unit. He referred this unit as the Main Fossiliferous Layer (MFL)(Figures 1 and 2). He proposed that this layer may have been the result of a tsunami following the impact during the K/Pg period. The tsunami hypothesis is supported by the finding of calcareous clay clasts in the basal 6 cm of the Paleocene from Bass River core. The clay clasts may have originated from erosion during a mega-earthquake triggered by the impact on the Cretaceous seabed (Olsson *et al.*, 1997). However, such a deposit could also be the result of normal deposition during a transgression or megastorm (Table 4).

One would expect to find graded bedding, exotic fragments, abrupt or an erosional contact with the underlying deposit to interpret a tsunami origin (Bourgeois *et al.*, 1988; Kidwell, 1989; Takashimizu and Masuda, 2000; van den Bergh *et al.*, 2003; Tuttle *et al.*, 2004; Fujino *et al.*, 2006; Morton *et al.*, 2007). Sedimentary structures such as hummocky cross stratification is strong evidence of a megastorm or hurricane origin (*e.g.*, Tuttle *et al.*, 2004; Morton *et al.*, 2007). Both tsunami and hurricane deposits also typically show grain size sorting (Bourgeois *et al.*, 1988; Kidwell, 1989; Takashimizu and Masuda, 2000; van den Bergh *et al.*, 2003; Tuttle *et al.*, 2004; Fujino *et al.*, 2006; Morton *et al.*, 2007). None of these sedimentary structures are found in the cores and sections that I examined.

The limited distribution of the fossiliferous MFL is additional evidence to support non-catastrophic sedimentation. At Search Farm this layer shows only mold of a *Cucullaea vulgaris*. The equivalent section of MFL at Meirs Farm and Low Meadow sites only show massive muddy, green glauconite sand (mgs-3). The restricted distribution contrasts with typically laterally extensive distribution of tsunamites and tempestites (*e.g.*, Tuttle *et al.*, 2004; Morton *et al.*, 2007).

A more reasonable explanation of the origin of MFL is that it is the result of normal marine deposition during a transgression (Landman *et al.*, 2004). The rise of sea level in the early Danian (Kominz *et al.*, 2005) cannibalized older deposits above fair-weather wave base (Swift, 1968). Sedimentation subsequently buried the bivalves and created a lag of siderite nodules (Landman *et al.*, 2007). Scattered siderite nodules found in the Burrowed Unit contained macrofossils which are present in the *Pinna* layer, thus supporting this hypothesis (Landman *et al.*, 2007). The presence of the reworked Upper Cretaceous fossil lag deposit at the MFL also favors the marine transgressive deposition hypothesis. Transgressive deposits are common in K/Pg boundary sections (*e.g.*, Savrda, 1993; Hargrove and Engelhardt, 1997; Johnson, 2002). This rationalization, however, does not negate the tsunami hypothesis following the impact nor does it imply that other K/Pg boundary deposits on New Jersey coastal plain or elsewhere are not result of such event. It is possible that the Florida platform blocked the tsunami wave to the northern part of US (Olsson *et al.*, 2002). It also possible that the mega-earthquake caused by the impact at Yucatan Peninsula (Norris *et al.*, 2000) did not generate slope failure and a tsunami on the New Jersey margin.

Glaucinitic mud (gm) (?New Egypt Fm.)

Glaucinitic mud (gm) is the only mud facies in the lowermost Paleogene sediment. It is only present at the most up dip section of Buck/Campo Pit (Figure 25). The presence of detrital kaolinite, chlorite, and vermiculite indicates contribution of sediment from land. The presence of glauconite combined with the abundance of mud indicates it was deposited in a low energy environment. However, quartz granules and scattered clay clasts suggest the environment of deposition was sometimes affected by a high-energy events, possibly during storms (*e.g.*, Saito, 1989). Another explanation could be subaqueous erosion from wave ravinement during transgression (early Danian). Based on the lithofacies characteristics glauconitic mud likely to have been deposited in the inner-shelf.

IV.2. K/Pg boundary placement

A complete K/Pg boundary section is found at Bass River, New Jersey (Olsson *et al.*, 1997; 2002) (Figure 37). This K/Pg deposit is only interrupted by ~6-cm thick spherule layer sandwiched between the Paleocene deposit above and the Maastrichtian deposit below (Olsson *et al.*, 1997; Olsson *et al.*, 2002). Olsson *et al.* (2002) placed the K/Pg boundary at the base of the spherule layer which has high concentration of Ir (~2 ppb). The Ir enrichment at the base of the spherule layer is believed to be the result of the post-depositional downward geochemical diffusion (Olsson *et al.*, 2002; Miller *et al.*, 2010). Thus, it indicates that the Ir at Bass River was deposited at the K/Pg boundary as it is at Global Stratotype Section and Point (GSSP), El Kef, Tunisia (Cowie *et al.*, 1979; Molina *et al.*, 2006). The Ir deposition at Bass River occurred within a few hours of the

impact at Chicxulub, which in a geologic sense is considered instantaneous (Olsson *et al.*, 1997).

Unlike the clear and straightforward K/Pg boundary at Bass River, the K/Pg boundary at K/Pg outcrop, *i.e.*, Manasquan River Basin, in the up dip section of New Jersey coastal plain is in ongoing debate (Landman *et al.*, 2007; Miller *et al.*, 2010). Landman *et al.* (2007) proposed that the K/Pg boundary is below the *Pinna* layer based on the position of elevated Ir values although this layer contains uppermost Maastrichtian species (Figure 2). On the other hand, Miller *et al.* (2010) studied four K/Pg cores and found that the Ir corresponds with the K/Pg boundary, except at the Tighe Park corehole. At Tighe Park, the elevated Ir was concentrated below the *Pinna* layer (Figure 19). Thus, they suggested that the K/Pg boundary is above the *Pinna* layer and hypothesized that the Ir is displaced downward due to differences in reduction-oxidation potential.

In other K/Pg cores, *i.e.*, Buck Pit and Search Farm, the K/Pg boundary is unambiguous. It coincides with the Ir anomaly linking it with the mass extinction at this period (Miller *et al.*, 2010). The elevated Ir value corresponds with the lowermost occurrence Danian index fossil *Senoniasphaera inornata* at Buck Pit (Figure 16) (Miller *et al.*, 2010). At Search Farm (Figure 23), the Iridium anomaly coincides with: (1) the contact between the Upper Cretaceous bioturbated, brown, muddy glauconite sand (mgs-b1) and the overlying lowermost Paleogene green, muddy glauconite sand (mgs-3); and (2) the decrease of echinoid epifaunal fecal pellets (Miller *et al.*, 2010). A mold of *Cucullaea vulgaris* is found at the contact which is equivalent with the Main Fossiliferous Layer (Landman *et al.*, 2004).

At Meirs Farm (Figure 21), the higher Ir value is considered immobilized and corresponds with: (1) clay clast below the bioturbated, brown, muddy glauconite sand (mgs-b1); and (2) the decrease of epifaunal fecal pellet (Miller *et al.*, 2010). However, it is also possible that the Ir at Meirs Farm is displaced. It was originally at the uppermost part of the Upper Cretaceous bioturbated, brown, muddy glauconite sand (mgs-b1) similar with the K/Pg deposit at Search Farm site. The downward displacement may be due to differences of redox potential (Miller *et al.*, 2010), bioturbation, or through pore water in more porous and permeable heavily bioturbated sand; the clay clast below the bioturbated sand acted as an aquitard.

The equivocal K/Pg placement at Meirs Farm is due to different interpretations of the stratigraphic formation with limited biostratigraphic data. Miller *et al.* (2010) considered the mgs-b1 is basal part of lowermost Paleogene Hornerstown Formation. This differs from this thesis which interprets the mgs-b1 to belong to the Upper Cretaceous New Egypt/Navesink Formation, consistent with the lithostratigraphic interpretation of the Search Farm core.

IV.3. Dynamics of sedimentation

Patterns of sedimentation are a function of the interplay between sediment flux, rate of change of accommodation space, and basin physiography (Posamentier and Allen, 1993). Accommodation space is controlled by tectonics (subsidence and uplift) and sea level (*e.g.*, Posamentier and Allen, 1993; Catuneanu, 2006). During K/Pg the New Jersey coastal plain was tectonically stable (Olsson, 1963; Kominz *et al.*, 1998; Kominz *et al.*, 2008). The geometry of the New Jersey margin across the K/Pg was a ramp-type basin

margin (Steckler *et al.*, 1999; Browning *et al.*, 2008). Thus, the sediment patterns were influenced mainly by sea level fluctuations (Kominz *et al.*, 1998; Kominz *et al.*, 2008) and sediment influx from the land.

Sea level was relatively high during the Maastrichtian, ~70 m above modern sea level (Figure 38; Miller *et al.*, 2005; Kominz *et al.*, 2008). Terrigenous material in nearshore settings (Figure 39) created a quartz-rich facies: muddy quartz sand (mqs) and quartzose sandy mud (qsm). A nearshore setting is also supported by the presence of detrital chlorite, kaolinite, or vermiculite. In deeper water there was little or no deposition of sediment from land. This condition is favorable for generating glauconite-rich facies, such as brown, muddy glauconite sand (mgs-1).

During the K/Pg transition, sea level fell gradually, but apparently did not create a sequence boundary (Miller *et al.*, 2005). However, Landman *et al.* (2004) identified a sharp contact between the Uppermost Cretaceous sediment from the New Egypt Formation and the lowermost Paleogene Hornerstown sediment at Parkers Creek, northeastern New Jersey. They considered that the sharp contact represents an erosional unconformity and estimated about 100 kyr time gap between the formations. This contact is highly burrowed and contains abundant fossils, which they referred to as the MFL (Landman *et al.*, 2004). They argued that the MFL was result of reworking from the underlying sediment that corresponded with the transgressive event in early Paleocene.

Two sharp contacts of K/Pg boundary deposits were noted in this study. They are sharp contacts between (1) indurated, muddy glauconite-quartz sand (mgs-2) and the overlying bioturbated, green, muddy glauconite sand (mgs-b3) at Tighe Park and (2) quartzose muddy sand (qsm) with the overlying glauconitic mud (gm) at Buck Pit.

Scattered siderite nodules found in the mgs-b1 may reflect reworking of nodules from the underlying mgs-2, which is supported by finding of same fossils within the nodule in both sediments (Landman *et al.*, 2007). These data may indicate that a minor hiatus (diastem) was formed after the Upper Cretaceous sediments were deposited. In addition, if we assume the ramp gradient is 1:1000, the environment of deposition of facies at Tighe Park would be approximately 10 m shallower than the facies at Buck Pit; thus, facies at Buck Pit would have been more affected by a drop sea level. Nonetheless, this diastem most probably only formed in the updip sections. Alternatively, the reworking was due to ravinement during the transgression in the earliest Danian. The presence of scattered clay clasts in glauconitic mud facies support this hypothesis.

Sea level slightly rose during the Danian (Miller *et al.*, 2005; Kominz *et al.*, 2008). As sea level rises, the shoreline migrated landwards (transgression) and accompanied by a tendency to have more sediment trapped in the alluvial and coastal plain environments (Cattaneo and Stell, 2003). This process results in a reduced sediment influx to the basin causing the generation of glauconite rich-facies (mgs-3 and mgs-b3). In the early transgression, strong erosive, cannibalizing activity (through ravinement) of previously deposited sediments (Cattaneo and Stell, 2003) created the Main Fossiliferous Layer, a transgressive lag deposit rich in shells and glauconitic mud (gm) with scattered clay clasts.

The sediment influx in the Danian possibly was lower compared to the Maastrichtian, creating condensed sections and generating glauconite throughout the basin, more widespread than in the Maastrichtian. The color of glauconite in the Upper Cretaceous and the lowermost Paleogene deposits is different. The dark green of

glauconite of lowermost Paleogene deposit may reflect a more reduced environment of deposition (Fanning *et al.*, 1989).

The Ir anomaly recorded in the New Jersey coastal plain K/Pg cores supported the hypothesis of mass extinction across the Cretaceous-Paleogene transition due to the Chicxulub impact (Miller *et al.*, 2010). However, it seems that the sedimentation patterns in the northern part of the coastal plain were not significantly affected by the impact. These sections lack spherules or shocked minerals characteristics of the ejecta layer which have been found at Bass River. There are no impact-related sedimentary structures, such as graded bedding, climbing ripples or unconformable lower contact observed in K/Pg cores to support the tsunami hypothesis. It is possible that the tsunami wave did not reach the northern part of US (Olsson *et al.*, 2002) or the earthquake caused by the impact at Yucatan Peninsula (Norris *et al.*, 2000) did not trigger slope failure on the New Jersey margin. Grain size analysis from Shatsky Rise in the Pacific Ocean (Ocean Drilling Program Site 1212) supports this hypothesis (Bralower, 2010). Alternatively, the depositional environment of the K/Pg sites were shallower than that at down dip Bass River; therefore, they would have been more affected by a drop of sea level at the end of Cretaceous. The subsequent transgression in the early Paleocene may have eroded and reworked the sedimentological evidence of the K/Pg event.

V. Conclusions

K/Pg cores from the New Jersey coastal plain are composed of five Upper Cretaceous lithofacies and three lowermost Paleogene lithofacies. The Upper Cretaceous lithofacies are brown, muddy glauconite sand (mgs-1); bioturbated, brown, muddy glauconite sand (mgs-b1); indurated, muddy glauconite-quartz sand (mgs-2); muddy quartzose sand (mqs); and quartzose sandy mud (qsm). The mgs-1 and mgs-b1 are very glauconite-rich and likely were deposited in deeper water where there was a little sediment input from the land, such as middle shelf region. The mgs-2, mqs, and qsm are quartz-rich and likely were deposited in upper-lower shoreface setting.

The lowermost Paleogene lithofacies are: green, muddy glauconite sand (mgs-3) and green, bioturbated, muddy glauconite sand (mgs-b3), and glauconitic mud (gm). The mgs-3 and mgs-b3 likely have been deposited in the middle shelf. The gm facies seems to have been deposited closer to the shore, possibly on the inner shelf.

The following sequence of events are interpreted for the K/Pg boundary section: (1) deposition in the near-shore setting (mqs; qsm; mgs-2) and slow sedimentation in the middle shelf (mgs-1 and mgs-b1) when sea level was falling, albeit still shelfal depth; (2) deposition of K/Pg lithofacies when sea level was falling possibly creating a diastem but not a sequence boundary; (3) a transgressive event immediately following the K/Pg boundary likely producing transgressive deposits (the MFL and gm); and finally (4) deposition in the middle shelf with perhaps decreased ocean productivity and a more reducing environment (mgs-3 and mgs-b3).

The K/Pg sections in the study area lack impact-related sedimentary structures such as graded bedding, climbing ripples or an unconformable lower contact to support a

tsunami hypothesis following the impact. This suggests that tsunami-related-impact activity at the K/Pg transition may not have reached the study area or the deposits were eliminated by bioturbation. Alternatively, the lack of sedimentological evidence of a post-impact tsunami suggests that the depositional environment of the K/Pg sites were impacted by a drop of sea level at the end of Cretaceous or by transgressive processes in the early Paleocene.

References

- Albani, A. E., Meunier, A., and Fürsich, F., 2005, Unusual occurrence of glauconite in a shallow lagoonal environment (Lower Cretaceous, northern Aquitaine Basin, SW France), *Terra Nova* 17, pp. 537 – 544.
- Alvarez, L. W., Alvarez, W., Asaro, F., and Michel, H. V., 1980, Extraterrestrial cause for the Cretaceous-Tertiary extinction – experimental results and theoretical interpretation, *Science* 208 (4448), pp. 1095–1108.
- Amorosi, A., 1995, Glaucony and sequence stratigraphy: a conceptual framework of distribution in siliciclastic sequences, *Journal of Sedimentary Research* 65, pp. 419–425.
- Amorosi, A., 1997, Detecting compositional, spatial, and temporal attributes of glaucony: a tool for provenance research, *Sedimentary Geology* 109, pp. 135–153.
- Arnot, R. W. C., 1995, The parasequence definition – are transgressive deposits inadequately addressed?, *Journal of Sedimentary Research* 65, pp. 1–6.
- Bambach, R. K., 2006, Phanerozoic biodiversity mass extinction, *The Annual Review Earth and Planetary Sciences* 34, pp. 127–155.
- Belknap, D. F., Kraft, J. C., and Dunn, R. K., 1994, Transgressive valley-fill lithosomes: Delaware and Maine, in Dalrymple, R.W., Boyd, R., and Zaitlin, B. A., eds., Incised-valley systems: Origin and sedimentary sequences, SEPM Special Publication 51, pp. 304–320.
- Bennington, J. B., Hesselbarth, S., Lee, M., and Mazza, J., 2010, Sediment analysis of a stratigraphic sequence across the K-T Boundary, Manasquan River Basin, NJ, *17th Annual Long Island Geologists Conference*, Stony Brook, New York, pp. 1–6.
- Benson, R.N., 2003, Age estimates of the seaward-dipping volcanic wedge, earliest oceanic crust, and earliest drift-stage sediments along the North American Atlantic in Hames, W.E., McHone, J.G., Ruppel, C., and Renne, P., eds., The Central Atlantic Magmatic Province: Insights from fragments of Pangea, Geophysical Monograph 136, American Geophysical Union, pp. 61–75.
- Bohor, B. F., Foord, E. E., Modreski, P. J., and Triplehorn, D. M., 1984, Mineralogic evidence for an impact event at the Cretaceous-Tertiary boundary, *Science* 224, pp. 867–868.
- Bourgeois, J., Hansen, T. A., Wiberg, P. L., and Kauffman, E. G., 1988, A tsunami deposit at the Cretaceous-Tertiary boundary in Texas, *Science* 241 (4865), pp. 567–570.

- Bourgeois, J., 1990, Boundaries: A stratigraphic and sedimentologic perspective, in Sharpton, V. L. and Ward, P. D., eds., *Global catastrophes in Earth history: An interdisciplinary conference on impacts, volcanism, and mass mortality*, Geological Society of America Special Paper 247, pp. 411–416.
- Bralower, T., Eccles, L., Kutz, J., Yancey, T., Schueth, J., Arthur, M., and Bice, D., 2010, Grain size of Cretaceous-Paleogene boundary sediments from Chicxulub to the open ocean: Implications for interpretation of the mass extinction event, *Geology* 38 (3), pp. 199–202.
- Browning, J. V., Miller, K. G., Sugarman, P. J., Kominz, M. A., McLaughlin, P. P., Kulpecz, A. A., and Feigenson, M. D., 2008, 100 Myr record of sequences, sedimentary facies and sea level change from Ocean Drilling Program onshore coreholes, US Mid-Atlantic coastal plain, *Basin Research* 20, pp. 227–248.
- Burst, J. F., 1958a, Glauconite pellets: their mineral nature and applications to stratigraphic interpretations, *Bulletin of the American Association of Petroleum Geologists* 42 (2), pp. 310–327.
- Burst, J. F., 1958b, Mineral heterogeneity in “glauconite” pellets, *The American Mineralogists* 43, pp. 481–497.
- Cattaneo, A. and Steel, R. J., 2003, Transgressive deposits: A review of their variability, *Earth-Science Reviews* 62, pp. 187–228.
- Catuneanu, O., 2006, *Principles of sequence stratigraphy*, Elsevier, New York, pp. 1–375.
- Chafetz, H. S. and Reid, A., 2000, Syndepositional shallow-water precipitation of glauconitic minerals, *Sedimentary Geology* 136, pp. 29–42.
- Chattoraj, S. L., Banerjee, S., and Saraswati, P. K., 2009, Glauconites from Late Palaeocene – Early Eocene Naredi Formation, Western Kutch and their genetic implications, *Journal of the Geological Society of India* 73, pp. 567–574.
- Chiu, T, Fairbanks, R. G., Mortlock, R. A., Bloom, A. L., 2005, Extending the radiocarbon calibration beyond 26,000 years before present using fossil coral, *Quaternary Science Reviews* 24, pp. 179–1808.
- Courtillot, V., Féraud, G., Maluski, H., Vandamme, D., Moreau, M.G., and Besse, J., 1988, Deccan flood basalts and the Cretaceous/Tertiary boundary, *Nature* 333, pp. 843–846.
- Cowie, J. W., Ziegler, W., Remane, J., 1989, Stratigraphic Commission accelerates progress, 1984 to 1989, *Episodes* 2 (2), pp. 79–83.

- Dashtgard, S. E., Gingras, M. K., and MacEachern, J. A., 2009, Tidally modulated shorefaces, *Journal of Sedimentary Research* 79 (11), pp. 793–807.
- Drake, A. A. Jr., Volkert, R. A., Monteverde, D. H., Herman, G. C., Houghton, H.F., Parker, R.A., and Dalton, R. F., 1996, I-2540-A, Bedrock Geology of Northern New Jersey, New Jersey Geological Survey.
- Donovan, A. D., Baum, G. R., Blechschmidt, G. L., Loutit, L. S., Pflum, C. E., and Vail, P. R., 1988, Sequence stratigraphic setting of the Cretaceous-Tertiary boundary in Central Alabama, in Wilgus, C. K., Posamentier, H., Hastings, B. S., Van Wagoner, J., Ross, C. A. and Kendall, C. G. St. C., eds., Sea-level changes: An integrated approach, Society of Economic Paleontologists and Mineralogists Special Publication 42, pp. 299–307.
- Duncan, R. A. and Pyle, D. G., 1988, Rapid eruption of the Deccan flood basalts at the Cretaceous/Tertiary boundary, *Nature* 333, pp. 841–843.
- Fanning, D. S., Rabenhorst, M. C., May, L., and Wagner, D. P., 1989, Oxidation state of iron in glauconite from oxidized and reduced zones of soil-geologic columns, *Clays and Clay Minerals* 37 (1), pp. 59–64.
- Fujino, S., Masuda, F., Tagomori, S., and Matsumoto, D., 2006, Structure and depositional processes of a gravelly tsunami deposit in a shallow marine setting: Lower Cretaceous Miyako Group, Japan, *Sedimentary Geology*, pp. 127–138.
- Gallagher, W. B., 1993, The Cretaceous/Tertiary mass extinction event in the northern Atlantic Coastal Plain, *The Mosasaur* 5, pp.75–155.
- Gallagher, W. B., 2002, Faunal changes across the Cretaceous-Tertiary (K-T) boundary in the Atlantic Coastal Plain of New Jersey: Restructuring the marine community after the K-T mass-extinction event, in Koeberl, C., and MacLeod, K. G., eds., Catastrophic events and mass extinctions: Impacts and beyond, Geological Society of America Special Paper 356, pp. 291–301.
- Harris, L. C. and Whiting, B. M., 2000, Sequence-stratigraphic significance of Miocene to Pliocene glauconite-rich layers, on- and offshore of the US Mid-Atlantic margin, *Sedimentary Geology* 134, pp. 129–147.
- Hargrove, D. C. and Engelhardt, D. W., 1997, Palynology of the Maastrichtian/Danian boundary at Savannah River Site, South Carolina, *Sedimentary Geology* 108, pp. 121–140.
- Hildebrand, A. R., Penfield, G. T., Kring, D. A., Pilkington, M., Camargo, A. Z., Jacobsen, S. B., and Boynton, W. V., 1991, Chicxulub crater: A possible Cretaceous/Tertiary boundary impact crater on the Yucatan peninsula, Mexico,

Geology 19 (9), pp. 867–871.

- Hein, J. R., Allwardt, A. O., and Griggs, G. B., 1974, The occurrence of glauconite in Monterey Bay, California, diversity, origins, and sedimentary environmental significance, *Journal of Sedimentary Petrology* 44 (2), pp. 562–571.
- Hesselbo, S. P. and Huggett, J. M., 2001, Glaucony in ocean-margin sequence stratigraphy (Oligocene–Pliocene, Offshore New Jersey, U.S.A.; ODP Leg 174A), *Journal of Sedimentary Research* 71 (4), pp. 599–607.
- Heward, A.P., 1981, A review of wave-dominated clastic shoreline deposits, *Earth-Science Reviews* 17, pp. 223–276.
- Hill, P. R., Meule, S., and Pee, H. L., 2003, Combined-flow processes and sedimentary structures on the shoreface of the wave-dominated Grande-Riviere-de-la-Baleine Delta, *Journal of Sedimentary Research* 73 (2), pp. 217–226.
- Hwang, In-Gul and Heller, P. L., 2002, Anatomy of a transgressive lag: Panther Tongue Sandstone, Star Point Formation, central Utah, *Sedimentology* 49 (5), pp. 977–999.
- <http://www.webmineral.com/MySQL/xray.php>
- Johnson, K.R., 2002, Megaflora of the Hell Creek and lower Fort Union Formations in the western Dakotas: Vegetational response to climate change, the Cretaceous–Tertiary boundary event, and rapid marine transgression, *in* Hartman, J. H., Johnson, K. R., Nichols, D. J., eds., *The Hell Creek Formation and the Cretaceous–Tertiary Boundary in the Northern Great Plains-An integrated continental record of the end of the Cretaceous*, Geological Society of America Special Paper 361, pp. 329–392.
- Keller, G., Adatte, T., Gardin, S., Bartolini, A., and Bajpai, S., 2008, Main Deccan volcanism phase ends near the K-T boundary: Evidence from the Krishna-Godavari Basin, SE India, *Earth and Planetary Science Letters* 268, pp. 293–311.
- Kelly, J. C. and Webb, J. A., 1999, The genesis of glaucony in the Oligo–Miocene Torquay Group, southeastern Australia: petrographic and geochemical evidence, *Sedimentary Geology* 125, pp. 99–114.
- Kidwell, S. M., 1989, Stratigraphic condensation of marine transgressive records: Origin of major shell deposits in the Miocene of Maryland, *Journal of Geology* 97, pp. 1–24.
- Kulpecz, A. A., 2008, Sequence stratigraphy of the mid-Atlantic Coastal Plain: An evaluation of eustasy, sediment supply variations, and passive-aggressive tectonism, *Ph.D. Thesis*, Rutgers University, US., pp. 1–252.

- Kulpecz, A. A., Miller, K. G., Sugarman, P. J., and Browning, J. V., 2008, Response of Late Cretaceous Migrating deltaic facies systems to sea level, tectonics, and sediment supply changes, New Jersey Coastal Plain, U.S.A., *Journal of Sedimentary Research* 78, pp. 1–252.
- Kominz, M. A., Miller, K. G., and Browning, J. V., 1998, Long-term and short-term global Cenozoic sea-level estimates, *Geology* 26, pp. 311–314.
- Kominz, M. A., Browning, J. V., Miller, K. G., Sugarman, P. J., Mizintseva, S., and Scotese, C. R., 2008, Late Cretaceous to Miocene sea-level estimates from the New Jersey and Delaware coastal plain coreholes: An error analysis, *Basin Research* 20, pp. 211–226.
- Kumar, N. and Sanders, J. E., 1976, Characteristics of shoreface storm deposits: Modern and ancient Examples, *Journal of Sedimentary Research* 46 (1), pp. 145–162.
- Landman, N. H., Johnson, R. O., and Edwards, L. E., 2004, Cephalopods from the Cretaceous/Tertiary boundary interval on the Atlantic Coastal Plain, with a description of the highest ammonite zones in North America. Part II., Northeastern Monmouth County, New Jersey, *Bulletin of the American Museum of Natural History* (287), pp. 1–107.
- Landman, N. H., Johnson, R. O., Garb, M. P., Edwards, L. E., and Kyte, F. T., 2007, Cephalopods from the Cretaceous/Tertiary boundary interval on the Atlantic Coastal Plain, with a description of the highest ammonite zones in North America. Part III, Manasquan River Basin, Monmouth County, New Jersey, *Bulletin of the American Museum of Natural History* (303), pp. 1–122.
- MacLeod, N. and Keller, G., 1991, How complete are Cretaceous/Tertiary boundary sections?, *Geological Society of America Bulletin* 103, pp. 1439–1457.
- Miller, K. G., Sugarman, P. J., Browning, J. V., Kominz, M. A., Hernandez, J. C., Olsson, R. K., Wright, J. D., Feigenson, M. D., and Van Sickel, W., 2003, A chronology of Late Cretaceous sequences and sea-level history: Glacioeustasy during the Greenhouse World, *Geology* 31, pp. 585–588.
- Miller, K. G., Sugarman, P. J., Browning, J. V., Kominz, M. A., Olsson, R. K., Feigenson, M. D., Hernandez, J. C., 2004, Upper Cretaceous sequences and sea-level history, New Jersey coastal plain, *Geological Society of America Bulletin* 116, pp. 368–393.
- Miller, K. G., Kominz, M. A., Browning, J. V., Wright, J. D., Mountain, G. S., Katz, M. E., Sugarman, P. J., Cramer, B. S., Christie-Blick, N., and Pekar, S. F., 2005, The Phanerozoic record of global sea-level change, *Science* 312, pp. 1293–1298.

- Miller, K. G., Sherrell, R. M., Browning, J. V., Field M. P., Gallagher, W. Olsson, R. K., Sugarman, P. J., Tuorto, S., and Wahyudi, H., 2010, Relationship between mass extinction and Iridium across the Cretaceous/Paleogene boundary in New Jersey, *Geology*, *in press*.
- Molina, E., Alegret, L., Arenillas, I., Arz, J. A., Gallala, N., Hardenbol, J., von Salis, K., Steurbaut, E., Vandenberghe, N., and Zaghbib-Turki, D., 2006, The global boundary stratotype section and point for the base of the Danian Stage (Paleocene, Paleogene, “Tertiary”, Cenozoic) at El Kef, Tunisia – Original definition and revision, *Episodes* 29 (4), pp. 263–273.
- Moore, D. M. and Reynolds, R. C., Jr., 1997, *X-Ray Diffraction and the Identification and Analysis of Clay Minerals*, Oxford University Press, Oxford, 2nd., pp. 1–378.
- Morton, R.A., Gelfenbaum, G., and Jaffe, B. E., 2007, Physical criteria for distinguishing sandy tsunami and storm deposits using modern examples, *in* Tappin, D.R., ed., *Sedimentary features of tsunami deposits-their origin, recognition, and discrimination*, *Sedimentary Geology* 200, pp. 184–207.
- North American Geologic-Map Data Model Science Language Technical Team, 2004, Report on progress to develop a North American science-language standard for digital geologic-map databases; Appendix C1 – Sedimentary materials: Science language for their classification, description, and interpretation in digital geologic-map databases; Version 1.0 (12/18/2004), *in* Soller, D.R., ed., *Digital Mapping Techniques '04 –Workshop Proceedings: U.S. Geological Survey Open-File Report 2004-1451*, pp. 1–595. Appendix C1 accessed at http://pubs.usgs.gov/of/2004/1451/sltt/appendixC/appendixC_pdf.zip.
- Odin, G. S. and Fullagar, P.D., 1988, Geological significance of the Glaucony Facies, *in* Odin, G.S., eds., *Green Marine Clay*, Elsevier, Amsterdam, pp. 295–332.
- Odin, G. S. and Letolle, G., 1980, Glauconitization and phosphatization environments: A tentative comparison, *in* Bendor, Y. K., eds., *Marine phosphorites*, *SEPM Special Publication* 29, pp. 227–237.
- Officer, C. B., and Drake, C. L., 1985, Terminal Cretaceous environmental events, *Science* 227, pp. 1161–1167.
- Olsson, R. K., 1963, Latest Cretaceous and earliest Tertiary stratigraphy of New Jersey Coastal Plain, *American Association of Petroleum Geologists Bulletin* 47(4), pp. 643–665.
- Olsson, R. K., 1975, Upper Cretaceous and Lower Tertiary stratigraphy, New Jersey coastal plain, Second Annual Field Trip Guidebook, *Petroleum Exploration Society of New York*, pp. 1–40.

- Olsson, R. K., 1987, Cretaceous stratigraphy of the Atlantic Coastal Plain, Atlantic Highlands of New Jersey, *Geological Society of America Centennial Field Guide-Northeastern Section*, pp. 87–90.
- Olsson, R. K. and Liu, C., 1993, Controversies on the placement of Cretaceous-Paleogene boundary and the K/P mass extinction of planktonic foraminifera, *Palaaios* 8, pp. 127–139.
- Olsson, R. K., Miller, K. G., Browning, J. V., Habib, D., and Sugarman, P. J., 1997, Ejecta layer at the Cretaceous-Tertiary boundary, Bass River, New Jersey (Ocean Drilling Program Leg 174AX), *Geology* 25 (8), pp. 759–762.
- Olsson, R. K., Miller, K. G., Browning, J. V., Wright, J. D., and Cramer, B. J., 2002, Sequence stratigraphy and sea-level change across the Cretaceous-Tertiary boundary on the New Jersey passive margin, in Koeberl, C., and MacLeod, K. G., eds., *Catastrophic events and mass extinctions: Impacts and beyond*, Geological Society of America Special Paper 356, pp. 97–108.
- Ortega-Huertas, M., Martinez-Ruiz, F., Palomo, I., and Chamley, H., 2002, Review of the mineralogy of the Cretaceous-Tertiary boundary clay: Evidence supporting a major extraterrestrial catastrophic event, *Clay Minerals* 37, pp. 395–411.
- Owens, J. P. and Gohn, G. S., 1985, Depositional history of the Cretaceous series in the U.S. Atlantic Coastal Plain: Stratigraphy, paleoenvironments, and tectonic controls of sedimentation, in Poag, C.W., ed., *Geologic evolution of the United States Atlantic Margin*: New York, Van Nostrand Reinhold, pp. 25–86.
- Owens, J. P., Sugarman, P. J., Sohl, N. F., Houghton, H. F., Volkert, R. A., Drake, A. A., Jr., Orndorff, R. C., 1998, Miscellaneous Investigations Series map I-25540-B (Sheet 3 of 4), Bedrock Geologic Map of Central and Southern New Jersey, United States Geological Survey – United States Department of the Interior in collaboration with New Jersey Geological Survey.
- Pasquini, C., Lualdi, A., and Vercesi, P. L., 2004, Depositional dynamics of glaucony-rich deposits in the Lower Cretaceous of the Nice arc, southeast France, *Cretaceous Research* 25, 179–189.
- Porrenga, D. H., 1966, Clay minerals in recent sediments off the Niger Delta., 14th Nat. Conf., *Clays and Clay Minerals*, pp. 221–233.
- Posamentier, H. W. and Allen, G. P., 1993, Variability of the sequence stratigraphic model: effects of local basin factors, *Sedimentary Geology* 86, pp. 91–109.
- Pospichal, J. J., 1994, Calcareous nannofossils at the K-T boundary, El Kef: No evidence for stepwise, gradual, or sequential extinctions, *Geology* 22 (2), pp. 99–102.

- Robertson, B. E., 1972, The paleoecology of the Tinton Formation, New Jersey Coastal Plain, *PhD Thesis*, Rutgers University, US., pp. 1–114.
- Saito, Y., 1989, Modern storm deposits in the inner shelf and their recurrence intervals, Sendai Bay, northeast Japan, *in* Taira, A and Masuda, F., eds., *Sedimentary Facies in the Active Plate Margin*, pp. 331–344.
- Savrda, C. E., 1993, Ichnosedimentologic evidence for a noncatastrophic origin of Cretaceous-Tertiary boundary sands in Alabama, *Geology* 21, pp. 1075–1078.
- Savrda, C. E., Ozalas, K., Demki, T. H., Huchison, R. A., and Scheiwe, T. D., 1993, Log-grounds and the ichnofossil *Teredolites* in transgressive deposits of the Clayton Formation (Lower Paleocene), western Alabama, *Palaio* 8, pp. 311–324.
- Schulte, P., 2003, The Cretaceous-Paleogene transition and Chicxulub impact ejecta in the northwestern Gulf of Mexico: Paleoenvironments, sequence stratigraphic setting and target lithologies, *Ph.D. Thesis*, University of Karlsruhe, Germany, pp. 1–204.
- Schulte, P., Alegret, L., Arenillas, I., Arz, J. J., Barton, P. J., Bown, P. R., Bralower, T. J., Christeson, G. L., Claeys, P., Cockell, C. S., Collins, G. S., Deutsch, A., Goldin, T. J., Goto, K., Grajales-Nishimura, J. M., Grieve, R. A. F., Gulick, S. P. S., Johnson, K. R., Kiessling, W., Koeberl, C., Kring, D. A., MacLeod, K. G., Matsui, T., Melosh, J., Montanari, A., Morgan, J. V., Neal, C. R., Nichols, D. J., Norris, R. D., Pierazzo, E., Ravizza, G., Rebolledo-Vieyra, M., Reimold, W. U., Robin, E., Salge, T., Speijer, R. P., Sweet, A. R., Urrutia-Fucugauchi, J., Vajda, V., Whalen, M. T., and Willumsen, P. S., 2010, The Chicxulub asteroid impact and mass extinction at the Cretaceous-Paleogene boundary, *Science* 327, pp. 1214–1218.
- Singer, A., 1984, The paleoclimatic interpretation of clay minerals in sediments – a review, *Earth-Science Reviews* 21 (4), pp. 251–293.
- Siringan, F. P. and Anderson, J. B., 1994, Modern shoreface and inner-shelf storm deposits off the east Texas coast, Gulf of Mexico, *Journal of Sedimentary Research* 64, pp. 99–110.
- Smit, J., 1999, The global stratigraphy of the Cretaceous–Tertiary boundary impact ejecta, *Annual Reviews in Earth and Planetary Sciences* 27, pp. 75–113.
- Snedden, J. W. and Bergman, K. M., 1999, Isolated shallow marine sand bodies; deposits for all interpretations, *in* Snedden, J. W. and Bergman, K. M., eds., *Isolated shallow marine sand bodies*, SEPM Special Publication 64, pp. 1–11.
- Stanford, S. D., Ashley, G. M., and Brenner, G. J., 2001, Late Cenozoic fluvial stratigraphy of the New Jersey Piedmont: A record of glacioeustasy, planation,

- and incision on a low-relief passive margin, *The Journal of Geology* 109, pp. 265–276.
- Steckler, M. S., Mountain, G. S., Miller, K. G., and Christie-Blick, N., 1999, Reconstruction of Tertiary progradation and clinoform development on the New Jersey passive margin by 2-D backstripping, *Marine Geology* 154, pp. 399–420.
- Stinnesbeck, W. and Keller, G., 1996, K/T boundary coarse-grained siliciclastic deposits in northeastern Mexico and northeastern Brazil: Evidence for mega-tsunami or sea-level changes?, in Ryder, G., Fastovsky, D and Gartner, S., eds., *The Cretaceous-Tertiary Event and other catastrophes in Earth history*, Geological Society of America Special Papers 307, pp. 197–209.
- Sugarman, P. J., Miller, K. G., Bukry, D., and Feigenson, M. D., 1995, Uppermost Campanian-Maestrichtian strontium isotopic, biostratigraphic, and sequence stratigraphic framework of the New Jersey Coastal Plain, *Geological Society of America Bulletin* 107, pp. 19–37.
- Swift, D. J. P., 1968, Coastal erosion and transgressive stratigraphy, *Journal of Geology* 76, pp. 444–456.
- Tamura, T., 2004, Preservation and grain-size trends of Holocene wave-dominated facies successions in eastern Japan: Implications for high-resolution sequence stratigraphic analysis, *Journal of Sedimentary Research* 74 (5), pp. 718–729.
- Tillman, R. W., 1999, The Shannon sandstone: A review of the sand-ridge and other models, in Snedden, J. W. and Bergman, K. M., eds., *Isolated shallow marine sand bodies*, SEPM Special Publication 64, pp. 29–54.
- Triplehorn, D. M., 1966, Morphology, internal structure, and origin of glauconite pellets, *Sedimentology* 6, pp. 247–266.
- Tuttle, M. P., Ruffman, A., Anderson, T., and Jeter, H., 2004, Distinguishing Tsunami from Storm Deposits in Eastern North America: The 1929 Grand Banks Tsunami versus the 1991 Halloween Storm, *Seismological Research Letters* 75 (1), pp. 117–131.
- van den Bergh, G. D., Boer, W., de Haas, H., van Weering, Tj. C. E., and van Wijhe, R., 2003, Shallow marine tsunami deposits in Teluk Banten (NW Java, Indonesia), generated by the 1883 Krakatau eruption, *Marine Geology* 197, pp. 13–34.
- Van Wagoner, J. C., Mitchum Jr., R. M., Campion, K. M., Rahmanian, V. D., 1990, Siliciclastic sequence stratigraphy in well logs, core, and outcrops: concepts for high-resolution correlation of time and facies, *American Association of Petroleum Geologists Methods in Exploration Series* 7, pp. 1–55.

- Vonhof, H. B. and Smit, J., 1997, High-resolution late Maastrichtian–early Danian oceanic $^{87}\text{Sr}/^{86}\text{Sr}$ record: Implications for Cretaceous-Tertiary boundary events, *Geology* 25 (4), pp. 347–350.
- Watts, A. B. and Thorne, J., 1984, Tectonics, global changes in sea level and their relationship to stratigraphical sequences at the US Atlantic continental margin, *Marine and Petroleum Geology* 1, pp. 319–339.
- Yancey, T. E. and Guillemette, R. N., 2008, Carbonate accretionary lapilli in distal deposits of the Chicxulub impact event: *Geological Society of America Bulletin* 120, pp. 1105–1118.

Table 1. Diffraction data for common clay minerals and their association.

Clay Mineral	Moore and Reynolds (1997)	webmineral.com
Chlorite	14.2 Å; 7.10 Å; 4.74 Å; 3.55 Å	-
Glauconite	10.1 Å; 5.00 Å (very weak); 3.38 Å	10.1 Å; 4.53 Å; 3.63 Å; 3.33 Å; 2.59 Å; 2.4 Å; 1.511 Å
Illite	10.1 Å; 5.00 Å; 3.38 Å	4.43 Å; 3.66 Å; 2.56 Å
Kaolinite	7.16 Å; 3.58 Å	7.17 Å; 3.58 Å; 1.49 Å
Vermiculite	14.4 Å; 7.16 Å; 4.80 Å; 3.58 Å	14.4 Å; 7.16 Å; 4.80 Å; 3.58 Å
Other mineral		
Calcite	3.86 Å; 3.04 Å; 2.50 Å	3.04 Å; 2.29 Å; 2.1 Å
Goethite	4.98 Å; 4.18 Å; 3.38 Å; 2.69 Å; 2.58 Å; 2.49 Å; 2.45 Å	4.98 Å; 4.18 Å; 3.38 Å; 2.69 Å; 2.45 Å
Gypsum	7.16 Å; 4.28 Å; 3.07 Å; 2.87 Å; 2.68 Å	7.63 Å; 4.28 Å; 3.07 Å; 2.87 Å; 2.69 Å
Halite	-	2.82 Å; 3.26 Å
Pyrite	3.13 Å; 2.71 Å; 2.43 Å	3.13 Å; 2.71 Å; 2.42 Å
Quartz	4.26 Å	4.26 Å
Siderite	3.59 Å; 2.80 Å; 2.35 Å	3.59 Å; 2.79 Å

Table 2. Authigenic glauconite and its environment of deposition in various locations.

Location	Age	Environment of deposition indicator/comment	Environment of deposition	Reference
Monterey Bay, California	Recent	Surface sediment	Continental slope (~100 - 200 m)	Hein, <i>et al.</i> (1974)
Niger Delta	Recent	Surface sediment	Shallow marine (~200 m)	Porrenga (1966)
ODP Leg 174A (Offshore New Jersey)	Pliocene	Benthic foraminiferal assemblage, seismic-reflection geometries	Shallow marine (<150 m)	Hesselbo and Huggett (2001)
	Oligocene - Miocene		Deep water (~600-1000 m)	
Torquay Basin, Southeastern Australia	Oligocene - Miocene	Ostracod and foraminiferal assemblage, sedimentary structure, textures	Mid-shelf (~120 m)	Kelly and Webb (1999)
Western Kutch, India	Early Eocene - Late Paleocene	Benthic foraminiferal assemblage	Mid-shelf (~10-50 m)	Chattoraj, <i>et al.</i> (2009)
Smithville, Texas	Eocene	Benthic foraminiferal assemblage	Nearshore - mid neritic	Burst (1958a)
Aquitaine Basin, SW France	Late Cretaceous	Invertebrate and vertebrate fossils assemblages	Shallow lagoon	Albani <i>et al.</i> (2005)
Nice Arc, Southeast France	Early Cretaceous	Vertical and lateral lithofacies	Outer platform (~60 - 550 m)	Pasquini <i>et al.</i> (2004)
Southwest USA	Cambro-Ordovician	Sedimentary structures, textures	Very shallow water - tidal flat	Chafetz and Reid (2000)

Table 3. Clay minerals and their interpretation of origin.

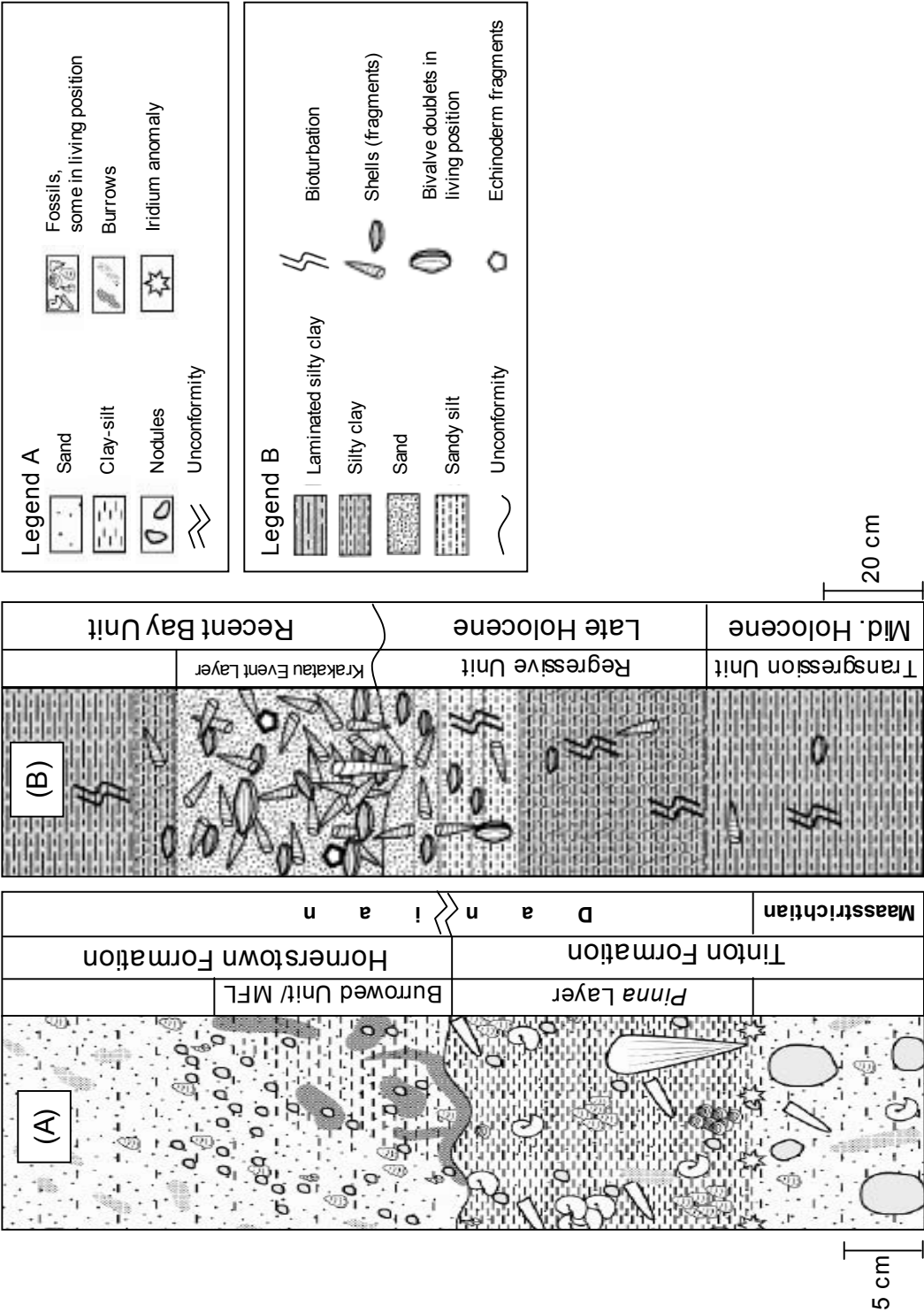
Clay Mineral	Interpretation of origin	References
Chlorite	Corresponding to relatively dry period. It can be diagenetic or detrital in origin.	Singer (1984), Moore and Reynolds (1997)
Glauconite	It forms at about the divide between outer shelves and continental slopes, areas of very slow accumulation of detritus, at temperatures <15°C, pH about 8, and an Eh right at the oxidation-reduction boundary.	Odin and Fullagar (1988), Moore and Reynolds (1997)
Illite	Corresponding to relatively dry period. It is formed at, and stable or metastable at, the earth's surface. Some of it is recycled, formed in pedogenic and weathering processes, and diagenetically formed.	Singer (1984), Moore and Reynolds (1997)
Kaolinite	Intensive chemical weathering in soils of warm to tropical temperatures, humid low-latitude regions, forming as residual weathering product, or sometimes by hydrothermal alteration, of other aluminosilicates, especially feldspar.	Moore and Reynolds (1997)
Vermiculite	Common in the well-drained soils of humid region if the parent materials contain a lot of micas (biotite, muscovite, and chlorite).	Moore and Reynolds (1997)

Table 4. Generic diagnostic sedimentological criteria of offshore tsunamite, tempestite, and transgressive fill deposits.

Deposits	Sedimentary attributes	Sources*
Tsunamite	<ul style="list-style-type: none"> - Up to 70 cm thick, but generally 5 – 25 cm thick; - Single, homogeneous bed that grades from coarser grained at the bottom to finer grained at the top, or a bed with only a few thin layers; - Rip up clasts, abundant reworked shell within, many exotic fragments from beach environments within the deposit; - Abrupt/erosional base lower contact; - Twig orientation or other indicators of return (seaward) flow during deposition of the sediment; - Mudcap usually present; - Bioturbation is absent in the bed, although this is common in the underlying or overlying deposits; - Deposits extend hundreds of meters inland from the beach and have an overall tendency to drape the preexisting landscape. 	<p>3, 9, 13, 15, 16 14, 16</p> <p>3, 9, 13, 15, 16</p> <p>3, 13, 15, 16 16 15, 16 9, 13 14, 16</p>
Tempestite	<ul style="list-style-type: none"> - Generally more than 30 cm thick; - Foresets bedding, climbing ripples, backsets, hummocky cross stratification, planar stratification, and numerous thin (millimeters to a few centimeters) lamina-sets of alternating coarse and fine grain size; - Abundant shell fragments organized in lamina, with no internal mud layers; - Abrupt lower contact; basal lag containing coarse gravel and rip up clasts may present - Mudcap rarely present; - Maximum deposit thickness is near the shore, and landward thinning of the deposit is commonly abrupt, which fill in topographic lows. 	<p>1, 14, 16 14, 16</p> <p>13, 16 1, 16 16 14, 16</p>
Transgressive fill deposits	<ul style="list-style-type: none"> - Relatively thin (usually less than 50 cm), may consist of coarse-grained beds that contain pebbles, shells fragment, shark teeth, intraclasts or other clasts or composed of mud-dominated beds; - Authigenic marine mineral such as glauconite and phosphate is common; - Part of upward deepening facies succession; - Extensive bioturbation may occur within the deposit; - Ravinement surface may or may not present; - The thickest, most complex and complete transgressive sequences are preserved in topographic hollows of the underlying surface, e.g., within (incised) valleys. 	<p>4, 5, 6, 11, 12</p> <p>4, 5, 8, 10, 12 4, 5, 8, 10, 12 4, 5, 6, 11, 12 5, 8, 12 2, 7</p>

* (1) Kumar and Sanders (1976); (2) Heward (1981); (3) Bourgeois *et al.* (1988); (4) Kidwell (1989); (5) Van Wagoner *et al.* (1990); (6) Savrda *et al.* (1993); (7) Belknap *et al.* (1994); (8) Amorosi (1995); (9) Takashimizu and Masuda (2000); (10) Harris and Whiting (2000); (11) Hwang and Heller (2002); (12) Cattaneo and Steel (2003); (13) van den Bergh *et al.* (2003); (14) Tuttle *et al.* (2004); (15) Fujino *et al.* (2006); (16) Morton *et al.* (2007).

Figure 1. Comparison of lithostratigraphic section of (A) the *Pinna* Layer and Main Fossiliferous Layer (MFL) from NJCP area (modified after Landman *et al.*, 2007 and Gallagher, 2002) and (B) Krakatau Event Layer (KEL) from TB area (modified after van den Bergh *et al.*, 2003). Van den Bergh *et al.* (2003) interpreted the KEL as a tsunami deposit triggered by the devastating Krakatau eruption in 1883. Figure is on the following page.



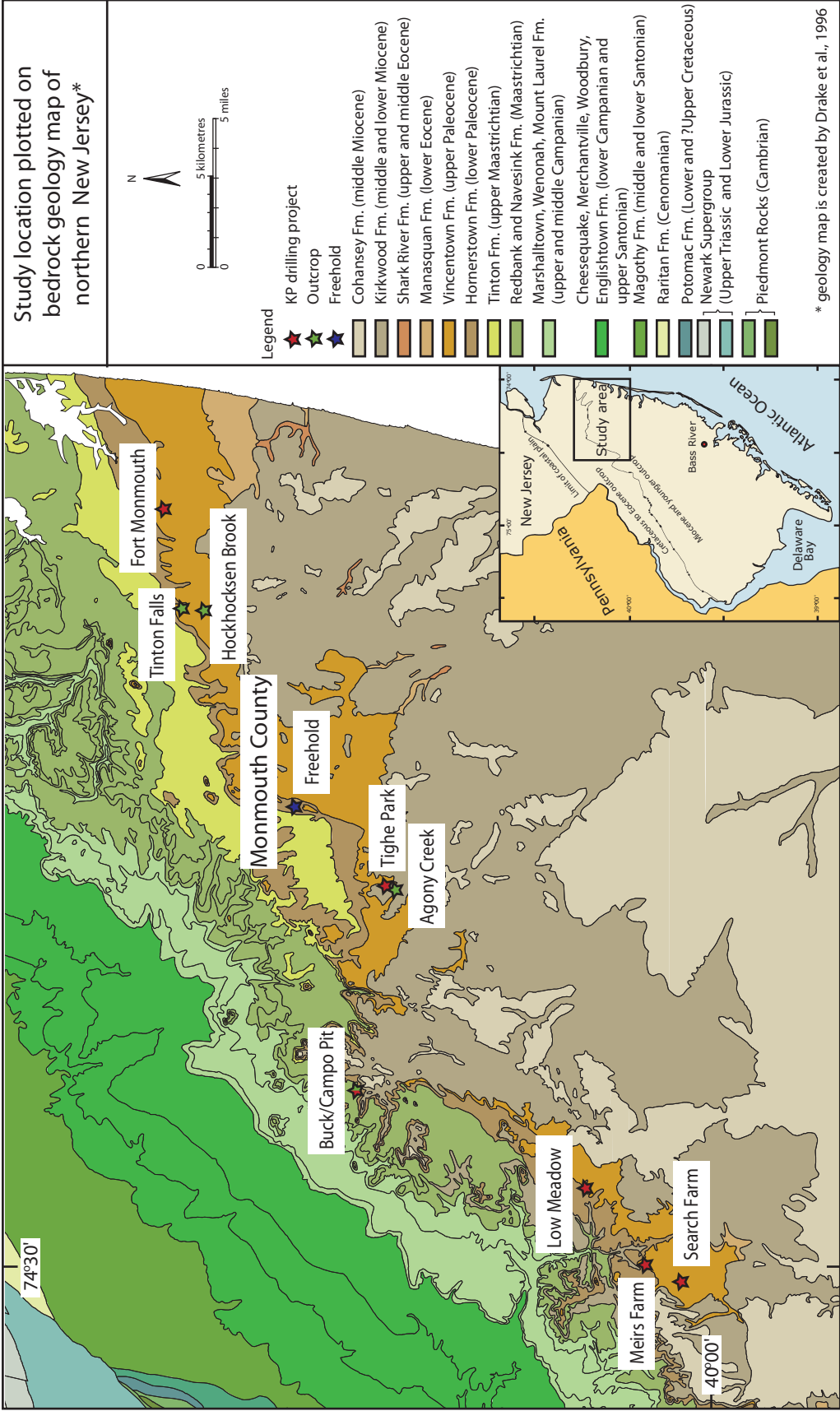


Figure 3. Study locations plotted on bedrock geology map of northern New Jersey (modified after Drake *et al.*, 1996).

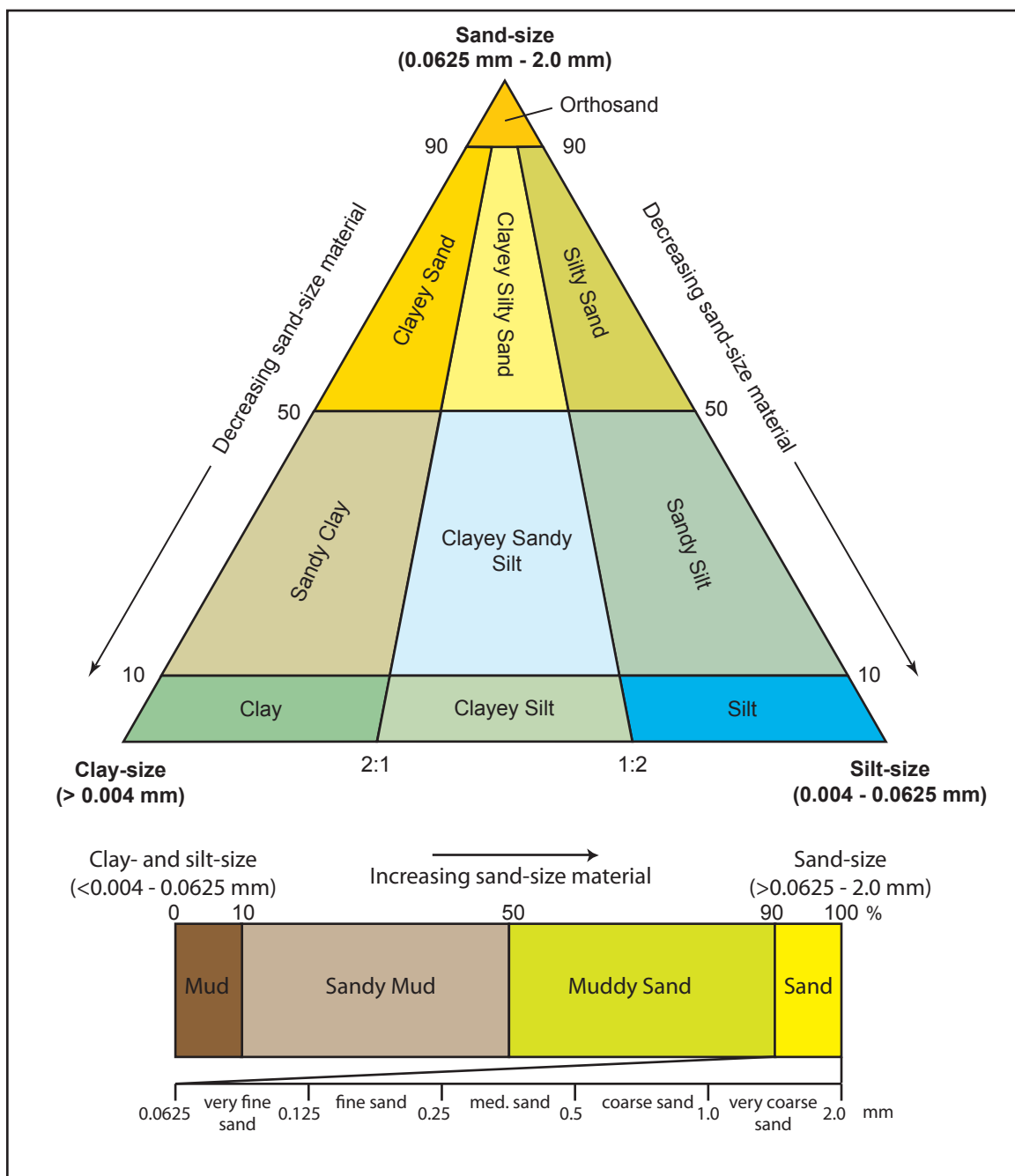


Figure 4. Fine-grained sediment classification based on percentage of grain sizes. Upper diagram is modified fine-grained sediment classification based on sand, silt, and clay percentage of Folk (1954) (taken from North American Geologic-Map Data Model Science Language Technical Team, 2004). Lower diagram is modified sediment classification based on sand/mud ratio used in this research.



Photo	Lithofacies	Description	Outcrop/Corehole	Code
	Brown, muddy glauconite sand	Very dark grayish brown (2.5Y 3/2)-black (5YR 2.5/1); dominantly sand-sized grains; non-faint lamination; composition: 54-86% glauconite, 11-43% mud, ~12% siderite, ~1-4% mica, ~1-3% fine quartz, ~1-3% coarse-medium quartz, <1% other; <i>Cucullaea vulgaris</i> and <i>Pecten</i> mold; thickness: 0.4-9.2 m (1.3-30.3 ft).	Corehole: Fort Monmouth 3, Low Meadow 1, Meirs Farm 1, Search Farm 1.	mgs-1
	Brown, bioturbated, muddy glauconite sand	Very dark grayish brown (2.5Y 3/2)-black (5YR 2.5/1); dominantly sand-sized grains; heavily bioturbated filled by greenish black muddy glauconite sand and/or brown clay; clay lamina; composition: 40-75% glauconite, 8-47% mud, 0-30% siderite, ~3-10% fine quartz, ~2-7% mica, <0.5% coarse-medium quartz, <0.5% other; thickness: 1.0-1.6 m (3.3-5.1 ft).	Corehole: Fort Monmouth 3, Low Meadow 1, Meirs Farm 1, Search Farm 1.	mgs-b1

Figure 5. The Upper Cretaceous sand-rich sediment from northern New Jersey Coastal Plain, showing photos, description, location, and code for each lithofacies in this study.



Photo	Lithofacies	Description	Outcrop/Corehole	Code
	Indurated, muddy glauconite-quartz sand	Dark grayish brown (10YR 4/1); indurated; non-faint lamination; dominantly sand-sized grains; granulariferous; composition 6-86% glauconite, 12-45% mud, 0.7-14% fine quartz, 0.3-65% medium-coarse quartz, <1% mica, <0.5% other materials; <i>Cucullaea vulgaris</i> and <i>Pecten</i> mold; thickness: 1.0 - 2.7 m (3.2-8.75 ft).	Corehole: Freehold, Tighe Park 1; Outcrop: Agony Creek, Hockhockson Br.	mgs-G
	Muddy quartz sand	Dark yellowish brown (10YR 4/4)-grayish brown (10YR 5/2); mottled; dominantly sand-sized grains: poorly sorted; angular-subrounded; composition: 55-90% medium-coarse quartz, 2-36% mud, 3-15% fine quartz, 1-6% glauconite, ~1% mica, <1% other minerals; thickness: 1.4-10 m (4.5-30.0 ft).	Corehole: Buck Pit 1, Freehold; Outcrop: Campo Pit, Hockhockson Br.	mqs

Figure 5 (cont'd). The Upper Cretaceous sand-rich sediment from northern New Jersey coastal plain, showing photos, description, location, and code for each lithofacies in this study.

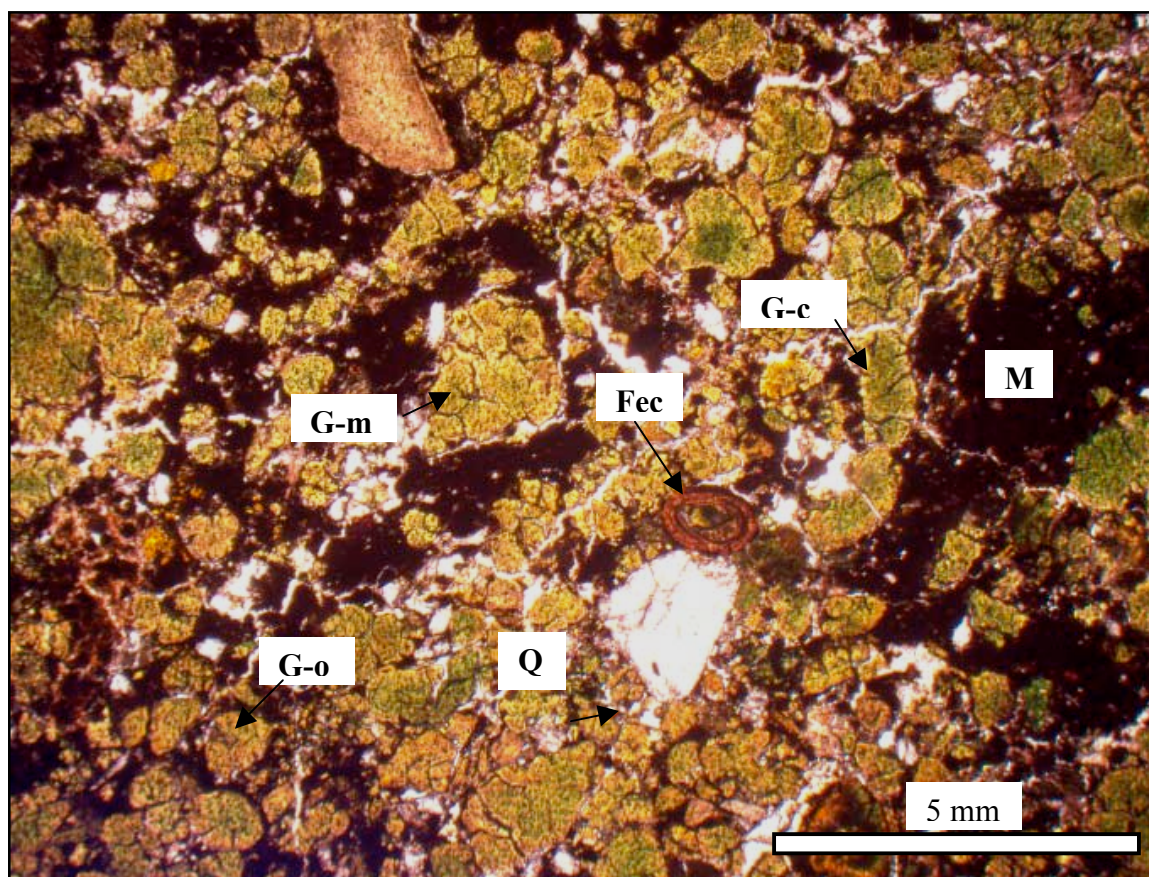


Figure 6. Microphotograph of brown, bioturbated, muddy glauconite sand (mgs-b1) from Meirs Farm 1 core. G-m = mammilated-lobate glauconite, G-o = ovoidal-spheroidal glauconite, G-c = capsule shaped glauconite, M=matrix, Q = quartz, Fec = fecal pellets. Note that glauconite grains show two-color variation, where core of the grains are dark green or cloudy brownish green and lighter green or yellowish green on their edge. Note also that glauconite replaces fecal pellet.



Figure 7. Bioturbated clay on granulariferous, indurated, muddy glauconite-quartz sand (mgs-2) from USGS-NJGS Freehold core.

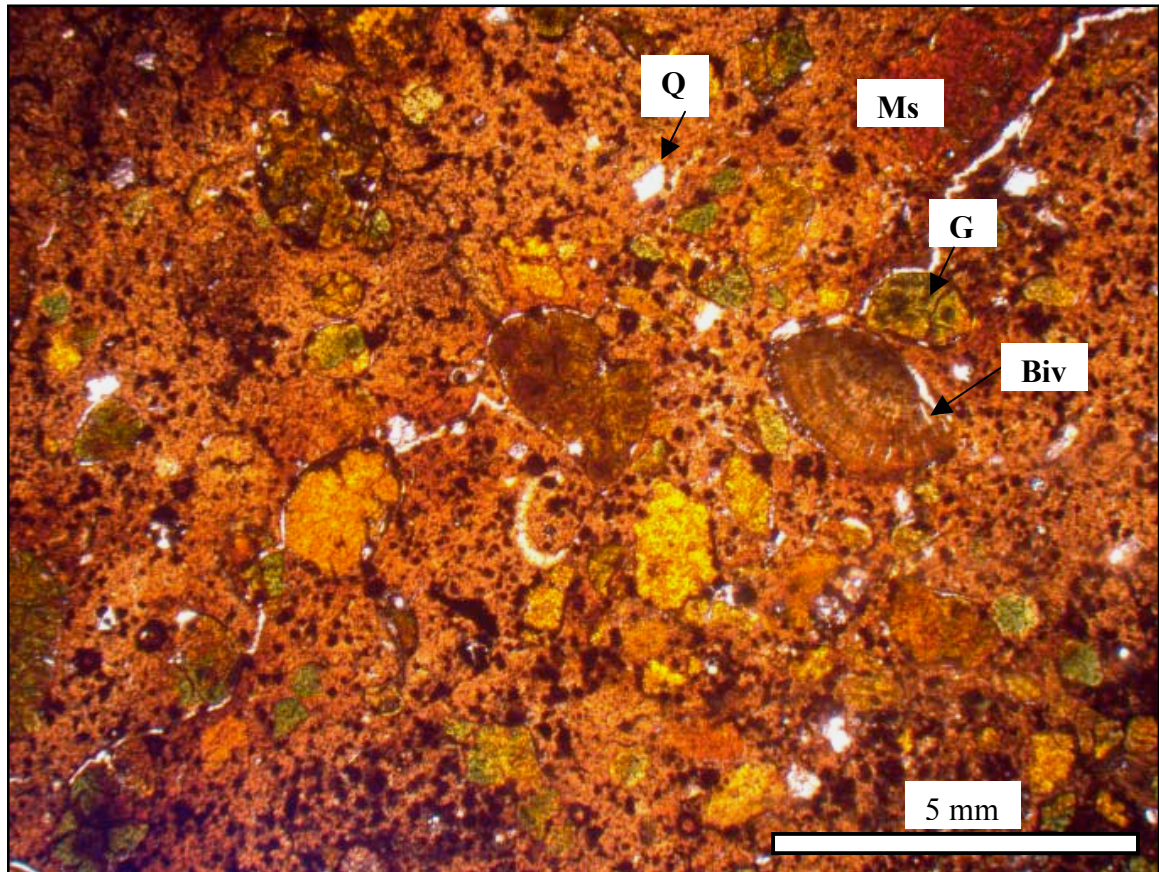


Figure 8. Microphotograph of indurated muddy glauconite-quartz sand (mgs-2) from Tighe Park 1 core. G = glauconite, Ms=sideritized matrix, Q = quartz, Biv = Bivalvia. The morphology of glauconite is difficult to observe due to heavily weathering.

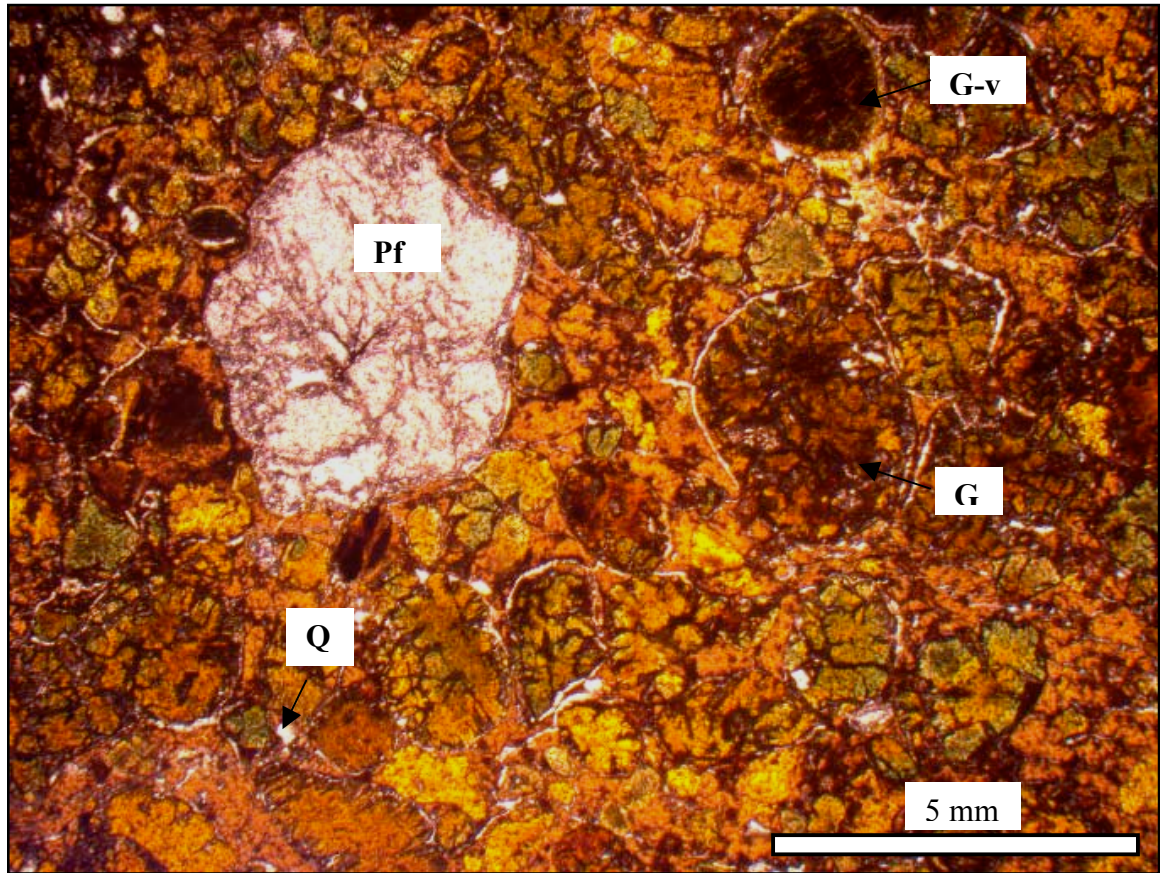


Figure 9. Microphotograph of indurated muddy glauconite-quartz sand (mgs-2) from Agony Creek outcrop. G = glauconite, G-v = glauconite-vermicular, Q = quartz, Pf = planktonic foraminifera.

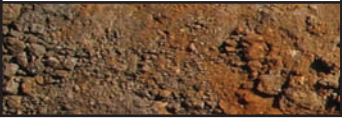
Photo	Lithofacies	Description	Outcrop/corehole	Code
	Quartzose sandy mud	Dark gray (5Y 4/1) to dark yellowish brown (10 YR 4/4); dominantly silt; sandy, angular- subrounded; composition: 66% mud, ~30% medium-coarse quartz, <3% fine quartz, <0.5% mica, ~0.2% glauconite, iron stain; thickness: 0.15m (0.5 ft).	Outcrop: Campo Pit Corehole: Buck Pit 1	qsm

Figure 10. The Upper Cretaceous mud-rich sediment from northern New Jersey coastal plain, showing photos, description, location, and code for each lithofacies in this study.



Photo	Lithofacies	Description	Outcrop/Corehole	
	Green, muddy glauconite sand	Very dark grayish green (GLY 1 3/5G); dominantly sand-sized grains; composition: 40-85% glauconite, 10-60% mud, <1-5% fine quartz, <1-2% coarse-medium quartz, <1-2% mica, <1% other materials; thickness: 1.0-10.6 m (3.3-35.0 ft).	All outcrops and coreholes	mgs-3
	Green, bioturbated, muddy glauconite sand	Very dark grayish olive (10Y-5GY 5GY/4) -olive (5Y 4/3); dominantly sand-size grains; heavily bioturbated; composition: 75-85% glauconite, 10-25% mud, <1% fine quartz, <1% medium-coarse quartz, <0.5% mica, <0.5% other materials; thickness: ~0.52-0.75 m (1.7-2.46 ft).	Outcrop: Agony Creek Corehole: Tighe Park 1	mgs-b3

Figure 11. The lowermost Paleogene sand-rich sediment from northern New Jersey coastal plain, showing photos, description, location, and code for each lithofacies in this study.

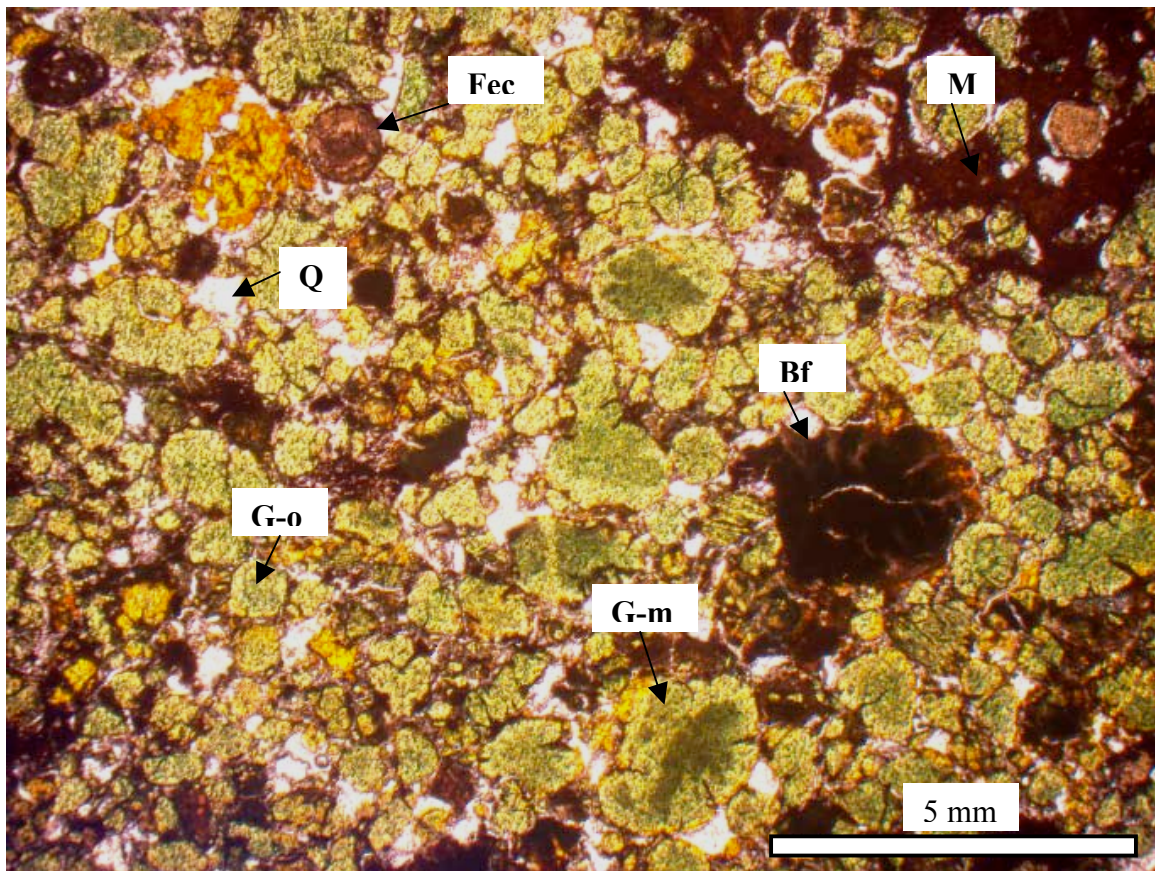


Figure 12. Microphotograph of green, muddy glauconite sand (mgs-3) from Meirs Farm 1 core. G-m = mammilated-lobate glauconite, G-o = ovoidal-spheroidal glauconite, G-c = capsule shaped glauconite, M = matrix, Q = quartz, Fec = fecal pellets, Bf = benthic foraminifera. Glauconite morphology classification is based on Triplehorn (1966).

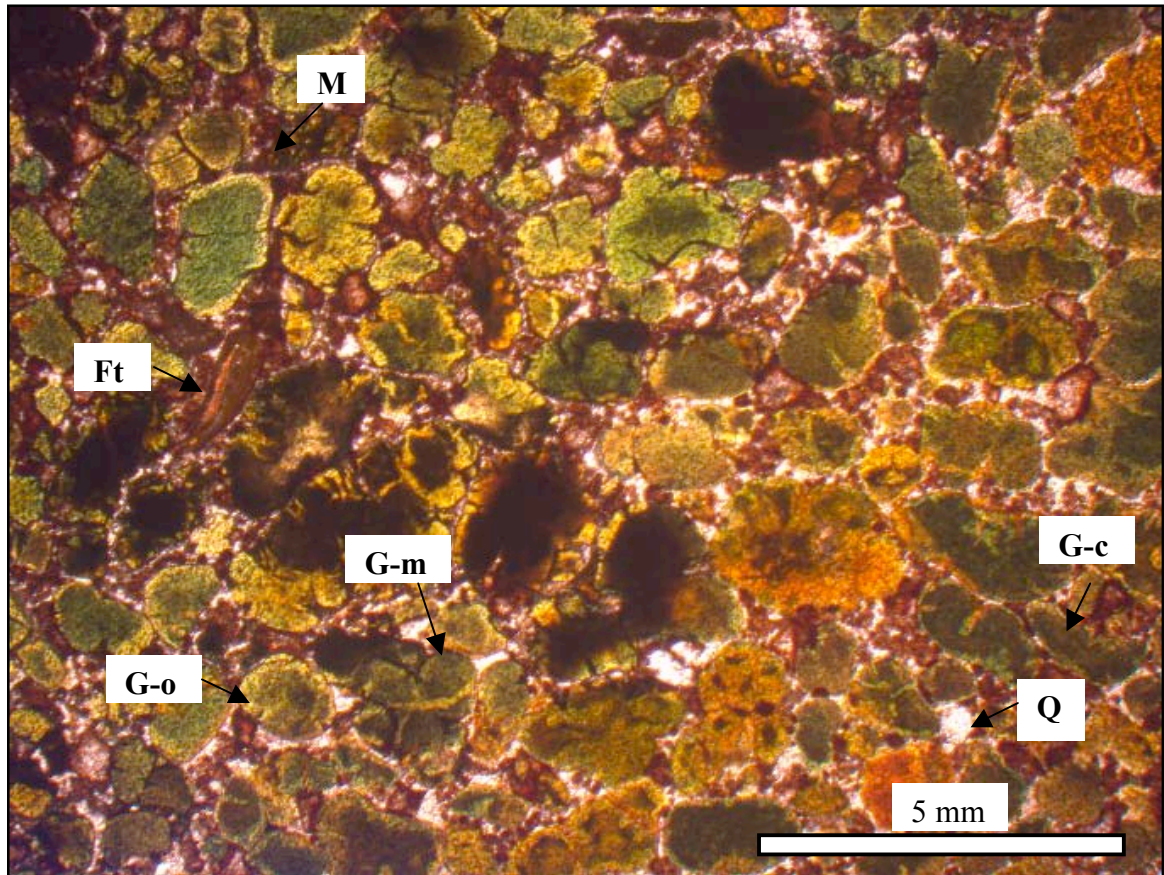


Figure 13. Microphotograph of green, bioturbated, muddy glauconite sand (mgs-b3) from Agony Creek outcrop. G-m = mammilated-lobate glauconite, G-o = ovoidal-spheroidal glauconite, G-c = capsule shaped glauconite, M = matrix, Q = quartz, Ft = fish teeth. Glauconite morphology classification is based on Triplehorn (1966).


Photo	Lithofacies	Description	Outcrop/corehole	Code
	Glauconitic mud	Olive (5Y 4/3) to dark gray (5Y 4/1); dominantly clay; composition: 93-97% mud, <0.5-4% glauconite, <2% medium-coarse quartz, <0.5% fine quartz, <0.2% mica, light brown clay clasts at bottom part of interval; thickness: ~0.3 m (1.0 ft).	Outcrop: Campo Pit Corehole: Buck Pit 1	gm

Figure 14. The lowermost Paleogene mud-rich sediment from northern New Jersey coastal plain, showing photos, description, location, and code for each lithofacies in this study.

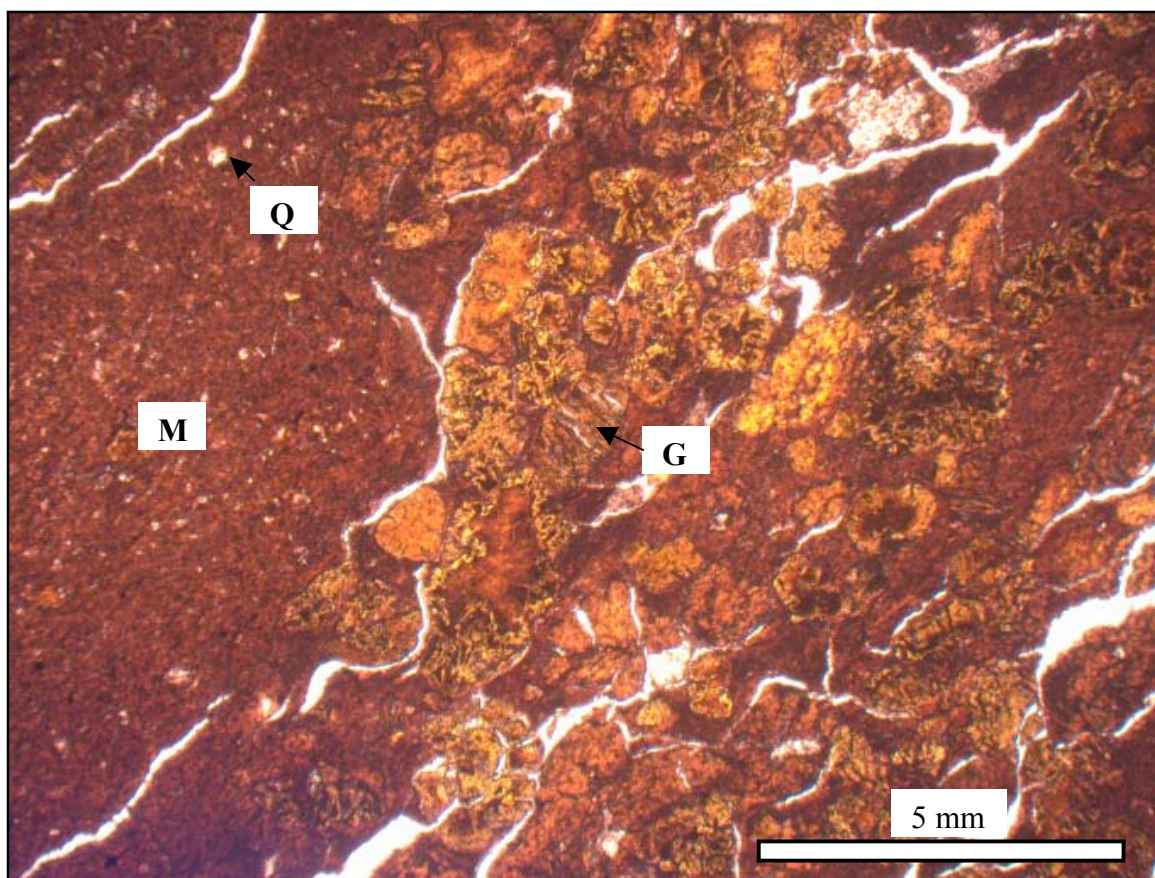
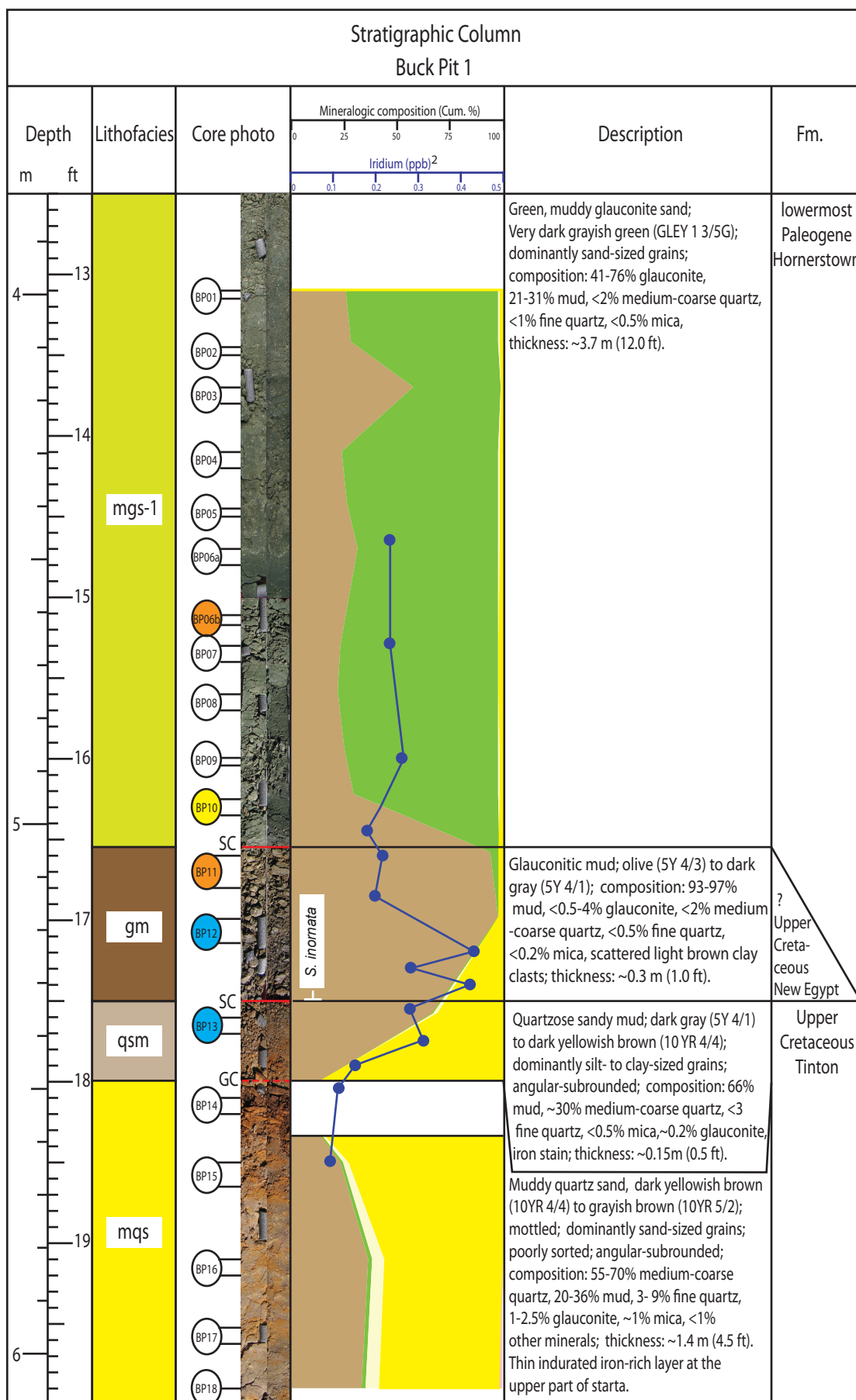


Figure 15. Microphotograph glauconitic mud (gm) facies from Buck Pit 1 corehole. G = glauconite, M = matrix, Q = quartz. Glauconite is mottled and show worm-like feature.

Figure 16. Stratigraphic column of Buck Pit 1 core. The muddy quartz sand grades upward into quartzose sandy mud. The contact between quartzose sandy mud and overlying glauconitic mud is sharp. The contact between the glauconitic mud and green, muddy glauconite sand is also sharp. The biostratigraphy age and Ir data are from Miller *et al.* (2010) study. *S. inornata* = *Senoniasphaera inornata*. BP01 = sample number 1 from Buck Pit 1 core. See legend for detail codes and color codes. Figure is on the following page.




















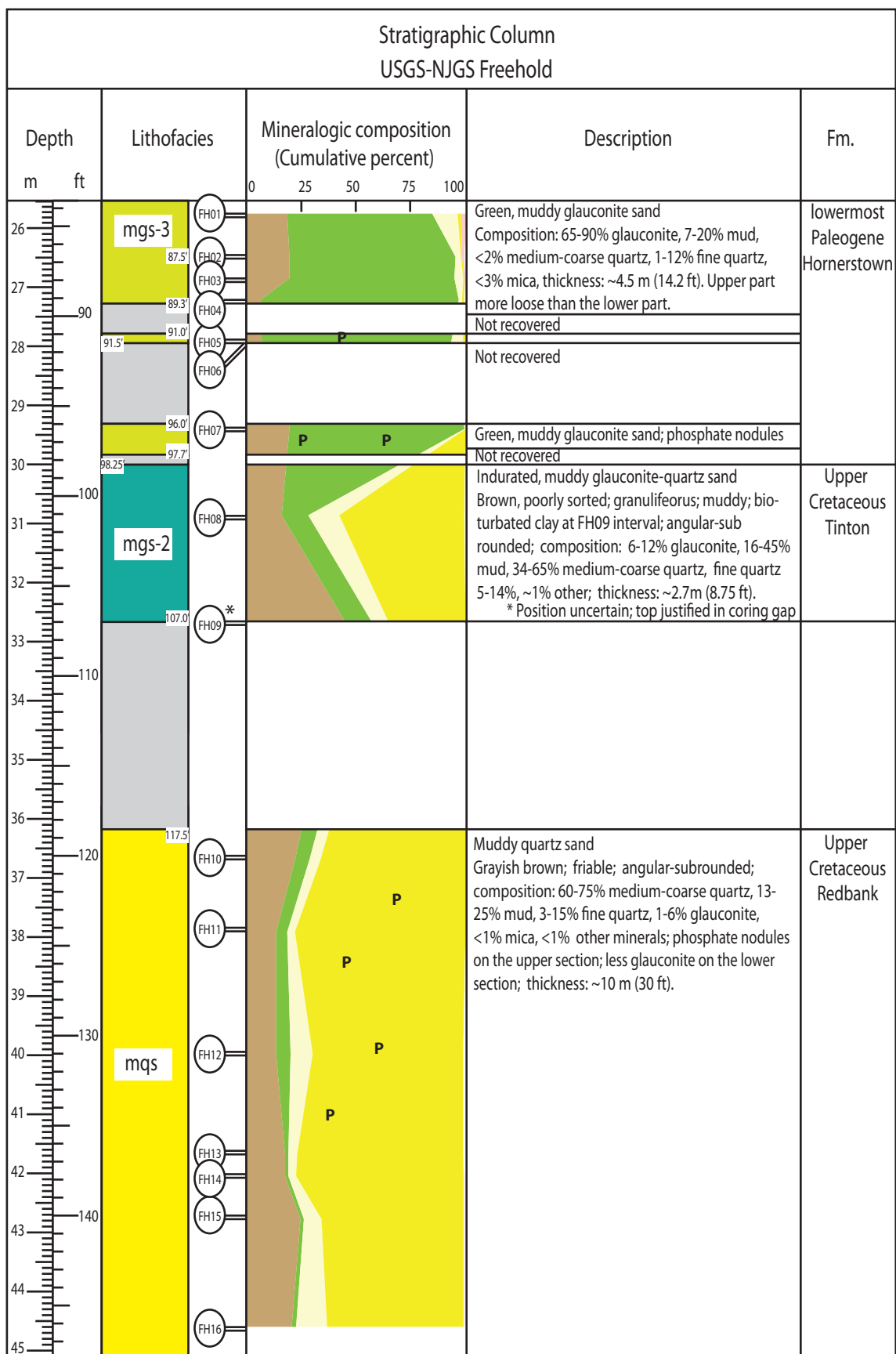
Legend:		
Lithofacies	Mineralogic composition (Cumulative percent)	P
 mgs-3	Green, muddy glauconite sand	 Phosphate nodule
 mgs-b3	Green, bioturbated, muddy glauconite sand	 Lithologic sample
 gm	Glauconitic mud	 Lithologic and petrographic samples
 qsm	Quartzose sandy mud	 Lithologic and microprobe samples
 mq	Muddy quartz sand	 Lithologic and XRD samples
 mgs-2	Indurated, muddy glauconite-quartz sand	 Lithologic, microprobe and XRD samples
 mgs-1	Brown, muddy glauconite sand	 Lithologic, petrographic and microprobe samples
 mgs-b1	Brown, bioturbated, muddy glauconite sand	 Sharp contact
		 Gradational contact

Figure 17. Stratigraphic column of USGS-NJGS Freehold core. This core is composed of muddy quartz sand; indurated, muddy glauconite-quartz sand; and green, muddy glauconite sand. The contact between these lithofacies are not present. FH01 = sample number 1 from Freehold core. See legend for detail codes and color codes. Figure is on the following page.



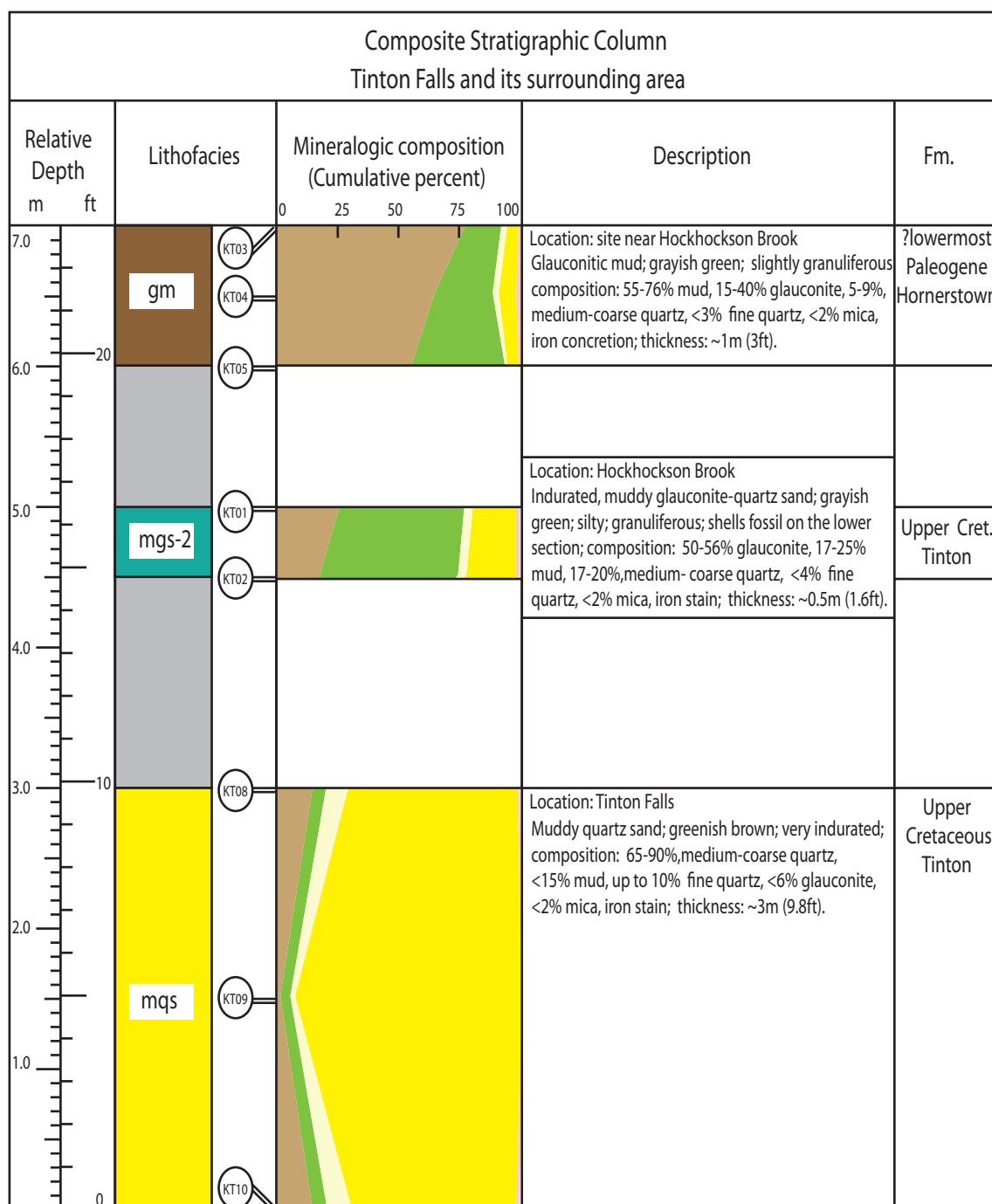
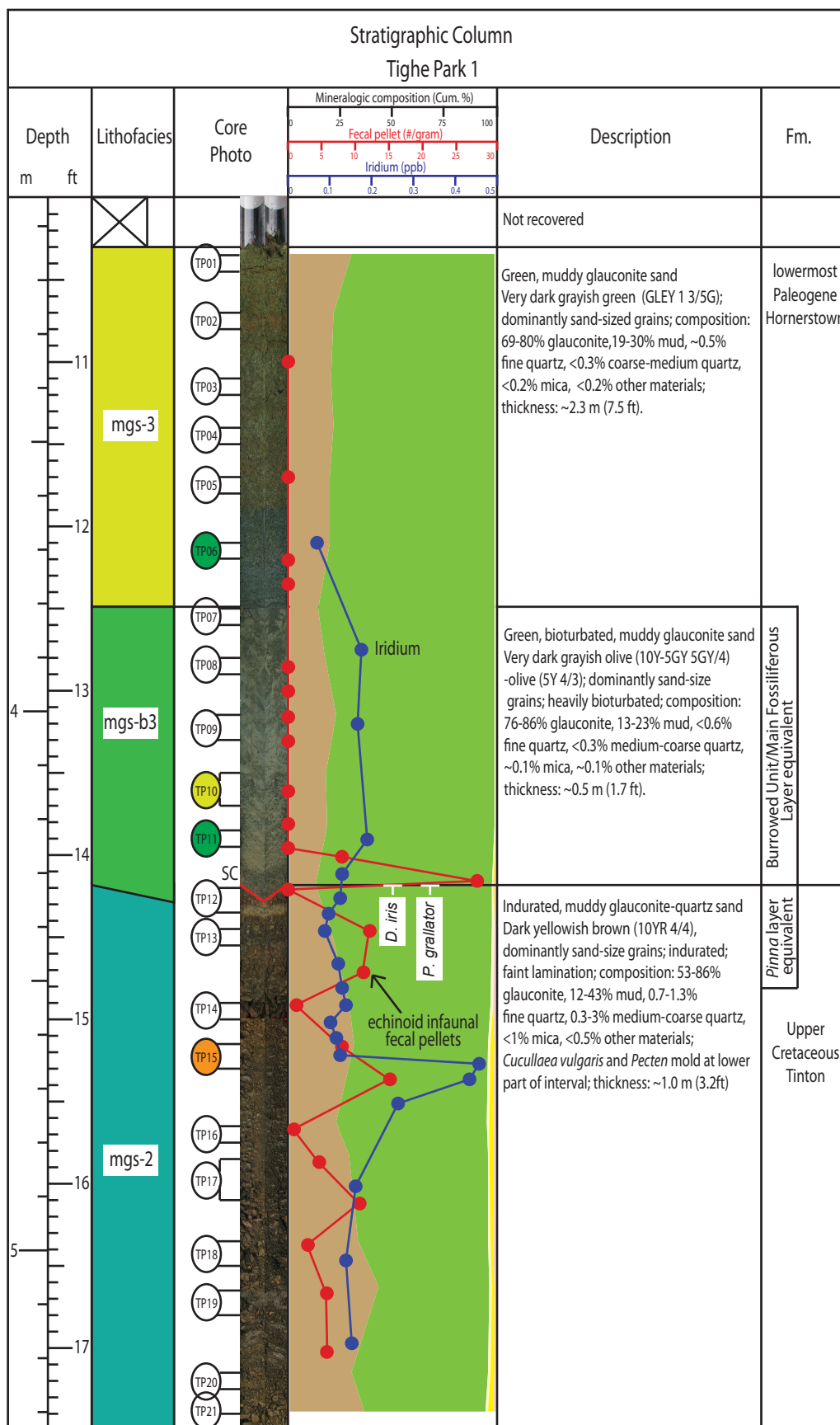


Figure 18. Stratigraphic column of Tinton Falls and its surrounding area. This core is composed of muddy quartz sand; indurated, muddy glauconite-quartz sand; and glauconitic mud. The contact between these lithofacies are not present. KT01 = sample number 1 from Cretaceous Tinton Formation. See legend for detail codes and color codes.

Figure 19. Stratigraphic column of Tighe Park 1. The indurated, muddy glauconite quartz sand sharply underlies the bioturbated, green, muddy glauconite sand. The upper part of indurated, muddy, glauconite quartz sand is the *Pinna* layer. The bioturbated, green, muddy glauconite sand grades upward into green, muddy glauconite sand. The bioturbated, green, muddy glauconite sand is the equivalent unit of the Burrowed Unit (Landman *et al.*, 2007) and the Main Fossiliferous Layer (Gallagher, 2002). The biostratigraphic age is from Landman *et al.*, 2007. *D. iris* = *Discoscaphites iris*; *P. grallator* = *Palynodinium grallator*. TP01 = sample number 1 from Tighe Park 1 core. See legend for detail codes and color codes. Figure is on the following page.



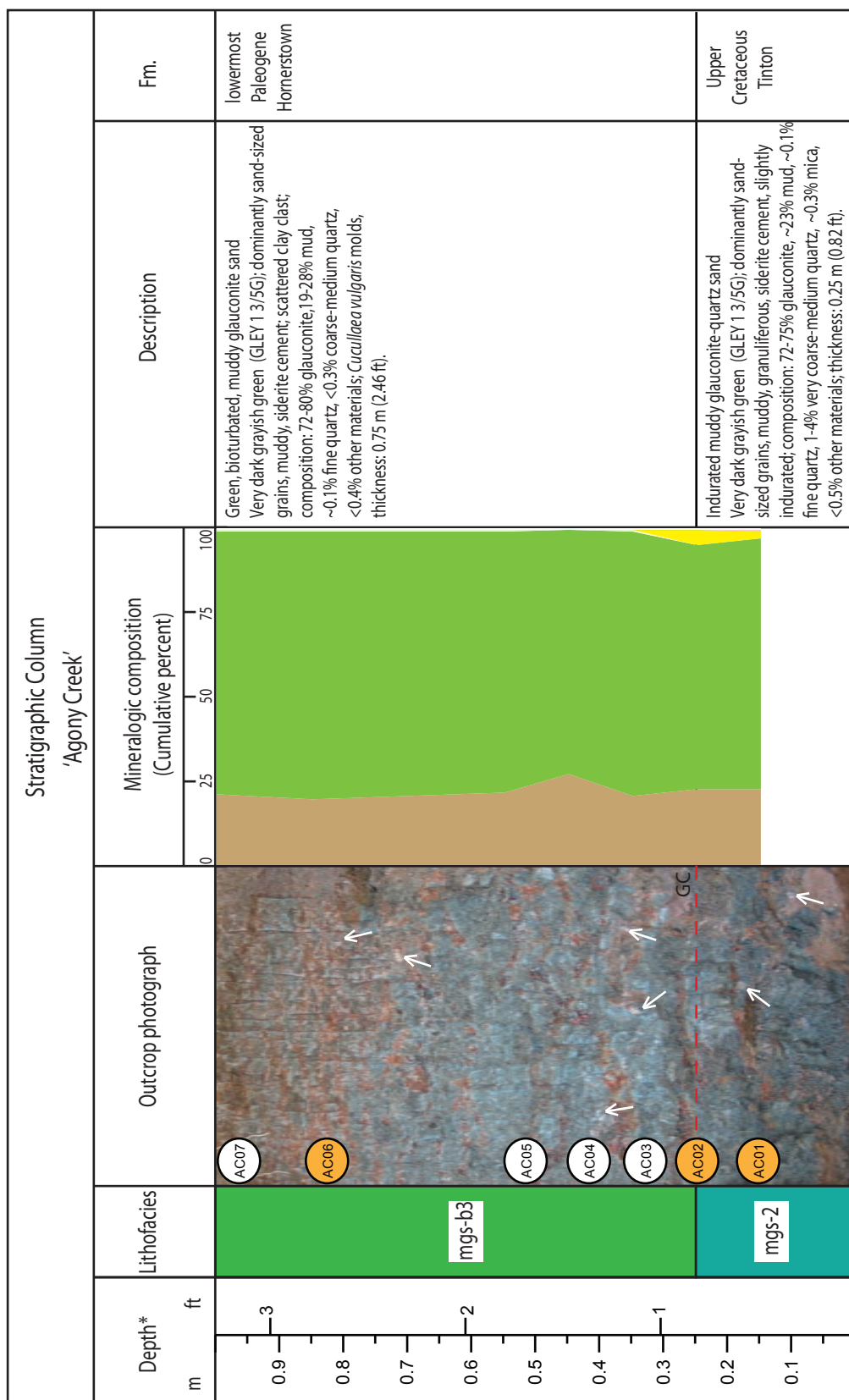


Figure 20. Stratigraphic column of Agony Creek outcrop. The indurated, muddy glauconite quartz sand grades to the bioturbated, green, muddy glauconite sand. The edge of the bioturbation is often times sideritized. White arrows show the siderite nodules. AC01 = sample number 1 from Agony Creek. See legend for detail codes and color codes.

Figure 21. Lithostratigraphic column of Meirs Farm 1 core. The brown, bioturbated, muddy glauconite sand grades upward into the green, muddy glauconite sand. Fecal pellets and Ir data are from Miller *et al.* (2010) study. Miller *et al.* (2010) placed the K/Pg contact at the Ir peak and sharp decrease of epifaunal echinoid fecal pellets corresponding with the clay clast. The K/Pg contact is placed at the upper part of brown, bioturbated, muddy glauconite sand suggesting the Ir is mobilized in this study. MF01 = sample number 1 from Meirs Farm 1 core. See legend for detail codes and color codes. Figure is on the following page.

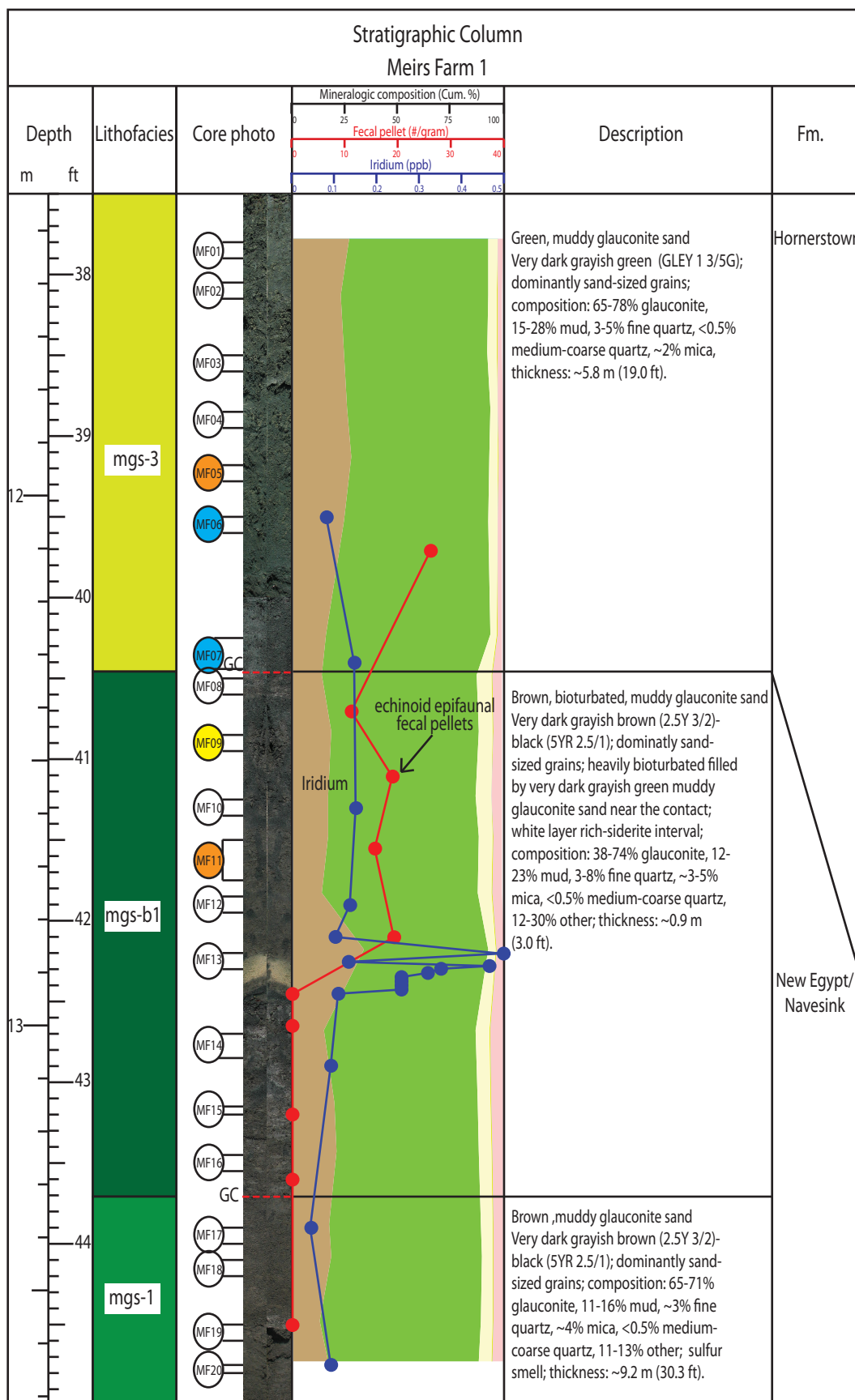


Figure 22. Stratigraphic column of Fort Monmouth 3 core. The brown, bioturbated, muddy glauconite sand underlies the green, muddy glauconite sand. The contact between these facies is sharp. The biostratigraphy age, fecal pellets, and Ir data are from Miller *et al.* (2010) study. FM01 = sample number 1 from Fort Monmouth 3 core. See legend for detail codes and color codes. Figure is on the following page.

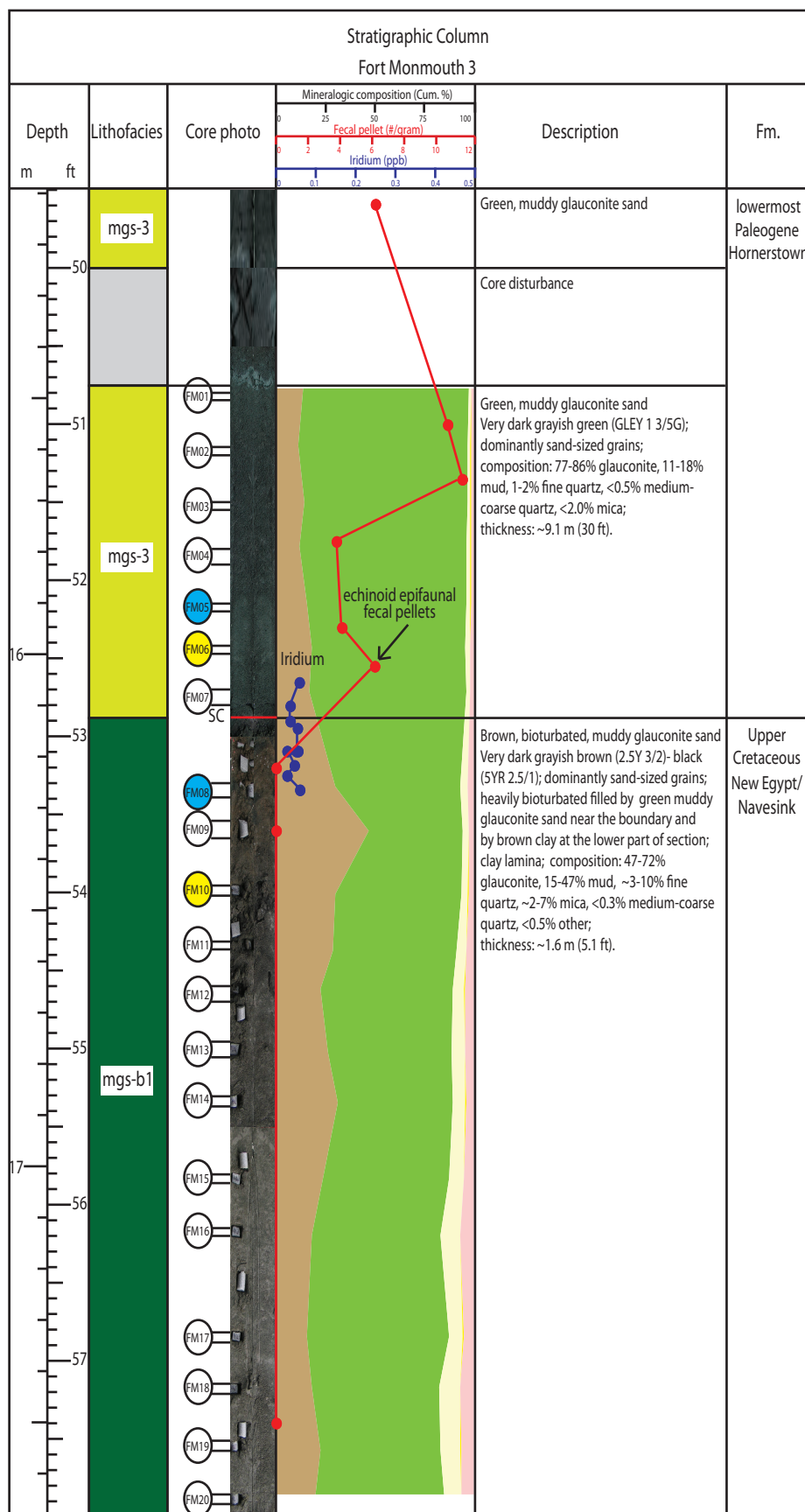


Figure 23. Stratigraphic column of Search Farm 1 core. The brown, bioturbated, muddy glauconite sand abruptly overlain by the green, muddy glauconite sand. *Cucullaea vulgaris* mold (the MFL) appear at the contact corresponds with the Ir peak. The fecal pellets and Ir data are from Miller *et al.* (2010) study. See legend for detail codes and color codes. Figure is on the following page.

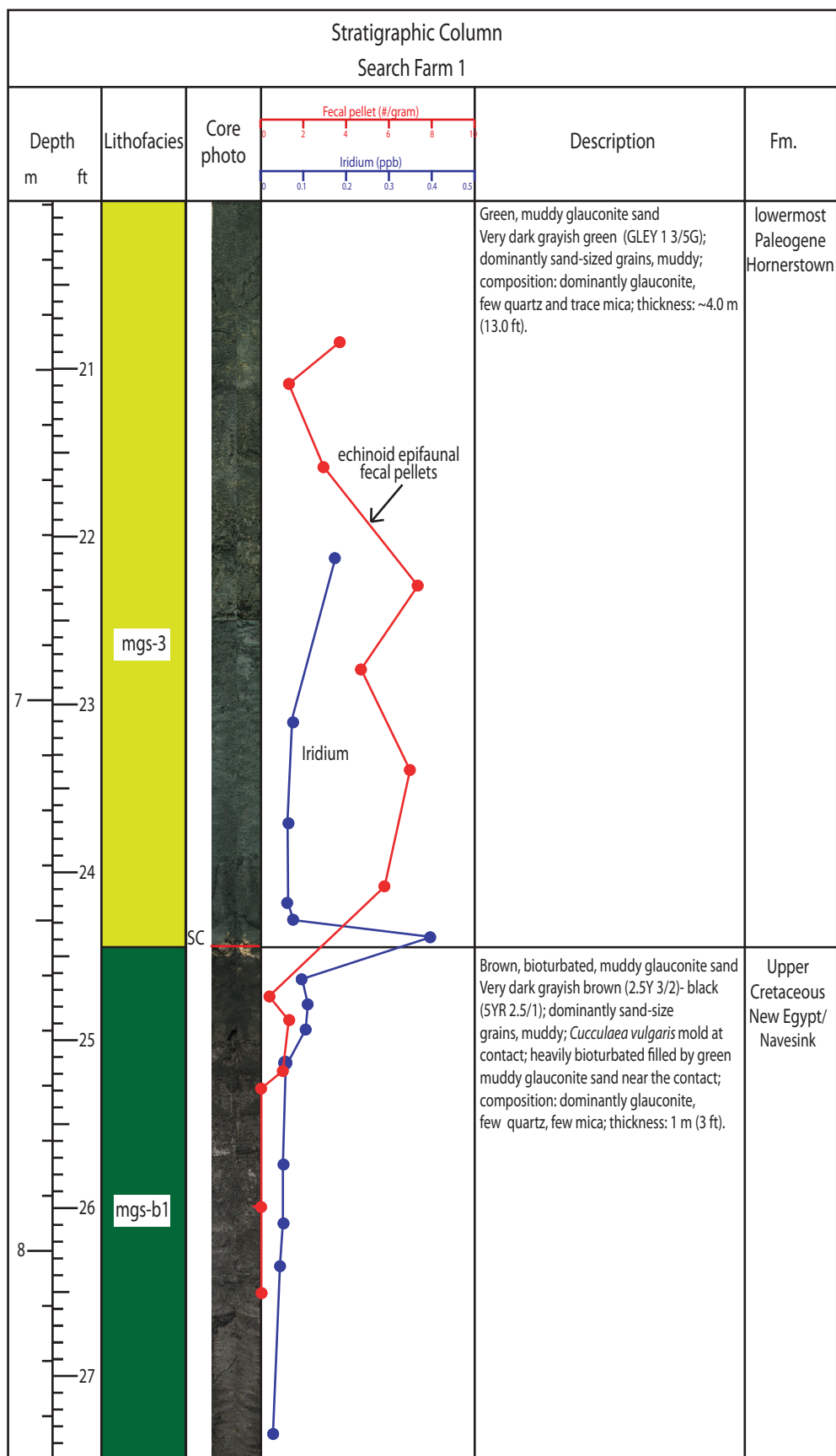


Figure 24. Stratigraphic column of Low Meadow 1 core. The brown, muddy glauconite sand grades into the green, muddy glauconite sand. See legend for detail codes and color codes. Figure is on the following page.

Stratigraphic Column Low Meadow 1				
Depth m ft	Lithofacies	Core Photo	Description	Fm.
			<p>Green, muddy glauconite sand Very dark grayish green (GLE 1 3/5G); dominantly sand-sized grains, muddy; composition: dominantly glauconite, few quartz and trace mica; thickness: ~10.6 m (35 ft).</p>	lowermost Paleogene Hornerstown
			<p>Brown, muddy glauconite sand Very dark grayish brown (2.5Y 3/2)- black (5YR 2.5/1); dominantly sand-size grains, muddy; slightly bioturbated; composition: dominantly glauconite, few quartz, few mica; thickness: 0.7 m (2.2 ft).</p>	Upper Cretaceous New Egypt/ Navesink

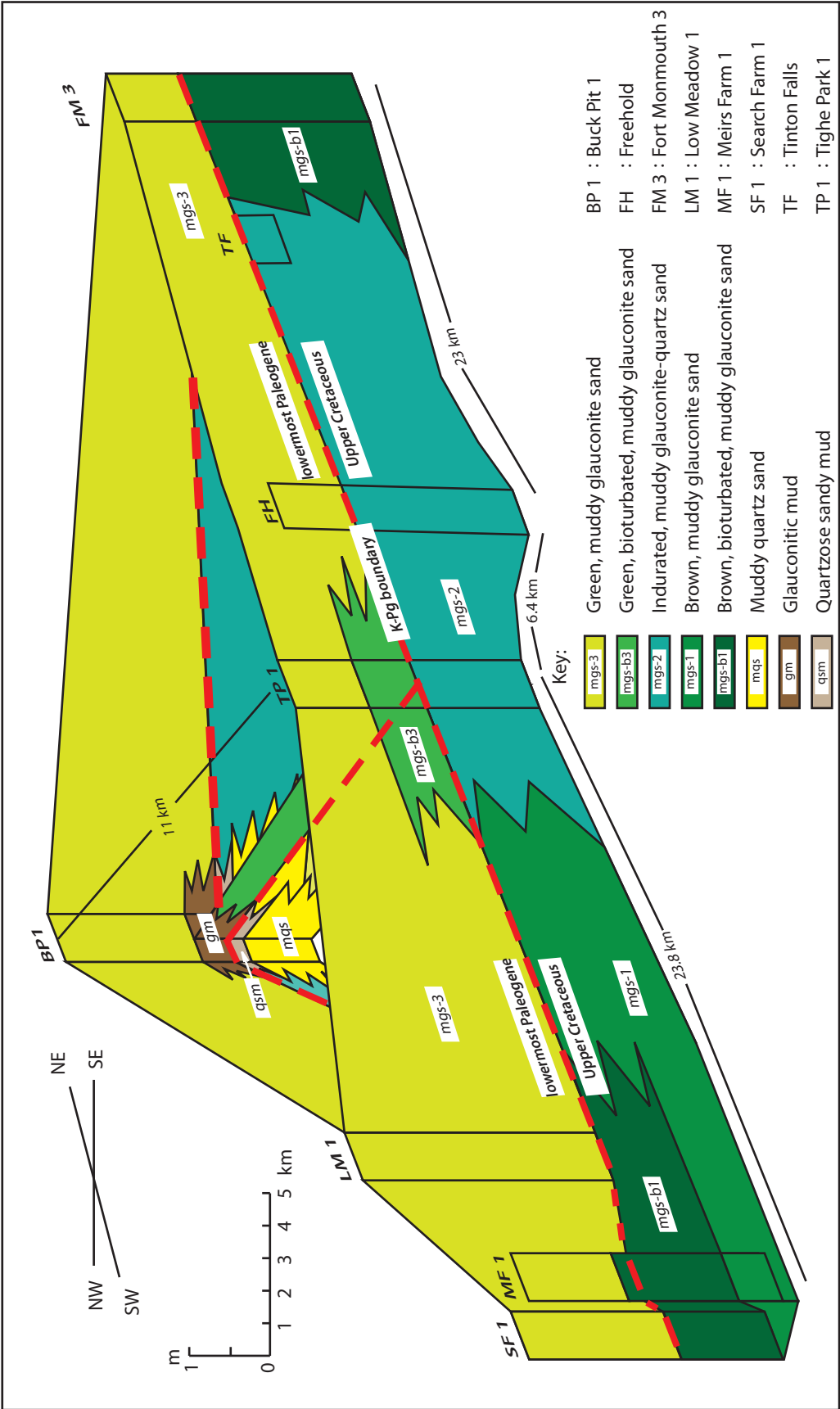


Figure 25. Fence diagram showing K/Pg sediment distribution (see map, Figure 3, for the core-hole location).

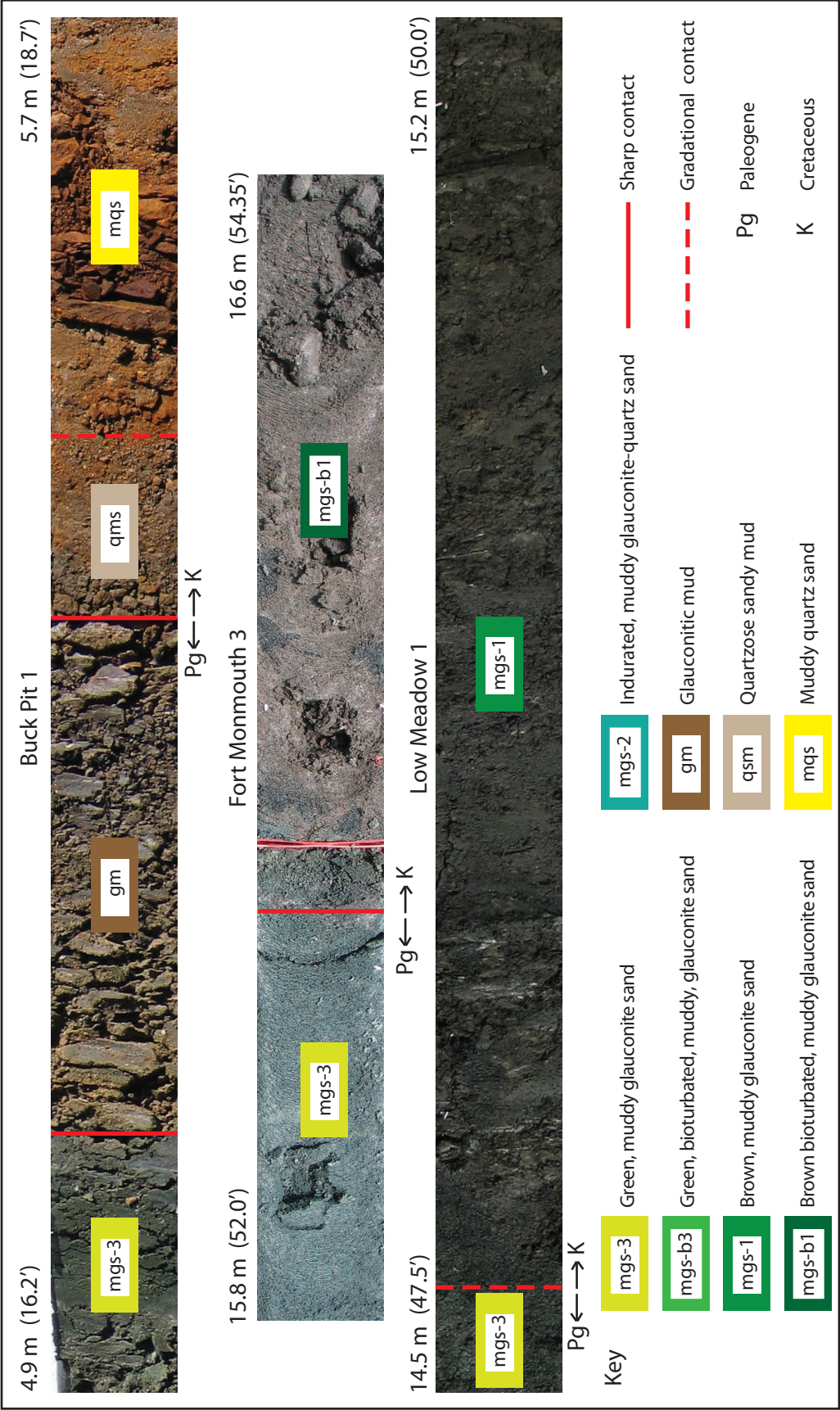


Figure 26. Sediment characteristics and lithofacies boundary of K/Pg deposits on New Jersey core-holes.

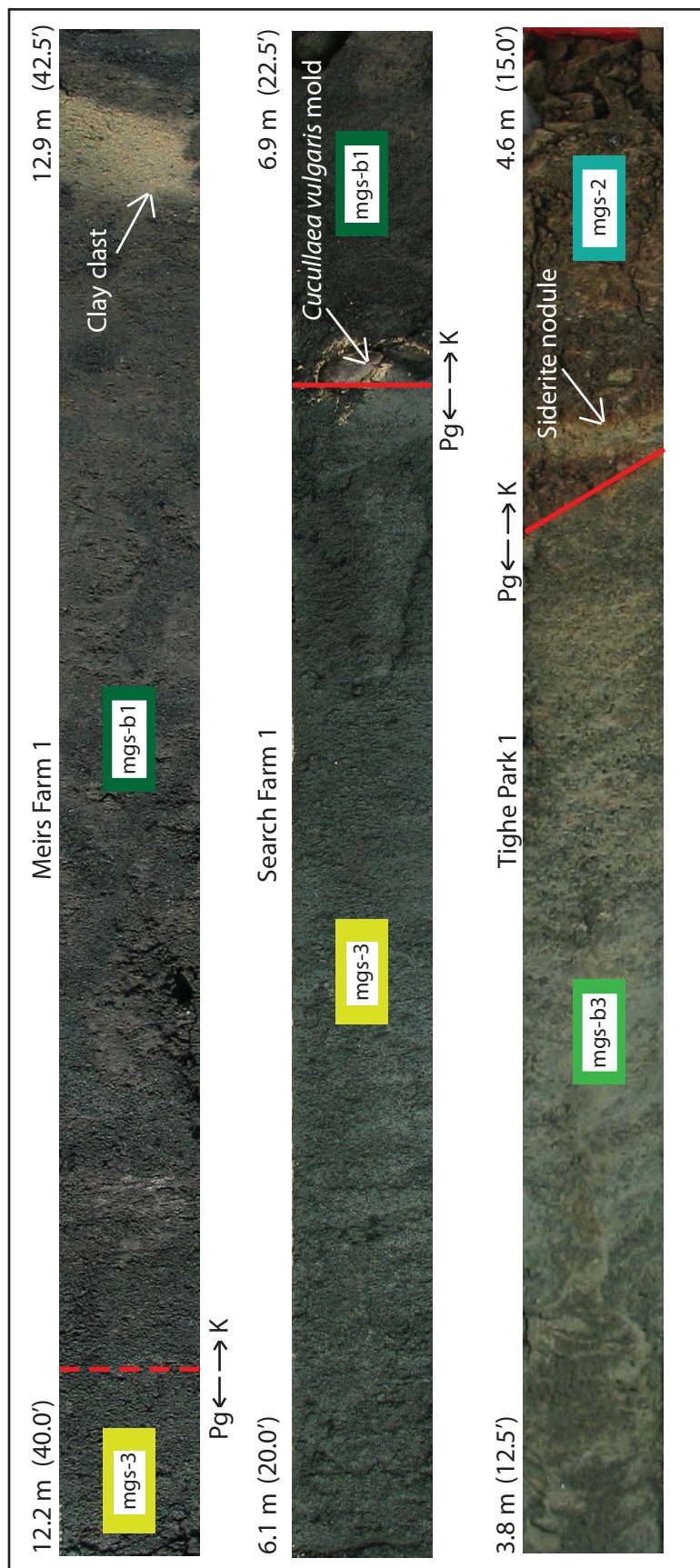


Figure 26 (cont'd). Sediment characteristics and lithofacies boundary of K/Pg deposits on New Jersey core-holes.

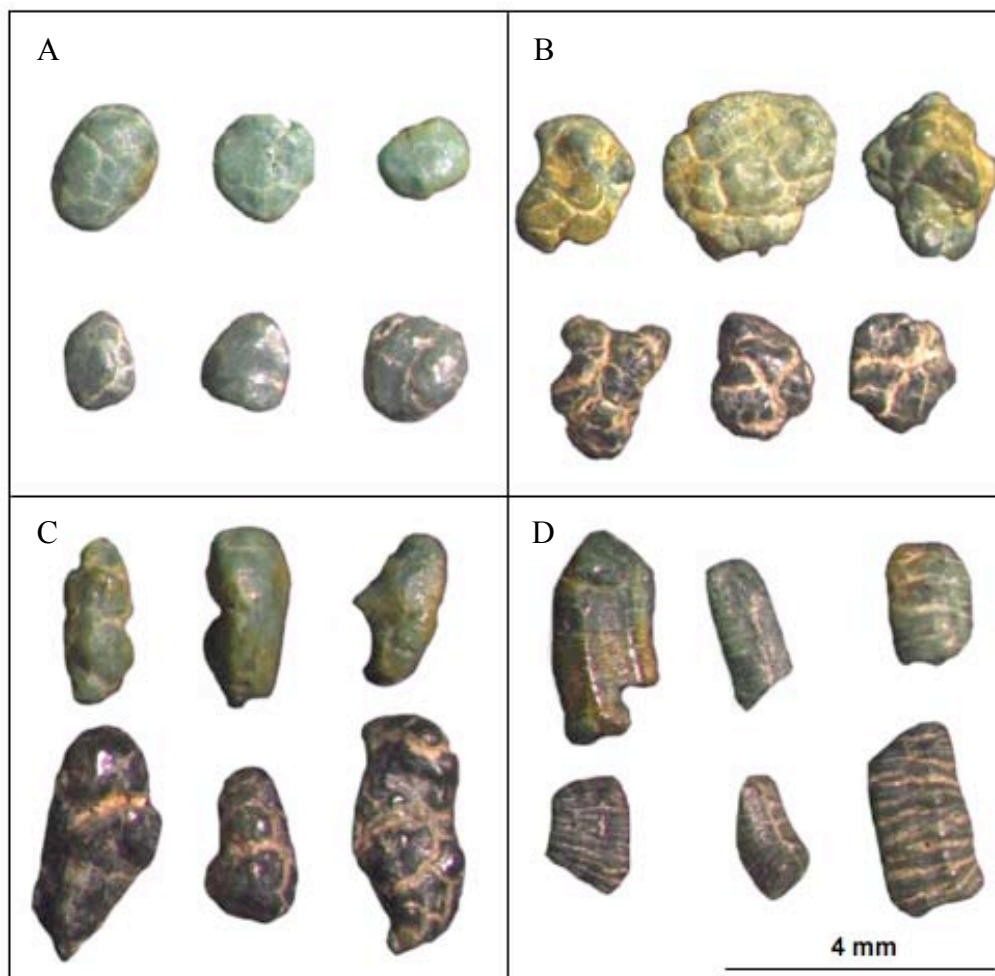


Figure 27. Different grain morphotypes of authigenic glauconite (Triplehorn, 1966) as viewed in reflected light. (A) Spheroidal-ovoidal grains. (B) Lobate-mammillated grains. (C) Capsule-shaped grains. (D) Vermicular grains. The lowermost Paleogene glauconite (upper) are dark green; the Upper Cretaceous glauconite (lower) are black. Samples are from Fort Monmouth 3 and sample location shown in yellow on Figure 22.

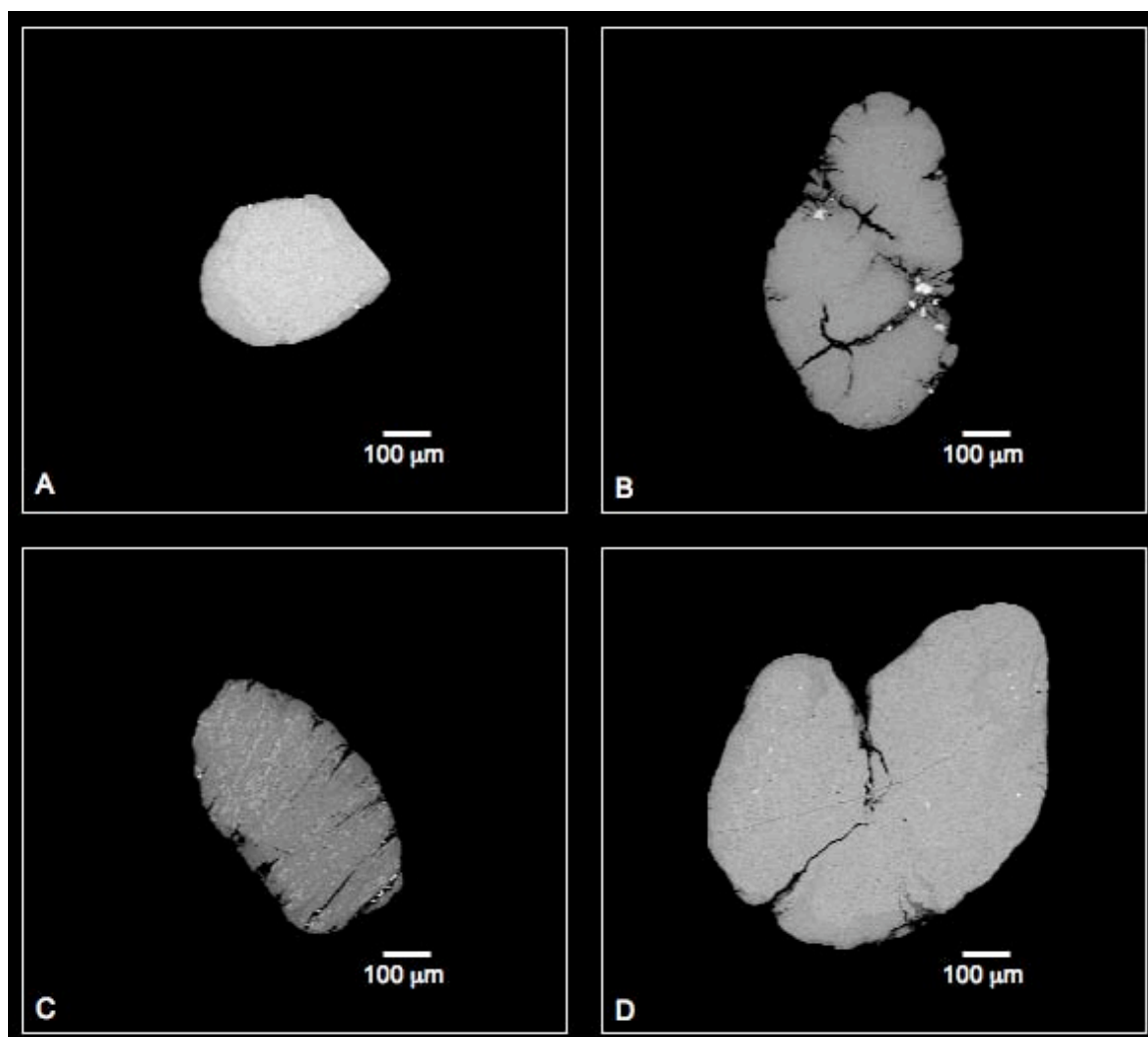


Figure 28. Backscattered electron images of different glauconite morphotypes (Triplehorn, 1966). (A) Spheroidal-ovoidal grain. (B) Capsule-shaped grain. (C) Vermicular grains. (D) Lobate-mammillated grains. Brighter spot in the grains represent a higher atomic number and Fe content.

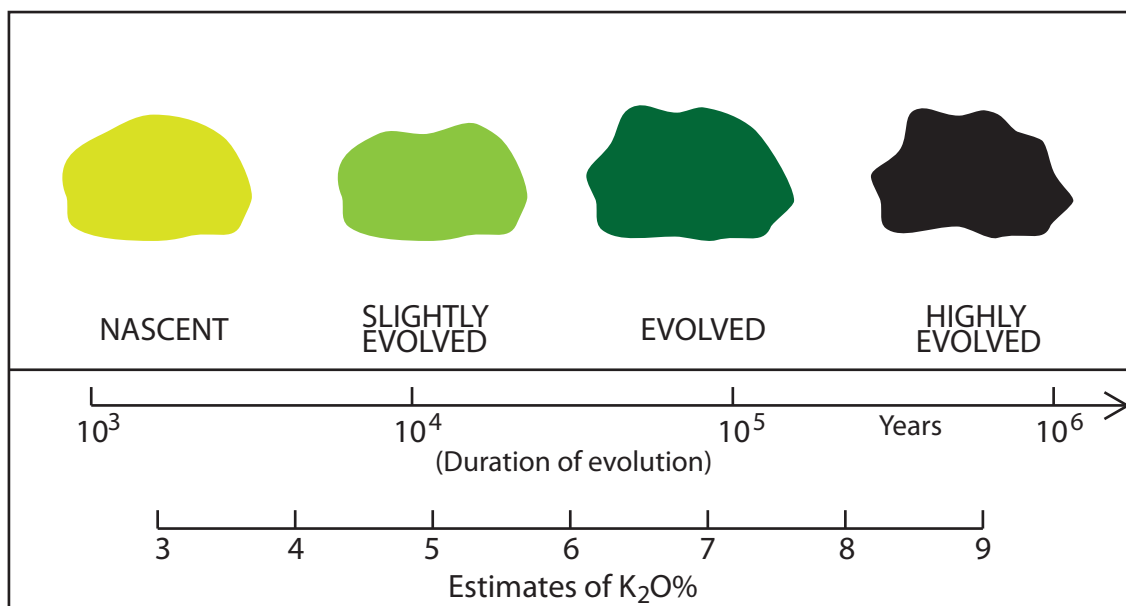


Figure 29. Stages of development of glauconitization in granular substrate (modified after Odin and Fullagar, 1988)

Figure 30. Relationship of K_2O with SiO_2 as determined by microprobe analysis. Total 9 black glauconites from the Upper Cretaceous and 17 dark green glauconites from the lowermost Paleogene formations were analysed, with data collected from the core midpoint, and rim for each grain. Green envelope represents dark green glauconite. Solid black represents black glauconite. Both type of glauconites fall into evolved (6-8% K_2O) to highly evolved (>8% K_2O) glauconite based on Odin and Fullagar classification (1988). Figure is on the following page.

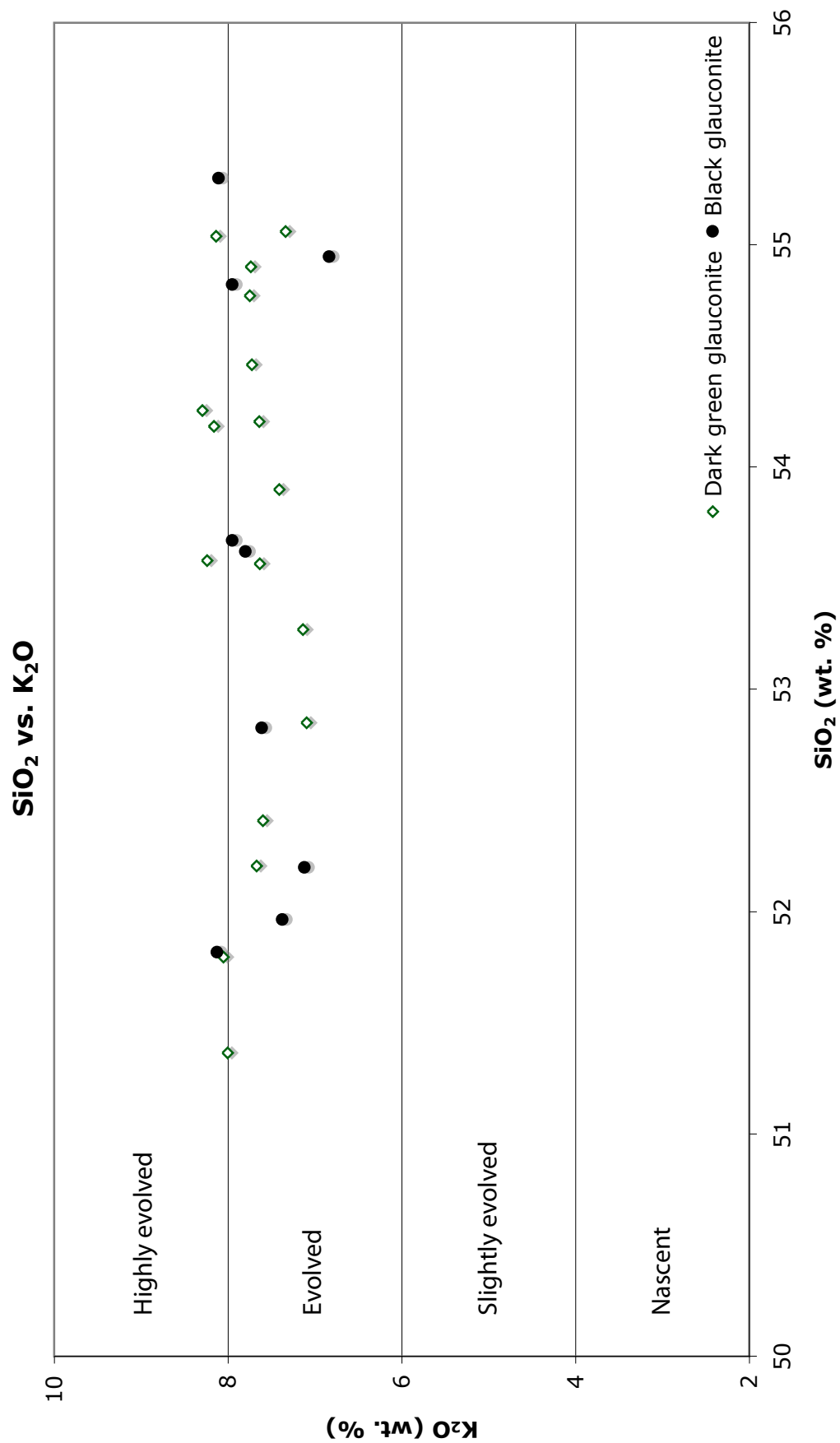


Figure 31. Relationship of K_2O with FeO as determined by microprobe analysis. Total 9 black glauconites from the Upper Cretaceous and 17 dark green glauconites from the lowermost Paleogene formations were analysed, with data collected from the core midpoint, and rim for each grain. Green envelope represents dark green glauconite. Solid black represents black glauconite. Both black and dark green glauconite demonstrate linear relationship of K_2O vs. FeO without significant difference. Thus, it is likely that these two oxides cannot be used to differentiate between black and dark green glauconite. Figure is on the following page.

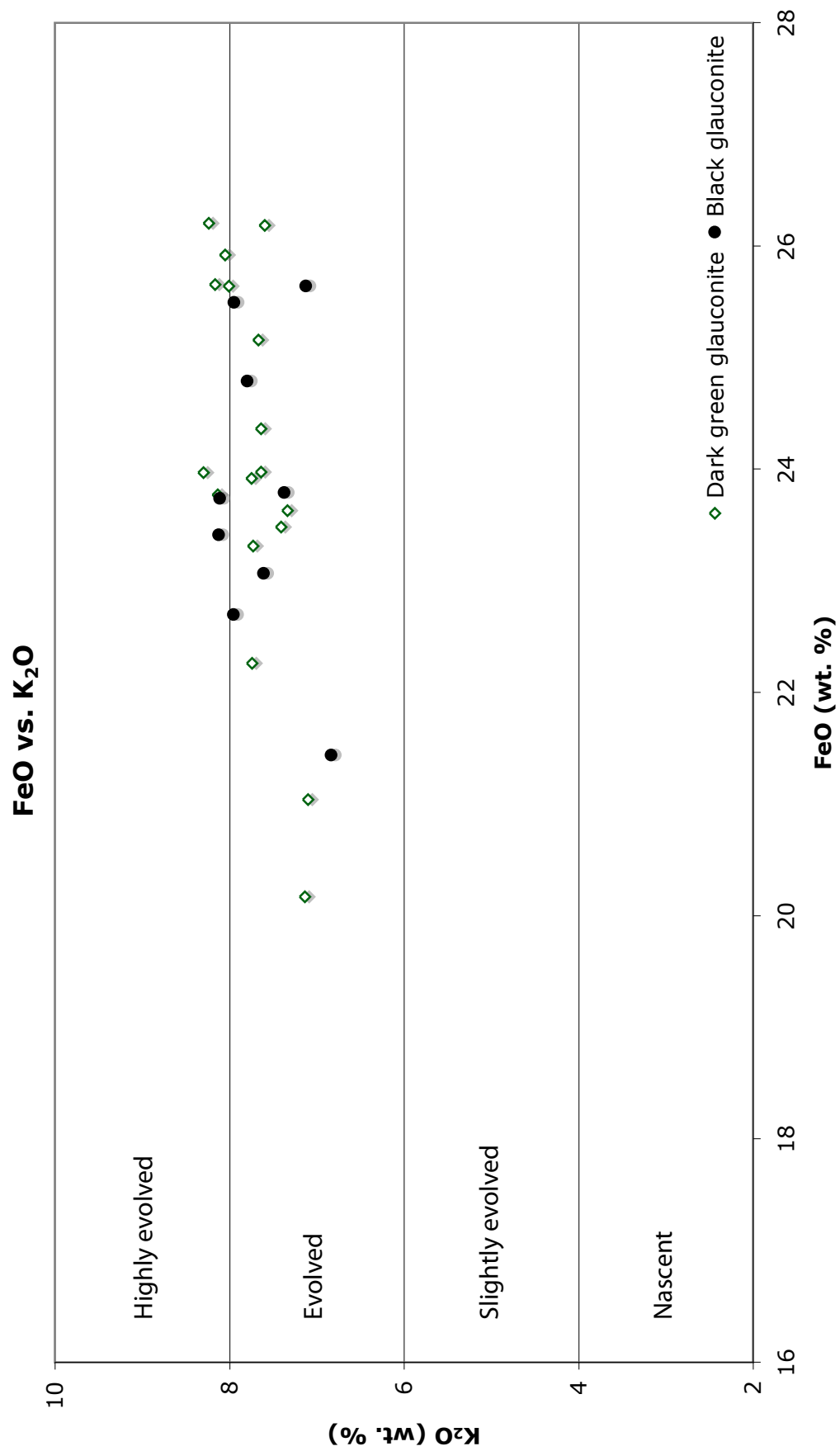


Figure 32. Relationship of K_2O with Al_2O_3 as determined by microprobe analysis. Total 9 black glauconites from the Upper Cretaceous and 17 dark green glauconites from the lowermost Paleogene formations were analysed, with data collected from the core midpoint, and rim for each grain. Green envelope represents dark green glauconite. Solid black represents black glauconite. Both black and dark green glauconite demonstrate linear relationship of K_2O vs. Al_2O_3 without significant difference. Thus, it is likely that these two oxides cannot be used to differentiate between black and dark green glauconite. Figure is on the following page.

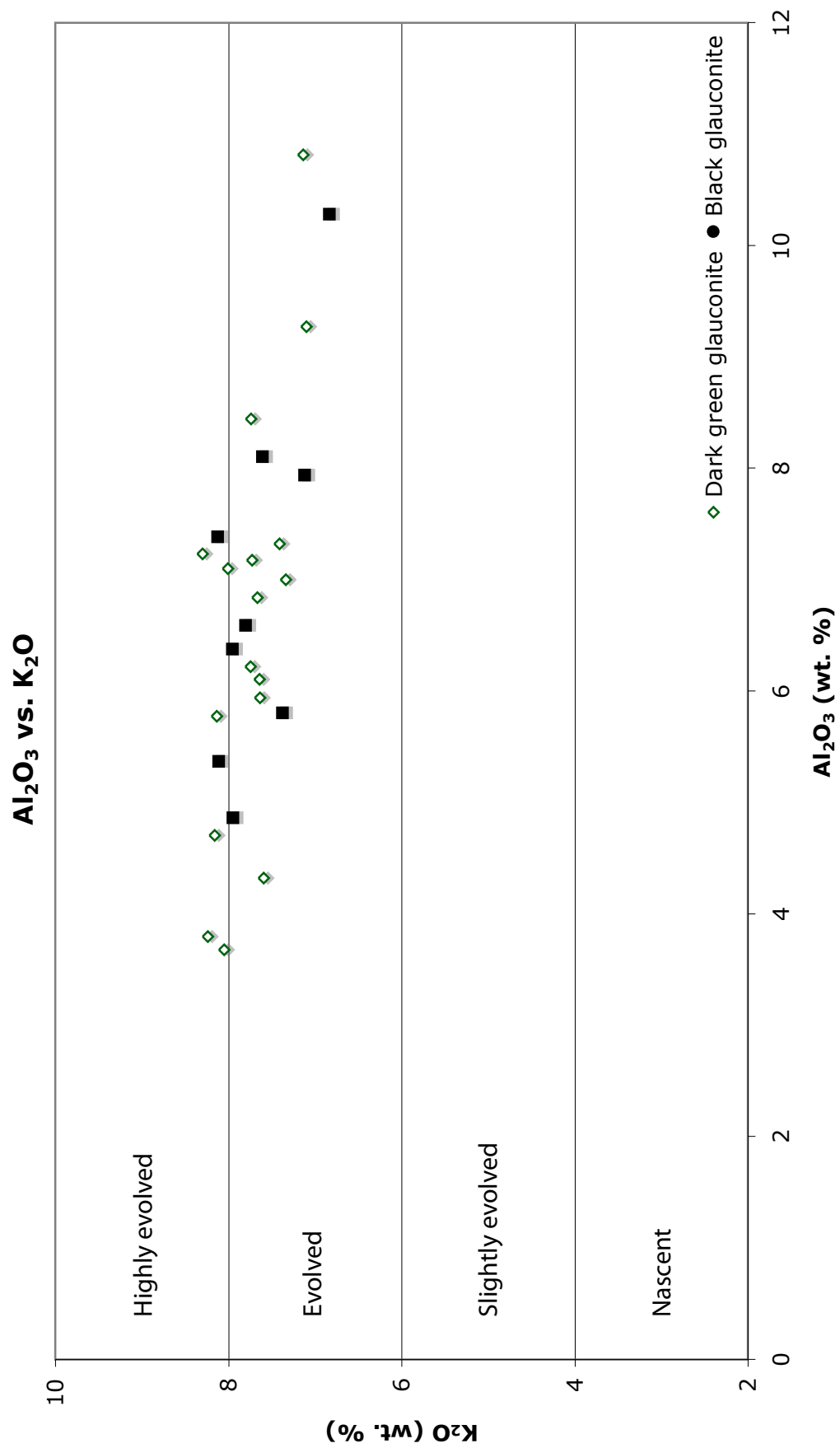
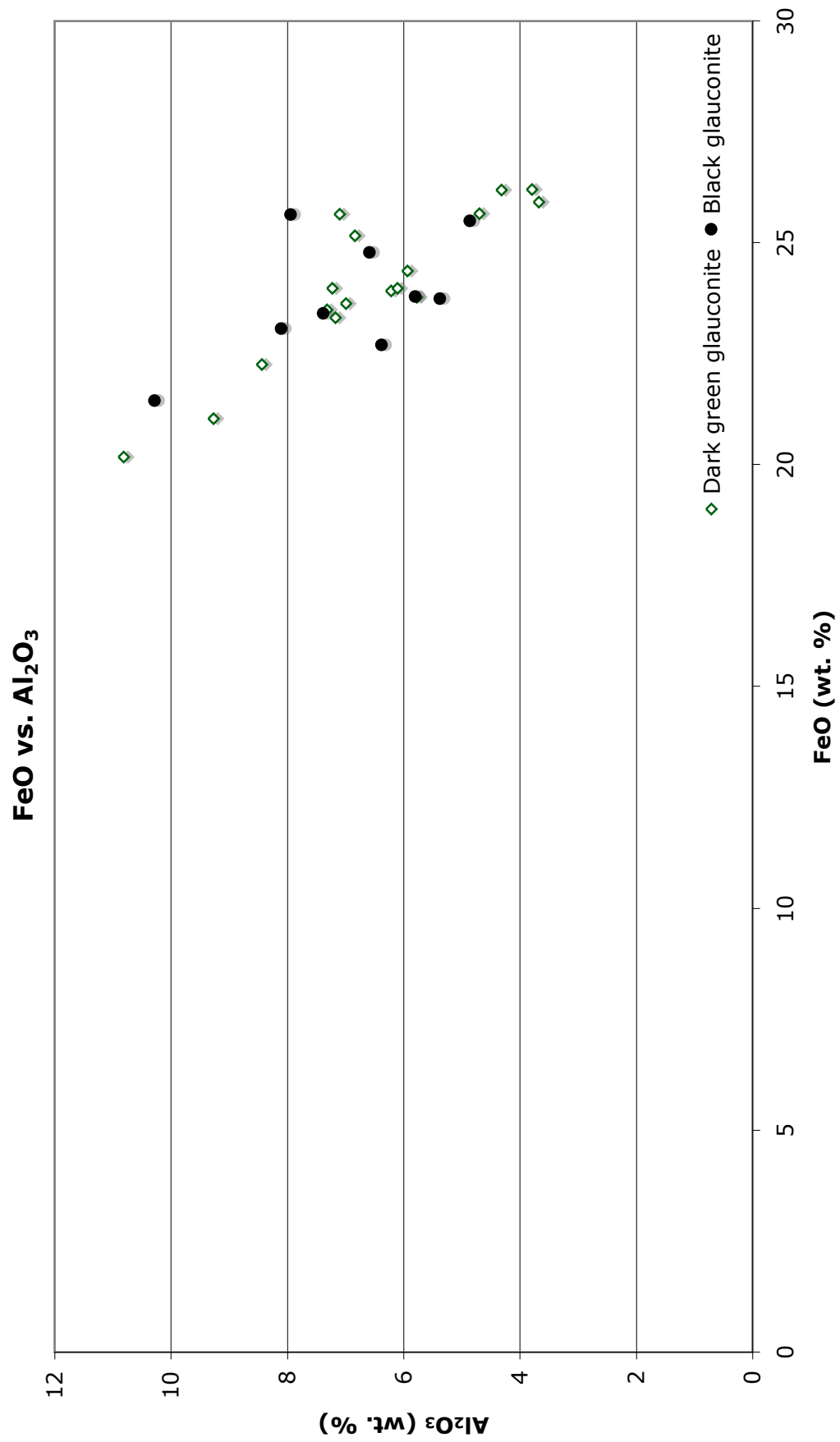


Figure 33. Relationship of FeO with Al_2O_3 as determined by microprobe analysis. Total 9 black glauconites from the Upper Cretaceous and 17 dark green glauconites from the lowermost Paleogene formations were analysed, with data collected from the core midpoint, and rim for each grain. Green envelope represents dark green glauconite. Solid black represents black glauconite. Both black and dark green glauconite demonstrate linear relationship of FeO vs. Al_2O_3 without significant difference. Thus, it is likely that these two oxides cannot be used to differentiate between black and dark green glauconite. Figure is on the following page.



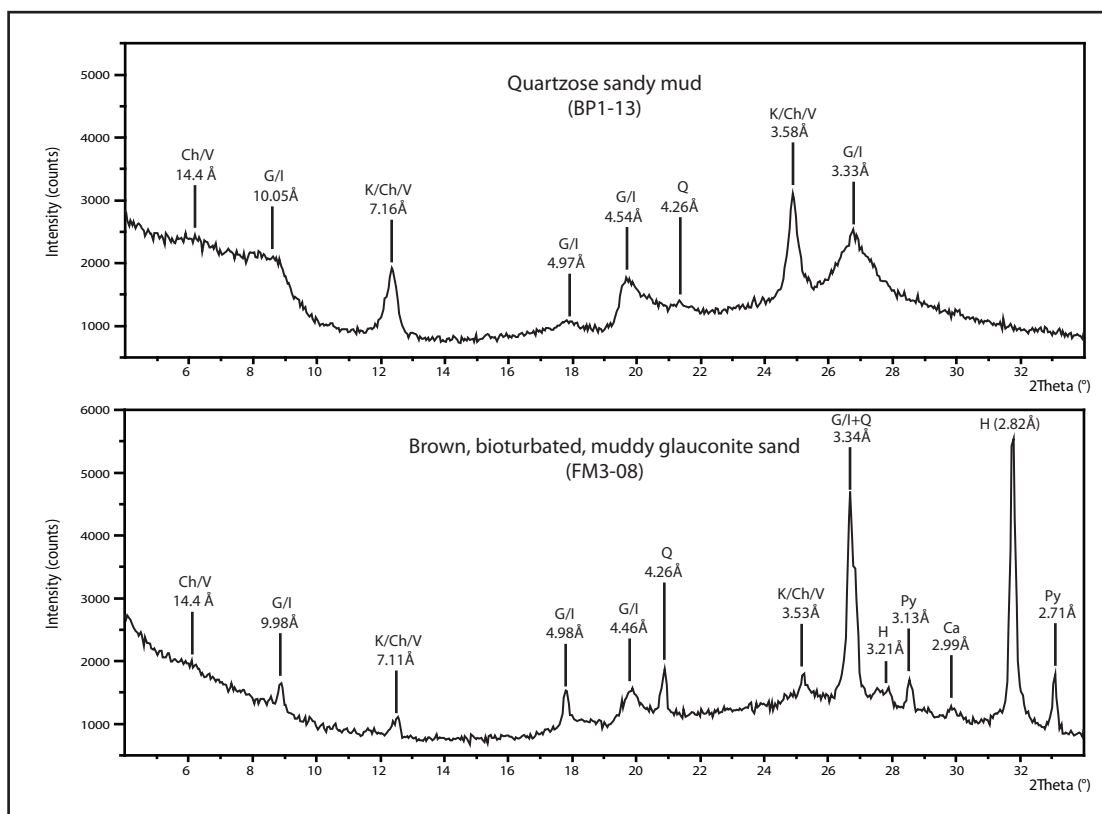


Figure 34. X-ray diffractograms derived from the Upper Cretaceous New Egypt/ Navesink samples. The upper diffractogram is from Buck Pit 1 and sample location shown in blue on Figure 16. The lower diffractogram is from Fort Monmouth 3 and sample location shown in blue on Figure 22. Ca = Calcite, Ch = Chlorite, G = Glauconite, H = Halite, I = Illite, K = Kaolinite, Py = Pyrite, Q = Quartz, V = Vermiculite. BP = Buck Pit, FM = Fort Monmouth.

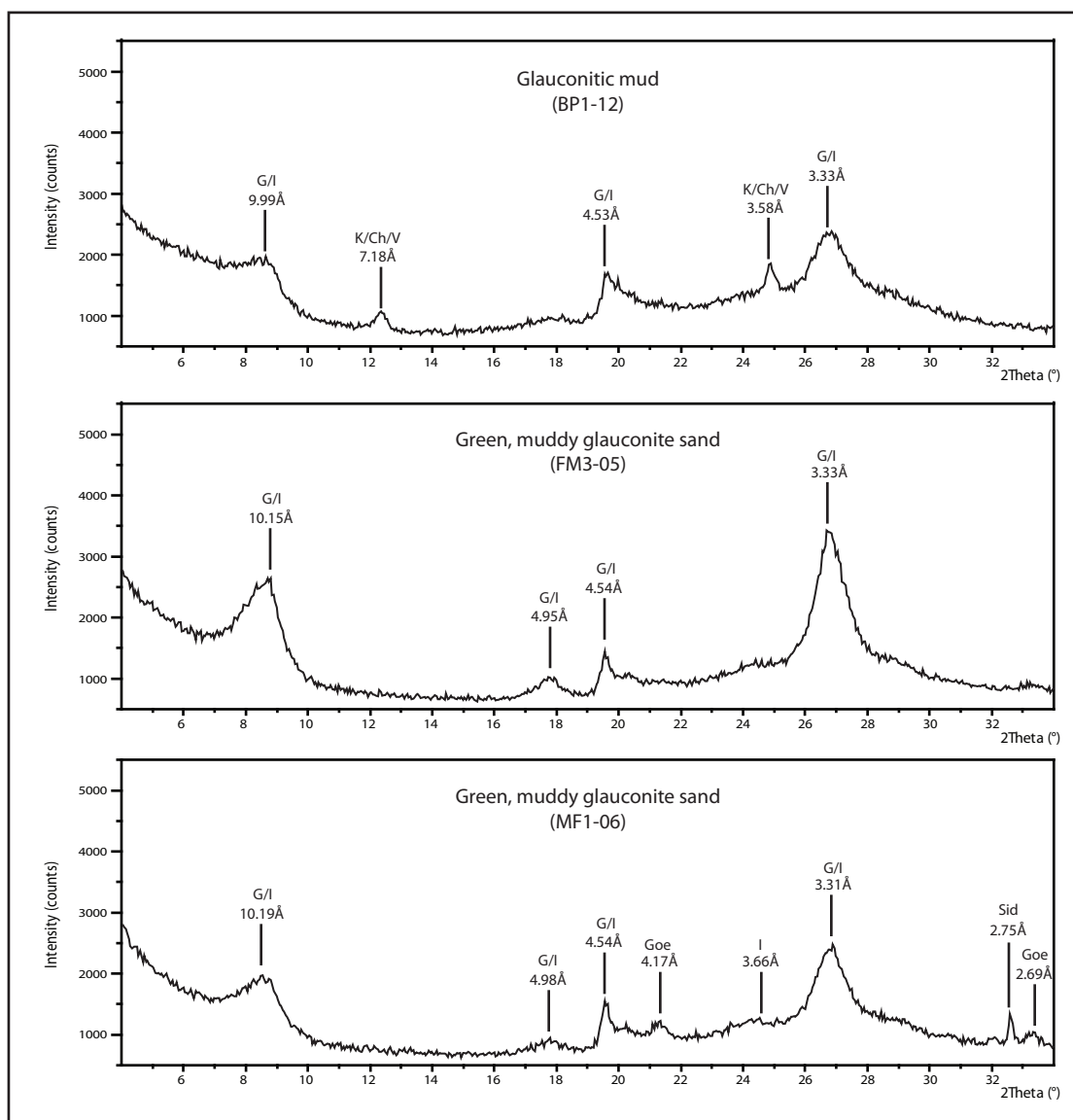


Figure 35. X-ray diffractograms derived from the lowermost Paleogene Hornerstown samples. The upper diffractogram is from Buck Pit 1 and sample location shown in blue on Figure 16. The middle diffractogram is from Fort Monmouth 3 and sample location shown in blue on Figure 22. The lower diffractogram is from Meirs Farm 1 and sample location shown in blue on Figure 21. Ca = Calcite, Ch = Chlorite, G = Glauconite, Goe = Goethite, Gy = Gypsum, I = Illite, Sid = Siderite. BP = Buck Pit FM = Fort Monmouth, MF = Meirs Farm.

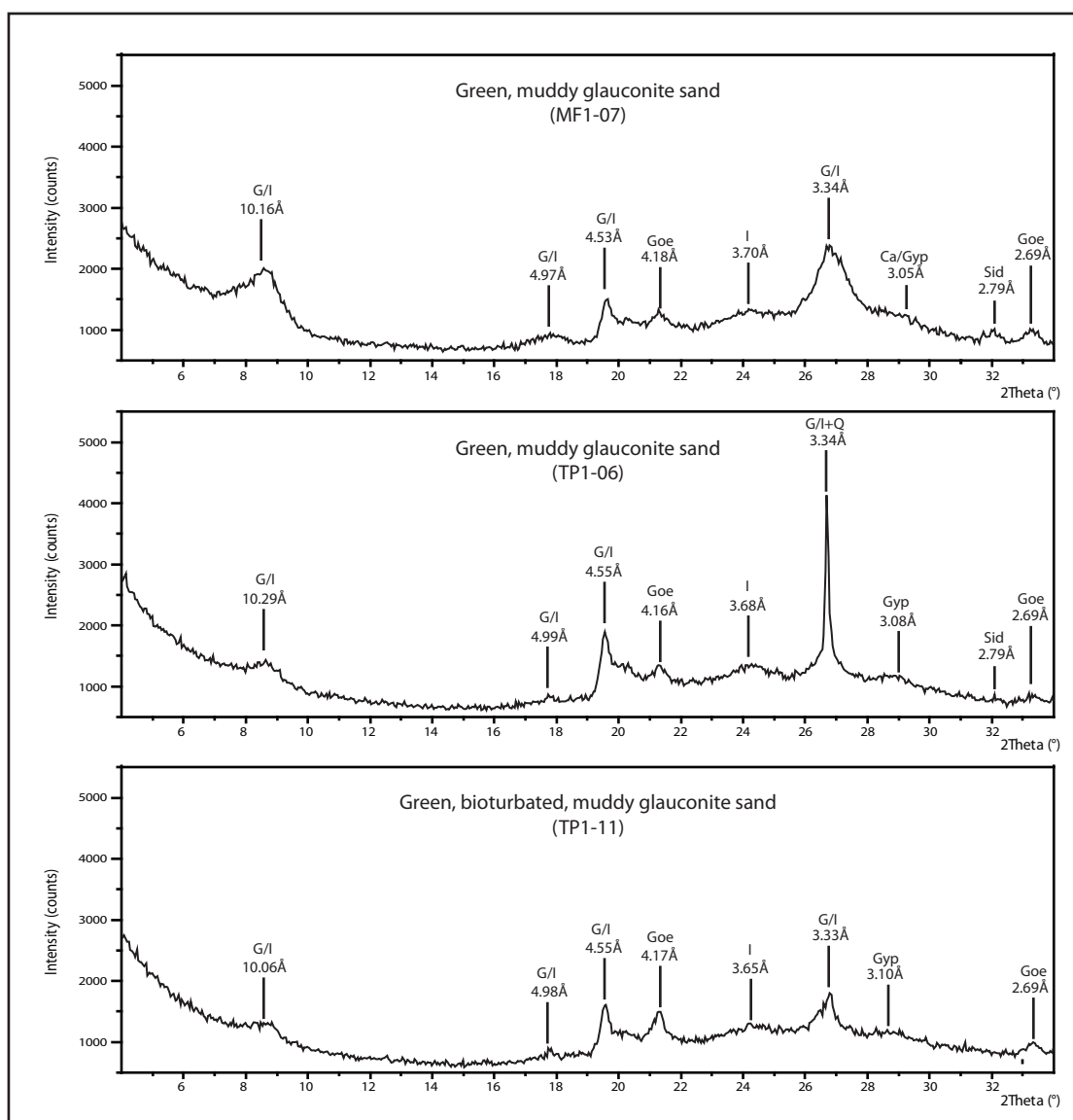


Figure 36. X-ray diffractograms derived from the lowermost Paleogene Hornerstown samples. The upper diffractogram is from Meirs Farm 1 and sample location shown in blue on Figure 21. The middle and lower diffractograms are from Tighe Park 1 and sample location shown in green on Figure 19. Ca = Calcite, Ch = Chlorite, G = Glauconite, Goe = Goethite, Gy = Gypsum, I = Illite, Sid = Siderite. MF = Meirs Farm, TP = Tighe Park.

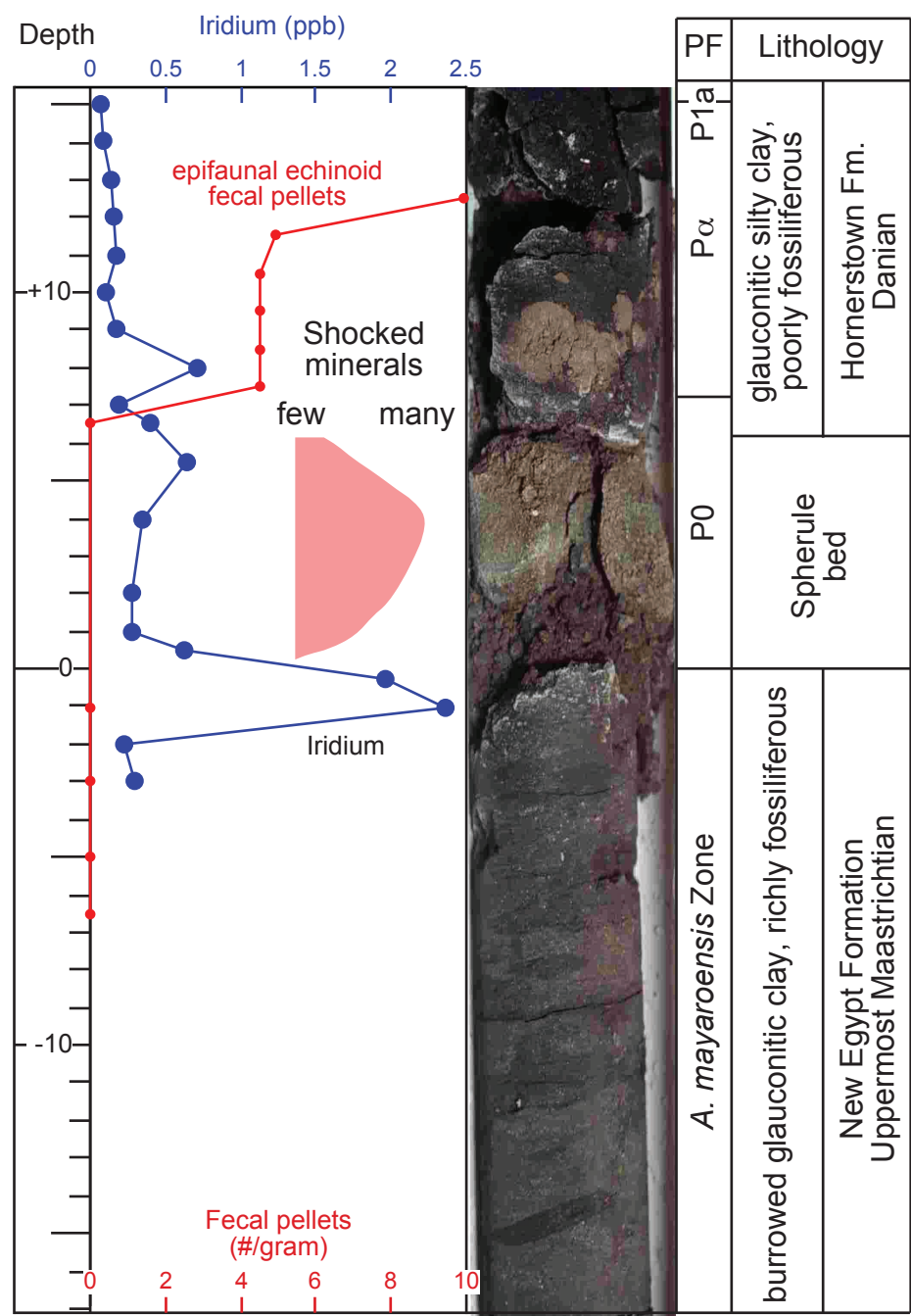


Figure 37. Complete K/Pg deposits from Bass River core-hole, New Jersey (modified after Olsson *et al.*, 1997; 2002). Core-hole location is shown on Figure 3.

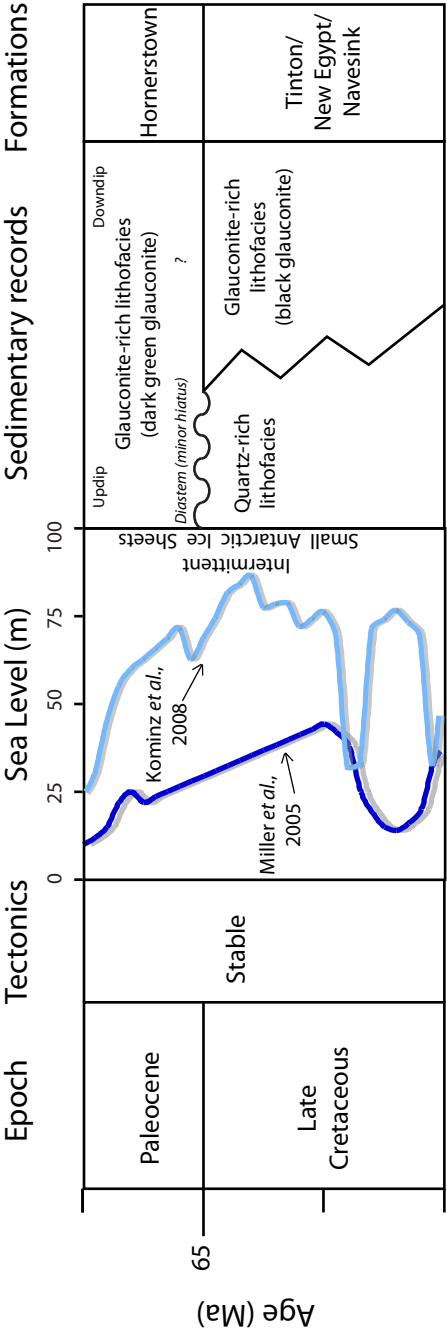


Figure 38. Sea level curve across the K/Pg boundary (modified after Miller *et al.*, 2005 and Kominz *et al.*, 2008).

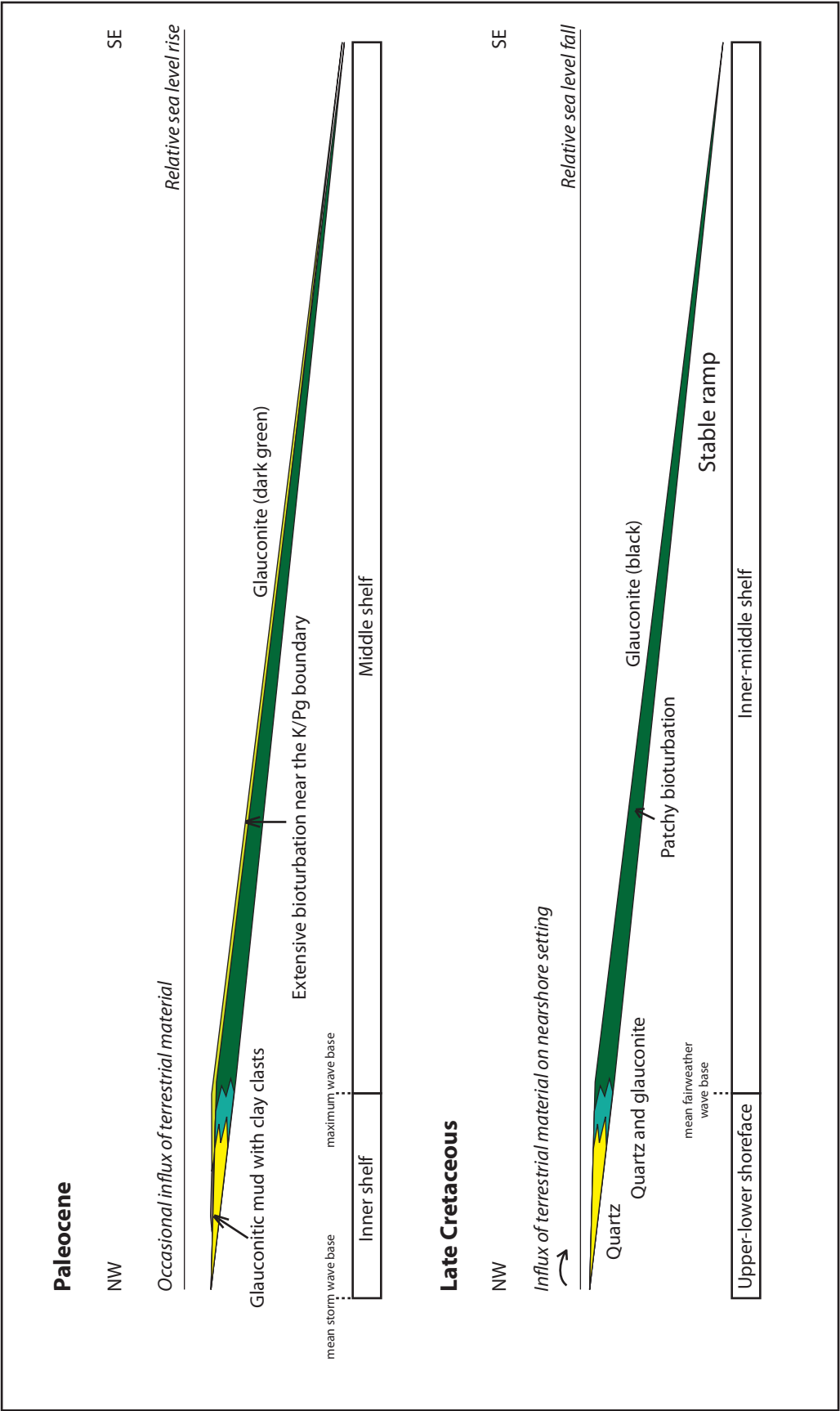


Figure 39. A dip section sketch of the proposed Late Cretaceous - Paleocene environment of deposition setting of New Jersey coastal plain.

Appendix 1. Location

Bore holes and outcrops	Location	
Agony Creek	40°14'18.79" N	74°24'45.85" W
Buck Pit 1	40°14'18.79" N	74°24'45.85" W
Fort Monmouth 3	40°18'37.18" N	74°02'46.25" W
Freehold	40°15'17" N	74°13'51" W
Hockhocks Brook	40°17'49" N	74°05'58" W
Low Meadow 1	40°07'57.96" N	74°28'36.78" W
Meirs Farm 1	40°06'15.48" N	74°31'37.48" W
Search Farm 1	40°05'29.20" N	74°32'16.10" W
Tighe Park 1	40°12'51.42" N	74°17'17.79" W
Tinton Falls	40°18'15.40"N	74°06'1.50"W

Appendix 2. Location and depth of petrographic, microprobe, and XRD samples.

Location	Depth		Sample code	Analysis		
	Meter	Feet		Petrography	Microprobe	XRD
Buck Pit	4.60-4.62	15.10-15.15	BP06b	✓		
	4.95-4.98	16.25-16.35	BP10		✓	
	5.06-5.12	16.60-16.80	BP11	✓		
	5.18-5.24	17.00-17.20	BP12			✓
	5.36-5.39	17.60-17.70	BP13			✓
Tighe Park	3.69-3.73	12.10-12.25	TP06		✓	✓
	4.11-4.18	13.50-13.70	TP10	✓	✓	
	4.22-4.25	13.85-13.95	TP11		✓	✓
	4.62-4.66	15.15-15.30	TP15	✓		
Meirs Farm	11.94-11.97	39.18-39.28	MF05	✓		
	12.05-12.09	39.55-39.65	MF06			✓
	12.27-12.33	40.25-40.45	MF07			✓
	12.45-12.48	40.85-40.95	MF09		✓	
	12.65-12.73	41.50-41.75	MF11	✓		
	13.02-13.06	42.70-42.85	MF14			
Fort Monmouth	15.90-15.91	52.15-52.20	FM05			✓
	15.98-15.99	52.42-52.47	FM06		✓	
	16.25-16.29	53.30-53.45	FM08			✓
	16.46-16.47	54.00-54.05	FM10		✓	
Agony Creek	0.65-0.75*	0.82-1.15	AC06	✓		
	0.25-0.35*	2.13-2.46	AC02	✓		
	0.15-0.25*	2.46-2.79	AC01	✓		

* Relative depth from the bench stream.

Appendix 3. XRD peaks list

- Quartzose sandy mud (BP1-13)

Position [$\infty 2\theta$.]	Height [counts]	FWHM [$\infty 2\theta$.]	d-spacing [Å]	Rel.Int. [%]	Tipwidth [$\infty 2\theta$.]	Interpretations
8.7972	651.42	0.3936	10.05	0.01	0.40	G/I
12.3653	1071.58	0.2460	7.16	0.02	0.25	K/Ch/V
17.8460	188.29	0.3936	4.97	0.00	0.40	G/I
19.5734	662.69	0.3444	4.54	0.01	0.35	G/I
24.8860	1779.74	0.2460	3.58	0.03	0.25	K/Ch/V
26.7683	1206.27	0.2460	3.33	0.02	0.25	G/I

Note:

Ch = chlorite; G = glauconite; I = illite; K = kaolinite; V = vermiculite.

- Brown, bioturbated, muddy glauconite sand (FM3-08)

Position [$\infty 2\theta$.]	Height [counts]	FWHM [$\infty 2\theta$.]	d-spacing [Å]	Rel.Int. [%]	Tipwidth [$\infty 2\theta$.]	Interpretations
8.8638	381.36	0.2952	9.98	0.01	0.30	G/I
12.4496	240.94	0.2952	7.11	0.00	0.30	K/Ch/V
17.7980	692.20	0.2952	4.98	0.01	0.30	G/I
19.9137	699.87	0.2460	4.46	0.01	0.25	G/I
20.8391	1003.44	0.2952	4.26	0.01	0.30	Q
25.2326	943.70	0.1968	3.53	0.01	0.20	K/Ch/V
26.6575	3900.11	0.2460	3.34	0.06	0.25	G/I
27.7949	729.25	0.3936	3.21	0.01	0.40	H
28.5305	857.30	0.1968	3.13	0.01	0.20	Py
29.9053	454.74	0.2952	2.99	0.01	0.30	Ca
31.7617	4361.50	0.2952	2.82	0.06	0.30	H
33.0599	805.33	0.2952	2.71	0.01	0.30	Py

Note:

Ca = calcite; Ch = chlorite; G = glauconite; H = halite; I = illite; K = kaolinite; Py = Pyrite; Q = quartz; V = vermiculite.

- Glauconitic mud (BP1-12)

Position [$\infty 2\theta$.]	Height [counts]	FWHM [$\infty 2\theta$.]	d-spacing [Å]	Rel.Int. [%]	Tipwidth [$\infty 2\theta$.]	Interpretation
8.8537	460.79	0.7872	9.99	0.01	0.80	G/I
12.3210	280.05	0.2952	7.18	0.00	0.30	K/Ch/V
17.9483	65.21	1.3776	4.94	0.00	1.40	G/I
19.5786	656.79	0.1968	4.53	0.01	0.20	G/I
24.8377	661.94	0.2460	3.58	0.01	0.25	K/Ch/V
26.7915	1121.98	0.8856	3.33	0.02	0.90	G/I

Note:

Ch = chlorite; G = glauconite; I = illite; K = kaolinite; V = vermiculite.

- Green, muddy glauconite sand (FM3-05)

Position [$\infty 2\theta$.]	Height [counts]	FWHM [$\infty 2\theta$.]	d-spacing [Å]	Rel.Int. [%]	Tipwidth [$\infty 2\theta$.]	Interpretation
8.7092	1304.28	0.2460	10.15	0.02	0.25	G/I
17.9205	287.93	0.3444	4.95	0.00	0.35	G/I
19.5591	555.68	0.1968	4.54	0.01	0.20	G/I
26.7431	2175.74	0.3444	3.33	0.03	0.35	G/I

Note:

G = glauconite; I = illite.

- Green, muddy glauconite sand (MF1-06)

Position [∞ 2Th.]	Height [counts]	FWHM [∞ 2Th.]	d-spacing [Å]	Rel.Int. [%]	Tipwidth [∞ 2Th.]	Interpretation
8.6742	655.96	0.6888	10.19	0.01	0.70	G/I
17.8234	153.92	0.3936	4.98	0.00	0.40	G/I
19.5535	693.60	0.1968	4.54	0.01	0.20	G/I
21.2947	309.86	0.3936	4.17	0.00	0.40	Goe
24.3341	240.18	0.5904	3.66	0.00	0.60	I
26.9169	1338.47	0.1968	3.31	0.02	0.20	G/I
32.6091	378.51	0.1968	2.75	0.01	0.20	Sid

Note:

G = glauconite; Goe = Goethite; I = illite; Sid = siderite.

- Green, muddy glauconite sand (MF1-07)

Position [∞ 2Th.]	Height [counts]	FWHM [∞ 2Th.]	d-spacing [Å]	Rel.Int. [%]	Tipwidth [∞ 2Th.]	Interpretation
8.5951	243.08	0.5904	10.29	0.00	0.60	G/I
17.7823	168.44	0.2952	4.99	0.00	0.30	G/I
19.5173	1205.77	0.1968	4.55	0.02	0.20	G/I
21.3347	624.18	0.3936	4.16	0.01	0.40	Goe
24.1929	605.36	0.9840	3.68	0.01	1.00	I
26.6915	2528.66	0.2952	3.34	0.04	0.30	G/I+Q
28.9804	377.74	0.7872	3.08	0.01	0.80	Gyp

Note:

G = glauconite; Goe = goethite; Gyp = gypsum; I = illite; Q = quartz..

- Green, muddy glauconite sand (TP1-06)

Position [∞ 2Th.]	Height [counts]	FWHM [∞ 2Th.]	d-spacing [Å]	Rel.Int. [%]	Tipwidth [∞ 2Th.]	Interpretations
8.7076	734.84	0.5904	10.16	0.01	0.60	G/I
17.8632	219.56	0.5904	4.97	0.00	0.60	G/I
19.5833	788.26	0.2460	4.53	0.01	0.25	G/I
21.2615	580.27	0.3936	4.18	0.01	0.40	Goe
24.0766	593.25	0.7872	3.70	0.01	0.80	I
26.7240	1605.70	0.2460	3.34	0.02	0.25	G/I
29.2430	508.49	0.7872	3.05	0.01	0.80	Ca/Gyp
32.1202	247.85	0.3936	2.79	0.00	0.40	Sid

Note:

Ca = calcite; G = glauconite; Goe = goethite; Gyp = gypsum; I = illite; Sid = siderite.

- Green, bioturbated, muddy glauconite sand (TP1-11)

Position [∞ 2Th.]	Height [counts]	FWHM [∞ 2Th.]	d-spacing [Å]	Rel.Int. [%]	Tipwidth [∞ 2Th.]	Interpretation
8.7863	192.89	0.2952	10.06	0.00	0.30	G/I
17.8117	207.18	0.2952	4.98	0.00	0.30	G/I
19.5125	929.71	0.2460	4.55	0.01	0.25	G/I
21.3209	839.28	0.2460	4.17	0.01	0.25	Goe
24.3651	608.15	0.7872	3.65	0.01	0.80	I
26.7864	1142.10	0.1968	3.33	0.02	0.20	G/I
28.8429	502.40	0.9840	3.10	0.01	1.00	Gyp
33.2677	319.05	0.2460	2.69	0.00	0.25	Goe

Note:

G = glauconite; Goe = goethite; Gyp = gypsum; I = illite.